Department of Physics
Indian Institute of Technology Guwahati
Ph.D. Thesis

Discontinuous percolation transition: Search for new models and scaling theory

Bappaditya Roy

Supervisor: Prof. S. B. Santra
November, 2017.

Discontinuous percolation transition: Search for new models and scaling theory

A thesis submitted by

Bappaditya Roy

to

Indian Institute of Technology Guwahati
in partial fulfillment of the requirements
for the award of the degree of
Doctor of Philosophy in Physics

Department of Physics
Indian Institute of Technology Guwahati
Guwahati - 781039, Assam, India

Statement

The work contained in the thesis entitled "*Discontinuous percolation transition: Search for new models and scaling theory*" has been carried out by me under the supervision of Prof. S. B. Santra, Professor, Department of Physics, Indian Institute of Technology Guwahati. This work has not been submitted elsewhere for the award of any degree.

(Bappaditya Roy)
Department of Physics
Indian Institute of Technology Guwahati
Guwahati - 781039

April 10, 2018

Certificate

It is certified that the work contained in the thesis entitled "*Discontinuous percolation transition: Search for new models and scaling theory*" by Mr. Bappaditya Roy, a Ph.D. student of the Department of Physics, Indian Institute of Technology Guwahati for the award of Doctor of Philosophy has been carried out under my supervision. This work has not been submitted elsewhere for the award of any degree.

(Prof. S. B. Santra)
Department of Physics
Indian Institute of Technology Guwahati
Guwahati - 781039

April 10, 2018

To my parents...

Acknowledgements

I express my sincere gratitude to all those people who made this dissertation possible. Foremost, I am very much indebted to my supervisor Prof. Sitangshu Bikash Santra for his motivation, patient guidance, invaluable suggestions, constant encouragement and support throughout my research work. I am also thankful to him for introducing me to many advanced subjects in physics like phase transitions and critical phenomena, percolation, self organized criticality, advanced statistical physics etc. I will remain ever grateful to him for his great assistance to make this thesis possible. I owe a deep gratitude to him and his family. Many many Thanks to my advisor Prof. Sitangshu Bikash Santra.

I convey my sincere thanks to my doctoral committee members, Prof. A. Srinivasan, Dr. T. N. Dey and Prof. S. N. Bora for constant encouragement, support, valuable suggestions and critical comments during the course of my work and specially during the annual review. I am thankful to all other faculty members of Physics department for being helpful in all regards. My special thanks to Prof. P. Poulose, Prof. S. Ghosh, Prof. S. Basu, Prof. P. Alagarsamy, Dr. A. K. Sharma Dr. D. Maity and Dr. Tapas K Mandal for their timely help and support. I am also thankful to my teachers Prof. R. C. B (IITKGP), Dr. Parthasarathi Das and Dr. Tanusri Pal from Midnapur college who help me to motivate towards the research.

I am grateful to have a discussion with Prof. Deepak Dhar, Prof. Parongama Sen, Prof. Hans J. Herrmann, Dr. Young Sul Cho, Prof. Satya N. Majumdar, Prof. Takahiro Hatano and Dr. Subir K. Das for many helpful suggestions.

I wish to thank Department of Physics, Indian Institute of Technology Guwahati (IITG), to provide me with necessary computational facilities. I wish to thank Indian Institute of Technology Guwahati for providing a great library facility and the computer center with outstanding network connectivity and various computational resources. I thank all the technical assistant of the department. I would specially

like to thank Mr. B. B. Purkayastha and H. Medhi in this regard. My special thanks goes to my senior Dr. Jahir Abbas Ahmed for his help, constant encouragement and support from the beginning of my research. I am also grateful to my senior Dr. S. Shina and Dr. K. Sen for their help and many research related discussion. I would also like to thank other seniors of our computational lab, Dr. B. Dutta, Dr. P. Dey, Dr. V. Prasad, Dr. S. Roy, Dr. B. Pal and Dr. Meera V. and all of my colleagues and juniors for their co-operation. I would like to thank my co-workers Brahmananda Sethi, Himangsu Bhaumik and Sourav Chattopadhyay for their co-operation and support. Special thanks to Kartik, Krishnanjan, Supriyo da, Kausik da and Amit for entertaining discussions over evening tea sessions.

I am grateful to IITG for the financial support.

I have been fortunate to come across excellent friends and juniors who made my stay at IITG cheerful. My special thanks go to Pankaj, Sukhomay, Najmul, Prasant, Amiya, Gaffar, Vipin, Amit, Suresh Babu, Apurba da, Kallol, Ramiz, Noor, Ashis, Shinananda, Kajjol, Anabil, Sudin, Kaushik, Tapas and Biswajit for their timely help, support and encouragement. I am also thankfull to my school and college friends for their encouragement, help and support.

I am deeply indebted to my parents, brothers, sisters, my sweet nephews, my beloved wife and other family members for their unconditional love, constant support and encouragement towards my thesis work. Their true love and strong trust made me always to keep my faith and road. They always stood behind me during the ups and downs of my life. Finally, I am blessed with my little princess Sanghavee (1yr old), who is a inspiration for my work which I have completed.

Bappaditya

Abstract

Percolation is one of the most studied models of Statistical Physics which found to have diverse application in a variety of problems ranging from physical sciences, mathematics as well as to computer science and sociology. It is well known to be a robust second order continuous geometrical phase transition from a disconnected phase to a connected or spanning phase. On the other hand, many connectivity problems in nature and society are found to be discontinuous or abrupt such as outbreak of epidemics, collapse of banking systems, power grids, computer networks, etc. It is therefore intriguing to look for a percolation model as it primarily describes connectivity problems that undergo first-order discontinuous transition. A new era in the study of percolation has started at the beginning of this century through the development of a series of new models. Among them, explosive percolation has taken the central stage in recent time after its introduction in 2009 which claimed to exhibit discontinuous percolation transition with sudden jump in the order parameter during a non-equilibrium growth process at an area fraction much higher than the percolation threshold. Though later it was found to be a continuous transition, such a claim triggered debates and detailed studies to confirm the existence of first order discontinuous transition in a percolation model. Explosive percolation was mostly studied constructing several non-equilibrium growth models. In most of them, the nature of transitions remain inconclusive because of slow convergence and found to be continuous in the thermodynamic limit. Moreover, except the existence of a discontinuous jump, the other properties of a first-order transition such as phase coexistence, nucleation, bimodal distribution of the order parameter etc. are found to be absent in most of the explosive percolation models. In this thesis, a number of lattice models are developed incorporating the essential ingredients like nucleation and growth in order to realize percolation as a first-order transition in static equilibrium properties of clusters as well as in a non-equilibrium growth process.

First, a new two-parameter percolation model (TPPM) with simultaneous growth of multiple clusters is developed. Two tunable parameters of the model are the ini-

tial seed concentration ρ and the constant cluster growth probability g. The model has an expand parameter space than that of original percolation model and incorporates partial hindrance in growing a cluster due to the presence of other clusters. Percolation transition is determined by the final static configurations of spanning clusters. It is found that the values of the critical exponents describing the scaling functions at the criticality in this model are that of original percolation for all values of ρ and the transitions belong to the same universality class of percolation. No discontinuous transition or tricritical point is observed in this model.

The model is improved by introducing suppressed cluster growth incorporating a cluster size dependent dynamic growth probability. This dynamically varying growth probability leads to correlated growth and expected to have stronger effect than partial hindrance in the previous model. The model is studied extensively following finite size scaling hypothesis. It is found that the values of the critical exponents describing the scaling functions at the criticality in this model are that of original percolation for $\rho \geq 0.2$. Whereas for $\rho < 0.2$, suppression of the growth of larger clusters seems to have non-trivial effect on the critical properties. The values of the critical exponents found to deviate from those of the original percolation and the model is found to belong in new universality classes. However, such suppression is found to be too weak to change the nature of the percolation transition.

Nucleation and preferential growth in cluster generation is further incorporated in TPPM, the above model. Following usual spanning cluster approach of original percolation, the model is found to exhibit distinctly a first-order transition as well as a continuous percolation transition at different regimes of initial seed concentration ρ. As ρ decreases starting from the percolation threshold p_c of the original percolation, a line of continuous transition encounters a coexistence region of percolating and non-percolating large clusters. At sufficiently small values of ρ (≤ 0.05), the value of g_0 exceeds p_c. First-order transitions are found to occur and are not only characterized by a discontinuous jump in the order parameter but also by the existence of coexistence of spanning and non-spanning large clusters, and the appearance of compact spanning clusters. For higher values of ρ (≥ 0.45), continuous transitions are found to occur that belong to the same universality class of original percolation. In the intermediate range of ρ ($0.05 < \rho < 0.45$), the nature of transition still remains inconclusive as the characteristic features of both continuous and discontinuous percolation transitions appear concurrently.

Finally a dynamical model of random cluster growth lattice filling percolation model with touch and stop rule is developed. Nucleation centers are continuously

added one at a time to the empty sites and clusters are grown from these nucleation centers with a growth probability g. The model is found to exhibit second order continuous percolation transitions as original percolation for $g \leq 0.5$ whereas for $g \geq 0.8$ it exhibits first order discontinuous percolation transitions. The transitions are characterized by estimating the values of the critical exponents associated with the order parameter and its fluctuation as well as the dimension of the spanning cluster over the whole range of g. Instead of a sharp tricritical point, a tricritical region is found to occur for $0.5 < g < 0.8$ within which the values of the critical exponents change continuously till the crossover from continuous to discontinuous transition is completed. The nature of transitions is confirmed by studying Binder cumulant, cluster size distribution, and order parameter distribution. Since the order parameter distribution is of a weak bimodal type for $g \geq 0.8$, the discontinuous transitions in this regime are weak first-order transitions.

The models are investigated via extensive numerical simulations. The scaling behaviour developed for these models are rigorously verified performing scaling analysis on the largest lattice as well as developing finite size scaling hypothesis. The thesis is finally able to identify criteria for the first-order transition in percolation models such as correlated growth, the rapid growth of smaller clusters than the larger clusters beside nucleation and overall growth instead of random growth. The models can be generalized to abrupt transition that occurs in science or nature.

Contents

Chapter 1

Introduction

S. R. Broadbent and J. M. Hammersley in 1957[1] introduced the theory of percolation to explain the process of flow of a fluid through a random medium though the phenomenon was already encounter by P. J. Flory during his study of polymerization of monomers in the early 1940's[2]. Soon after the introduction of the percolation theory various applications in physical problems were considered by Cyril Domb, Michael Fisher, John Essam and M. F. Skyes and others[3]. Further extension of the theory in the context of phase transition and critical phenomena was made by a large number of physicists including Krikpatrick, Stanley, Herrmann, Stauffer, Aharony, Havlin and many others. Percolation is one of the most studied models of Statistical Physics which found to have diverse application in a variety of problems ranging from physical sciences, mathematics as well as to computer science and sociology. For example: oil recovery from porous media[4], epidemic modeling[5], networks[6], fracture[7], metal-insulator transition[8], ionic transport in glasses and composites[9], earthquakes in rocks and ground water flow[10] many others. One of the simplest models of Statistical Physics is possibly percolation in which sites or bonds of a lattice are randomly occupied with certain probability p and one looks for a long range connectivity, spanning the system from one side to the other at a critical threshold p_c. It is well known to be a robust second order continuous geometrical phase transition from a disconnected phase to a connected or spanning phase[11]. As $p \to p_c$, the critical point, the geometrical quantities obtained from the second moment of the cluster size distribution and the connectivity (or correlation) length diverges. The order parameter of the transition, the probability to find a site in the spanning cluster, continuously goes to zero as p is decreased to p_c from above. The spanning cluster becomes a self-similar fractal object. The percolation transition (PT) not only has one-to-one correspondence with thermal critical phenomena but

also the model can be mapped to $q = 1$ Potts model that involves Ising spins of q-states[12,13]. Such mapping of the percolation model to the Potts model lead to evaluation of exact values of the critical exponents of percolation in two dimensions as well as the scaling relations among the critical exponents[14]. Furthermore, the critical exponents are found to be universal in the sense that they are independent of the type of percolation model (site or bond) and the lattice structure in a given dimension as happens in thermal critical phenomena[15]. Percolation thus has all the critical properties of a second-order continuous phase transition.

On the other hand, the first-order phase transitions are those that involve a latent heat and usually associated with structural change in the system. During such a transition, a system either absorbs or releases a fixed amount of energy. There are changes in entropy and volume corresponding to discontinuous change in the first derivatives of the Gibbs free energy[16]. The change from one phase of the system to the other is sudden or abrupt. Because energy cannot be instantaneously transferred between the system and its environment, first-order transitions are associated with "mixed-phase regimes" or "phase co-existence" in which some parts of the system have completed the transition and others have not. A familiar phenomenon is boiling of water where a phase transition from a liquid to a gas phase (vapour) happens with abrupt jump in the entropy and volume. As the water does not instantly turn into vapour, it forms a turbulent mixture of liquid water and water vapour bubbles. Many important phase transitions fall in this category, including the solid-liquid, liquid-gas, solid-gas transitions. In nature and society, many connectivity problems are also found to be discontinuous or abrupt such as outbreak of epidemics, collapse of banking systems, power grids, computer networks, etc.[17]. It is therefore intriguing to look for a percolation model as it primarily describes connectivity problems that undergoes first-order transition.

In fact, a new era in the study of percolation has started at the beginning of this century through development of a series of new models[18–20] such as percolation on growing networks[21], percolation in the models of contagion[22,23], k-core percolation[24,25], jamming percolation[26], explosive percolation[27–29], percolation on interdependent networks[30–32], agglomerative percolation[33,34], percolation on hierarchical structures[35], drilling percolation[36,37], two-parameter percolation[38] with preferential growth[39] and many others. Among these models, explosive percolation (EP) has taken the central stage in recent time after its introduction by Achlioptas *et al.* (2009)[27] which claimed to exhibit discontinuous PT with sudden jump in the order parameter during a non-equilibrium growth proces at an area fraction

p much higher than the percolation thresholds. Though later it was found to be a continuous transition, such a claim triggered debates and detailed studies to confirm the existence of first order discontinuous transition in a percolation model which in general incorporate random processes. The study reveals, instead of robust second order (continuous) transition with formal finite size scaling (FSS) as observed in ordinary percolation[11,40], a variety of new features. Sometimes the transitions are characterized as a first-order transition[41–44], sometimes a crossover from second order to first order with a tricritical point (or region) are observed[23,39,45–47], sometimes features of both first and second order transitions are simultaneously exhibited in a single model[48–50], sometimes second order transitions with unusual FSS are found to appear[51–54]. In most of the cases, except a jump in the order parameter, the other aspects of a first-order transition such as compact spanning cluster, phase coexistence, nucleation, bimodal distribution of order parameter, etc., which are essential features of a first-order thermal phase transition are found to be absent. However, such activity not only enriches the understanding of a variety of physical problems but also leads to creation of newer models beside extension of the existing models for deeper understating of the existence of such non-universal but intriguing behaviour. Therefore, the search for a equilibrium or non-equilibrium percolation models that exhibit true discontinuous first-order transitions remain open.

In this thesis, such a challenging task has been taken up. New percolation models will be constructed, appropriate scaling theory will be developed and the order of transition will be characterized. First a brief review will be given on phase transition, critical phenomena and first order transition. The ordinary percolation model and its features will be then described. Recent literature on explosive percolation will be summarized and a plan of the thesis problem will be provided at the end of this chapter.

1.1 Phase transition and critical phenomena

A phase is a state of matter in thermodynamic equilibrium. The system could be in several different states or phases depending upon the macroscopic condition (Temperature, Pressure, etc.) of the system. Different phases of water are our everyday experience. Ice, water and vapour are three different states or phases of a collection of large number of H_2O molecules. Given a macroscopic condition, the system spontaneously goes to a particular phase corresponding to the lowest free energy. At equilibrium, the Gibbs free energy $G(N, P, T)$ is found to be the lowest

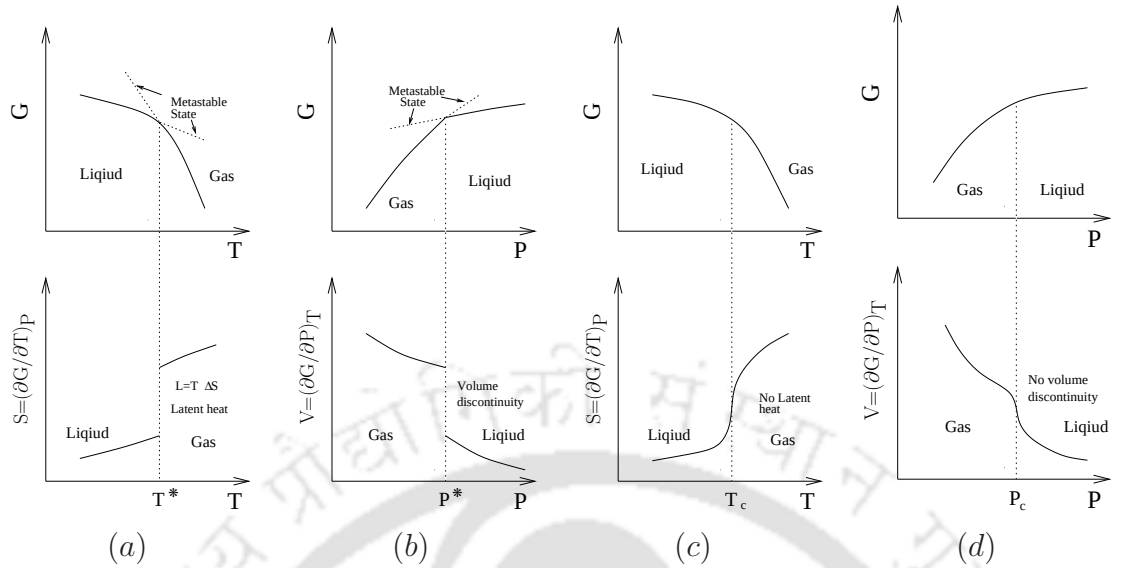

Figure 1.1: Variation of Gibbs free energy $G(T, P)$ and its first derivatives with respect to T and P around (T^*, P^*) below (T_c, P_c), a second order transition point in (a) and (b). In (c) and (d), same plots are shown around (T_c, P_c), a second order transition point.

for a system whose state is described by number of particles N, pressure P and temperature T.

There is a wide variety of phase transitions starting from liquid to gas, paramagnet to ferromagnet, antiferromagnet to paramagnet, ferrimagnet to paramagnet, para-electric to ferro-electric, normal to superconductor, normal to superfluid, liquid to liquid crystal, order disorder, percolation and many others. A good description of phase transition and critical phenomena can be found in a number of classic books[15,55,56]. Most phase transitions belong to one of the two types: first-order transition or second-order transition. In principle, all macroscopic properties can be obtained from the free energy function of a given system near to the critical point. As per Ehrenfest's criteria, nth order phase transition corresponds to the discontinuity or divergence of the nth derivative of the free energy functions. Thus, in a first-order transition, the first derivative of the free energy becomes discontinuous whereas in the second order phase transition, the second derivative of the free energy becomes discontinuous or diverges at the transition point. First and second order phase transitions then can be understood qualitatively in terms of non-analyticity in the free energy function. We will describe qualitatively the variation of the Gibbs free energy $G(T, P)$ and its derivatives to demonstrate order of transition in a fluid system. In Fig.1.1(a) and (b), the free energy curves of the two phases meet with difference in slopes and both stable and meta-stable states exist for some region of temperature

and pressure. At the transition point (T^*, P^*), the tangents to the curves change discontinuously and yield discontinuity in entropy $S = -(\partial G/\partial T)_P$ (corresponds to latent heat $L = T\Delta S$) and discontinuity in the volume $V = (\partial G/\partial P)_T$. At a second order transition, however, the free energy curves of two phases meet tangentially at the critical point (T_c, P_c). The slopes of the curves changes continuously across the critical point. Therefore, there is no discontinuity either in entropy or in volume as shown in Fig.1.1(c) and (d). Since there is no entropy discontinuity in second order transition, there is no emission (or absorption) of latent heat in this transition. In the case of second order transition, the system then goes continuously from one phase to another without any supply of latent heat and known as continuous phase transition.

Fluid system:

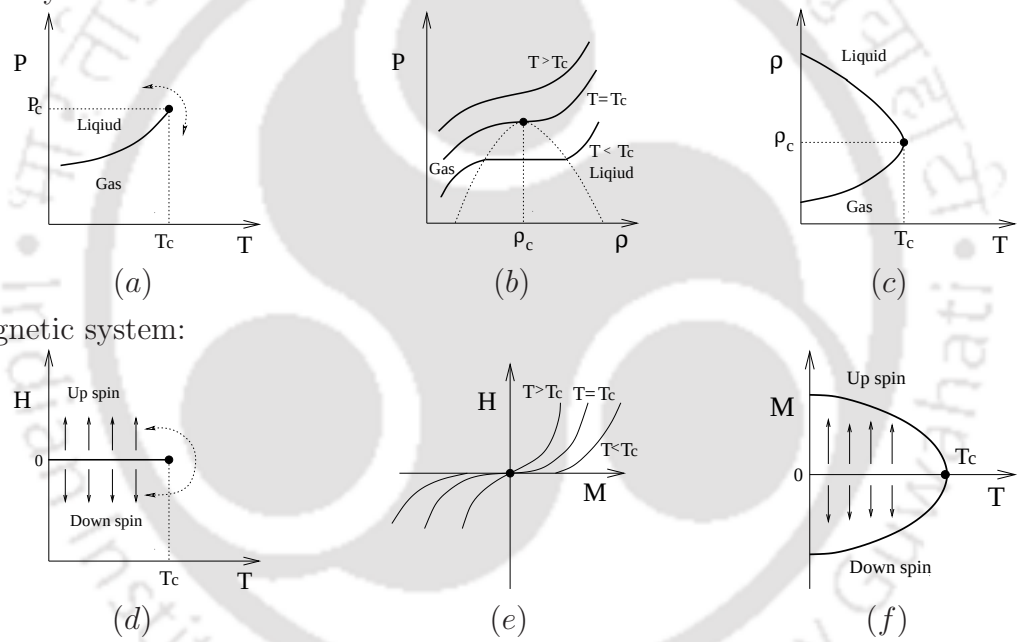

Magnetic system:

Figure 1.2: (a) Plot of vapour pressure curve in the $P-T$ plane. (b) Plot of isotherms curves in the $P-\rho$ plane. (c) Plot of ρ versus T in the $\rho-T$ plane. (d) Plot of phase separation curve in the $H-T$ plane. (e) Plot of isotherms in the $H-M$ plane. (f) Plot of M versus T in the $M-T$ plane.

Phase transition can be understood by considering different phase diagrams. Below we present different phase diagrams for the fluid and magnetic systems whose equation of states in terms of pressure P, temperature T and density ρ for a fluid system and magnetic field H, magnetization M and temperature T for a magnetic system are given by $f(P, \rho, T) = 0$ and $f(H, M, T) = 0$ respectively. The vapour pressure curve in the $P-T$ plane in (a) or the phase separation curve in $H-T$ in (d), the line of first-order phase transitions, terminates at a critical point around which a

continuous conversion of a phase to the other is possible without crossing the vapour pressure or phase separation curve (or costing latent heat). As the temperatures decreases, the isotherms in both the cases develop curvature and become flat at the critical point in the $P-\rho$ and $H-M$ plane as shown in (b) and (e). At $T = T_c$, the response functions, the isothermal compressibility $\kappa_T = \frac{1}{\rho}\partial\rho/\partial P$ or the isothermal magnetic susceptibility $\chi_T = \partial M/\partial H$, the second derivative of the respective free energy, diverge as $T \to T_c$ as expected for a second-order phase transition. The density difference and spontaneous magnetization are the order parameters in theses cases and it can be seen in (c) and (f) that they are deceases as T increases to t_c and vanish above T_c.

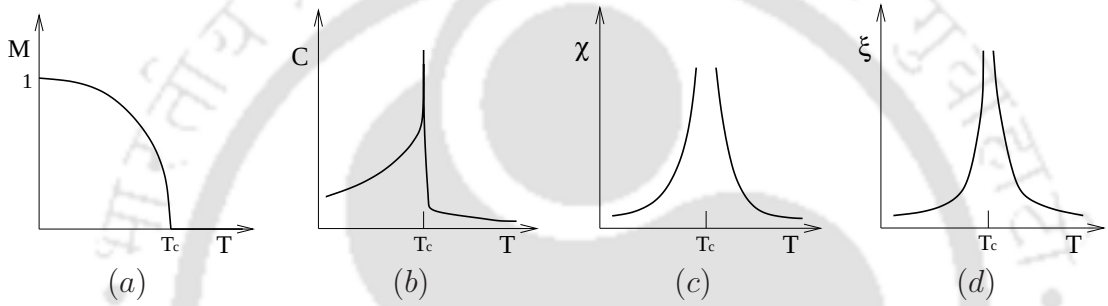

Figure 1.3: Plot of (a) M versus T, (b) C versus T, χ versus T and (d) ξ versus T.

The characteristic features that appear at the critical point where a second-order continuous transition occurs are: order parameter continuously goes to zero, response functions diverge, fluctuations (in density or in spin orientation) appear at all length scales, long range order appears in density-density or spin-spin correlation, *i.e.*; correlation length diverges. On the other hand, the first-order discontinuous transitions are characterized by jump in the order-parameter, exchange of latent heat, coexistence of two phases, nucleation and growth, etc. The singularities in the order parameter M, specific heat C, susceptibility χ and the correlation length ξ in a second order phase transition as $T \to T_c$ for a magnetic system are given by $M \sim (T - T_c)^{\beta}$, $C \sim |T - T_c|^{-\alpha}$, $\chi \sim |T - T_c|^{-\gamma}$, $\xi \sim |T - T_c|^{-\nu}$ where α, β, γ and ν are the respective critical exponents. The variations of theses thermodynamic quantities and the correlation length ξ versus temperature around the critical point are shown in Fig.1.3. At $T = T_c$, the scaling of the critical isotherm and the correlation function are given by $H \sim M^{\delta}$ and $\Gamma(r) \sim r^{-(d-2+\eta)}$ where δ and η are two exponents.

There exists a well defined prescription to study the critical behaviour of the thermodynamic quantities near the critical point $T \to T_c$. Since the thermodynamic

quantities can be obtained as different derivatives of the free energy, the whole problem is then boiling down to the estimation of free energy of a given system. The free energy G is obtained in terms of the canonical partition function Z as

$$G = -k_{\mathrm{B}} T \ln Z \tag{1.1}$$

where T is the temperature of the system and k_{B} is the Boltzmann constant. Estimating the partition function or the free energy in the vicinity of the critical point, the critical behaviour of the thermodynamic quantities can be obtained. As the thermodynamic quantities are obtained by taking different derivatives of the free energy, the critical exponents describing their singularities then can not be all independent. As $T \to T_c$, the Gibbs free energy $G(T, H)$ becomes a generalized homogeneous function of reduced temperature t and reduced field h, a set of scaling relations among the critical exponents are obtained as: $\alpha + 2\beta + \gamma = 2$, $\alpha + \beta(1 + \delta) = 2$, $\beta(\delta - 1) = \gamma$ and two more relations by hyper-scaling: $\nu(2 - \eta) = \gamma$ and $d\nu = 2 - \alpha$ where d is the space dimension.

Phase transition can be qualitatively understood by the phenomenological theory of Landau[55,56]. The theory provides a description of both first order and second order phase transitions and their interplay[57]. We will briefly present Landau theory below and highlights the essential points.

1.1.1 Landau Theory of phase transition

Landau developed a theory of phase transition guessing the form of the thermodynamic potential without involving detailed interactions among the particles in the system. The Landau potential $A(T, m)$ where $m = M/N$ is an intensive parameter is constructed with fundamental assumptions that the free energy is analytic and can be expanded in a power series of the order parameter m, and should have the same symmetry of the Hamiltonian with $h = 0$, *i,e*; $A(T, m) = A(T, -m)$. Therefore, only even powers of the order parameter would appear in the expansion. It is intriguing that such an analytic function incorporates non-analyticities in the process of minimization.

The Landau free energy $A(t, m)$ then can be written as

$$A(t, m) = a(t) + \frac{1}{2} b(t) m^2 + \frac{1}{4} c(t) m^4 + \frac{1}{6} d(t) m^6 + \cdots \tag{1.2}$$

where $t = (T - T_c)/T_c$ is the reduced temperature and the fractional pre-factors are

taken for simplification of later calculations. Depending on which function $b(T)$, $c(T)$, $\cdots$ changes sign and at which temperature it will lead to continuous and first-order phase transitions as well as tricritical points.

Case-I: Continuous Transition

Let us consider that the coefficients of m^4 and all other higher order terms are positive, *i.e.*; $c(t), d((t), \cdots > 0$ and $b(t)$ can change sign at $t = 0$ (or $T = T_c$). Let us assume $b(t) = b_0 t$ only the linear term in the power series of $b(t)$, with $b_0 > 0$. The free energy $A(t, m)$ must have extrimum with respect to m. To identify those extrimum, $A(t, m)$ is minimized with respect to m. Hence,

$$\frac{\partial A}{\partial m} = 0 = b_0 t m + c(t)m^3 + d(t)m^5 + \cdots = m\left[b_0 t + c(t)m^2 + d(t)m^4 + \cdots\right] \quad (1.3)$$

Thus $m = 0$ is always a solution. Ignoring m^4 and higher order terms in the bracket, one has $m = \pm\sqrt{-b_0 t/c(t)}$. Therefore,

$$m = \begin{cases} 0 & \text{for } \; t \geq 0, \\ 0, \; \pm\sqrt{\frac{b_0|t|}{c_0}} & \text{for } \; t < 0 \end{cases} \quad (1.4)$$

where $c(t)$ is approximated as c_0 as $t < 0$. The minima and maxima corresponding to these solutions can be identified by taking the second derivative of $A(t, m)$. It is found that for $t \geq 0$, there is a minimum at $m = 0$. But for $t < 0$, there is a maximum at $m = 0$ and two minima at $m = \pm\sqrt{b_0|t|/c_0}$. Plot of the Landau potential $A(t, m)$ against m for different t is shown in Figure 1.4(a) and the values of $m(T)$ obtained from the positions of minima of $A(t, m)$ are plotted against T in Figure 1.4(b). It can be seen that $m(T)$ is zero for $T = T_c$ but is a double valued function below T_c that describes a second order continuous phase transition.

Case-II: Discontinuous Transition

Let us consider now that $c(t)$ has a sign change at $T^* > T_c$: such that $c(t) < 0$ for $T < T^*$ and $c(T) > 0$ for $T > T*$. The stability of the system has to be ensured by $d(T)$, $e(T) > 0$. Again, minimization of $A(t, m)$ requires,

$$\frac{\partial A}{\partial m} = 0 = b(t)m + c(t)m^3 + d(t)m^5 = m\left[b_0 t + c(t)m^2 + d(t)m^4\right] \quad (1.5)$$

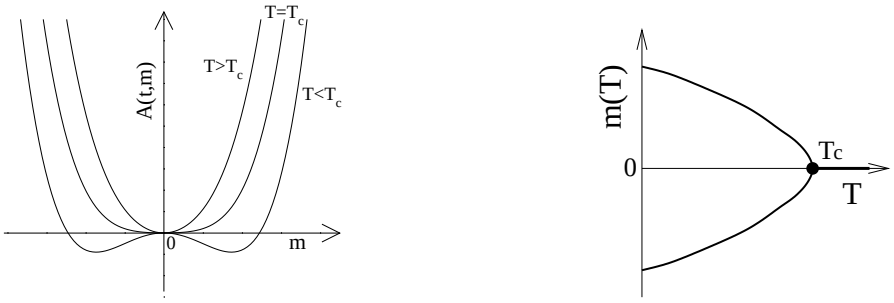

(a) (b)

Figure 1.4: (a) Plot of $A(t,m)$ against m for different values of t. The values of the constants are taken as $a(t) = 0$, $b_0 = 4$ and $c_0 = 1/2$. The positions of minima $m(t)$ for different values of t are shown in (b).

Hence, $m = 0$ is still a solution. The solutions of $0 = b + cm^2 + dm^4$ are

$$m_{\pm}^2 = -\frac{c}{2d} \pm \frac{1}{2d}\sqrt{c^2 - 4db}. \tag{1.6}$$

As $t, t^* > 0$ ($T, T^* > T_c$), b is always positive. For $t > t^*$, we also have $c, d > 0$. Then the square root is either imaginary (no real solution for m^2) or less than c (no positive solution for m^2). Hence, $m = 0$ remains the only solution. Whereas, for $t < t^*$ (but $t > 0$ ot $T > T_c$), $b, d > 0$ and $c < 0$. Then $-c/(2d) > 0$, and if $c^2 - 4db > 0$ there might be 2 positive solutions for m^2, hence 4 additional solutions for m, $\pm m_+$ and $\pm m_-$ (symmetric about $m = 0$). Due to stability and symmetry, the 5 extrema must be ordered as: *min* - *max* - *min* - *max* - *min*. A competition within the system will then arise between the minimum at $m = 0$ and the two minima at $m = \pm\left[-\frac{c}{2d} + \frac{1}{2d}\sqrt{c^2 - 4db}\right]^{1/2}$ to become the global minimum of the free energy. The phase transition will happen if they all have the same free energy at some temperature, say t'. Therefore, one solves for

$$A(m, t') - A(0, t') = \frac{1}{2}b(t')m^2 + \frac{1}{4}c(t')m^4 + \frac{1}{6}d(t')m^6 = 0. \tag{1.7}$$

Besides $m = 0$, other solutions can be obtained as

$$\frac{1}{2}b(t') + \frac{1}{4}c(t')m^2 + \frac{1}{6}d(t')m^4 = 0. \tag{1.8}$$

Inserting the other equation $b(t') = -c(t')m^2 - d(t')m^4$, one has

$$m^2 = -\frac{3c(t')}{4d(t')} \tag{1.9}$$

as the values of m where the phase transition happens. As there is a sudden jump in the value of the order parameter, the phase transition at $T = T'$ is a *first-order discontinuous phase transition.*

Case-III: Tricritical Point

The situation corresponding to both $b(t)$ and $c(t)$ change sign simultaneously at exactly the same temperature could lead to new types of critical behaviour. This situation is expected to occur if there is at least a second tuning parameter besides temperature. Let us introduce a new intensive tuning parameter Δ. Still assuming symmetry with respect to the sign of the order parameter, the Landau free energy is given as

$$A(m, t, \Delta) = a(t, \Delta) + \frac{1}{2}b(t, \Delta)m^2 + \frac{1}{4}c(t, \Delta)m^4 + \frac{1}{6}d(t, \Delta)m^6. \tag{1.10}$$

The line of critical points is given by $b(t, \Delta) = 0$, which defines a curve in the $t - \Delta$ plane. A unique point in this plane (t_t, Δ_t), called the tricritical point is given by $b(t_t, \Delta_t) = c(t_t, \Delta_t) = 0$.

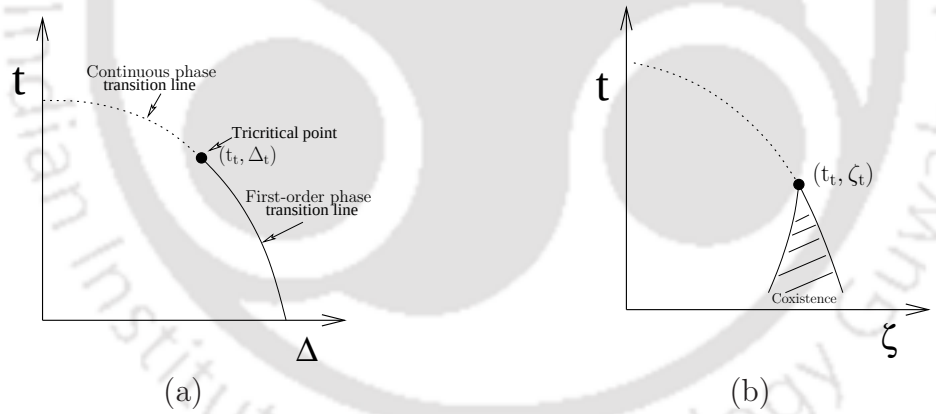

Figure 1.5: (a) Plot of t against Δ. Dotted and solid lines represent the continuous and first-order phase line respectively. The black point represents the tricritical point at $(\mathrm{t_t}, \Delta_\mathrm{t})$. (b) Plot of t against ζ. A coexistence region is shown below the point $(\mathrm{t_t}, \zeta_\mathrm{t})$
.

Assume that $\Delta > \Delta_t$ and $c(t)$ becomes negative at a higher temperature than $b(t)$ does. This will correspond to first order transition. On the other hand, for $\Delta < \Delta_t$ and $c(t)$ becomes negative at a lower temperature than $b(t)$ does would correspond to second-order continuous transition. The line of first-order transitions would join the line of critical points of continuous transition in a smooth manner. The line of first-order transitions can be obtained by incorporating the value of m

given in Eq.1.9 into the expression of $b(t)$ as

$$b(t,\Delta) - \frac{3c^2(t,\Delta)}{16d(t,\Delta)} = 0. \tag{1.11}$$

The slope of the line $b(t,\Delta) = 0$ for the critical points on the $t-\Delta$ plane at $b = 0$ is given by

$$\left.\frac{d\Delta}{dT}\right|_{\text{crit}} = -\frac{(\partial b/\partial t)_\Delta}{(\partial b/\partial \Delta)_t} = -\frac{b_T}{b_\Delta} \tag{1.12}$$

where the subscripts indicate partial differentiation and the slope of Eq.1.11 for the first-order line is given by

$$\left.\frac{d\Delta}{dT}\right|_{\text{first order}} = -\frac{b_T - (3/8)cc_T + bd_T}{b_\Delta - (3/8)cc_\Delta + bd_\Delta} \tag{1.13}$$

At the tricritical point, $b \to 0$, $c \to 0$, hence both the slopes become the same and the transition lines join smoothly as shown in Fig. 1.5(a).

Coexistence of two phases that occur in the first-order transition for $\Delta > \Delta_t$ can be visualized introducing an intensive parameter ζ conjugate to Δ as $\zeta = -(\partial A/\partial\Delta)_T$, where the sign is an arbitrary convention. Along the first-order transition line, using the values for m at both sides of the transition one has

$$\zeta_+ \approx -a_\Delta, \quad \zeta_- \approx -a_\Delta + \frac{3}{8d}(b_\Delta c + c_\Delta b). \tag{1.14}$$

keeping lowest order terms. Then

$$\delta\zeta = \zeta_+ - \zeta_- \approx -\frac{3}{8d}(b_\Delta c + c_\Delta b), \tag{1.15}$$

is positive. In the $t-\zeta$ plane, a coexistence region is opening up below t_t as shown in Fig. 1.5(b).

A few examples of systems exhibiting tricritical points are the mixtures of ^{3}He and ^{4}He, the antiferromagnet $FeCl_2$, the solid NH_4Cl, the ferroelectric $KDPO_4$, etc.

A detailed theory of first-order transition and finite size scaling hypothesis can be found in Ref.[58,59].

1.2 Percolation as a critical phenomena

Classical percolation is a typical geometrical phase transition. The model along with its numerous variations have been extensively studied since 1940s and applied

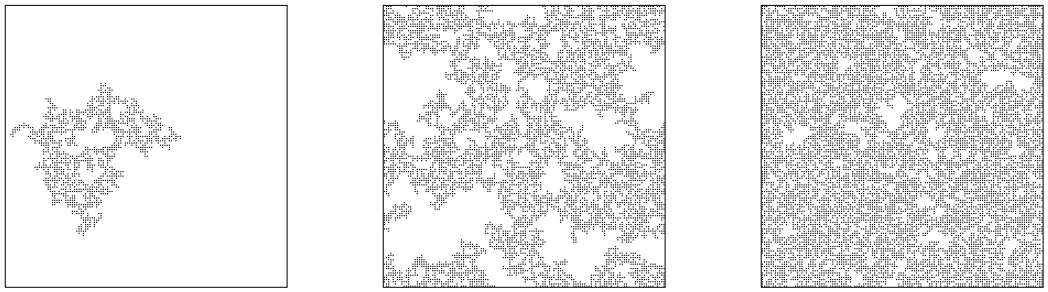

$p = 0.57$ $p = 0.59274621$ $p = 0.65$

Figure 1.6: The largest clusters at different site occupation probabilities p. These are obtained populating a square lattice lattice of size 128×128.

in many different branches of science[10,60–64]. In recent times, percolation model is applied to oil recovery in porous media[65,66], epidemic modeling[67], networks[68,69], business firm growth[70], fragmentation of solids[71], poly-atomic species[72], electrical conductivity of colloidal dispersion[73], conductivity of DNA[74], living neural networks[75], propagation of information on scale free networks[76], seismic process[77], gelation[78], hydration water in bio-systems[79], solar dynamo[80] and many others. In all these systems, the common ingredient is randomness or disorder and a transition from connectivity to non-connectivity or propagation to non-propagation, etc., occurs in the system at a sharply defined parameter value.

The percolation model and its elaborate theory developed by several authors during last few decades are well documented in enormous literature and can be found in[11,40,81,82]. A brief description, however, will be provided here. There are two versions of the model, namely site and bond. The site percolation model is defined on a square lattice of linear size L in 2 dimensions (2d). Sites of an empty are randomly occupied with a probability p or remains unoccupied with a probability $q = 1-p$. A cluster of occupied sites is defined as a collection of a number of occupied sites connected by nearest neighbor bonds. For small values of p, only small isolated clusters of occupied sites are generated without a spanning cluster. As p increases from a small value, a spanning cluster of occupied sites appears for the first time in the system at a particular value of p between 0 and 1, say p_c, called the percolation threshold. Below p_c there is no spanning cluster and above p_c there is always a spanning cluster present in the system. This is known percolation transition. For an infinitely large lattice, p_c has a sharp and unique value determined by the lattice structure and the dimension d of the lattice. For a finite lattice, the value of p_c has a small spread. A few largest clusters are shown in Figure 1.6. A spanning cluster appears in the system for the first time at $p = 0.59274621$, the percolation threshold

on the square lattice for site percolation. It should be mentioned here that it has been shown rigorously by Grimmett[83] that there is no percolating infinite cluster at $p = p_c$ for $d = 2$. The large but finite clusters that emerge at $p = p_c$ are called 'incipient infinite clusters'. However, throughout this thesis, the incipient infinite clusters at $p = p_c$ will be referred as percolating spanning clusters.

1.2.1 Finite clusters and scaling

As thermodynamic quantities exhibit critical behaviour at the critical point, the geometrical properties of the finite clusters (excluding the spanning cluster) are expected to exhibit critical behaviour at the percolation threshold $p = p_c$. Such geometrical quantities, can be obtained by define a cluster generating function G similar to free energy function in thermodynamic critical phenomena. The generating function in case of percolation is defined as

$$G = \sum_{h} {\sum_{s}}' n_s(p) e^{-sh} \tag{1.16}$$

where $n_s(p)$ is the number of s-sited clusters per lattice site at the site occupation probability p and h is a fictitious field that has no physical meaning. The primed sum is over all finite clusters. The relevant geometrical quantities are now obtained by taking different derivatives of the generating function G.

The function G at $h = 0$, given by

$$G\Big|_{h=0} = {\sum_{s}}' n_s(p) \sim |p - p_c|^{2-\alpha} \tag{1.17}$$

gives total number of finite clusters per lattice site and scales with $|p - p_c|$ with and exponent α as $p \to p_c$.

The order parameter P_∞ of the percolation transition, defined as the probability that a site belongs to the spanning cluster, can be obtained from the first derivative $(\partial G/\partial h)_{h=0} = {\sum_s}' s n_s(p)$ of the generating function as

$$P_\infty = p - {\sum_{s}}' s n_s(p) \sim (p - p_c)^\beta, \tag{1.18}$$

that scales with $p - p_c$ with an exponent β. The order parameter $P_\infty = 0$ for $p < p_c$ as ${\sum_s}' s n_s(p) = p$. At $p = 1$, ${\sum_s}' s n_s(p) = 0$ and thus $P_\infty = 1$. As $p \to p_c^+$, P_∞ continuously goes to zero from $p = p_c$ with an exponent β, as spontaneous

magnetization does in the case of magnetic transition.

The average cluster size χ can be obtained from the second derivative $(\partial^2 G/\partial h^2)_{h=0} = \sum_s' s^2 n_s(p)$ of the generating function. As $\sum_s' s n_s(p) = p$, χ is defined as

$$\chi = \frac{\sum_s' s^2 n_s(p)}{\sum_s' s n_s(p)} = \frac{1}{p} \sum_s' s^2 n_s(p) \sim |p - p_c|^{-\gamma}, \tag{1.19}$$

and scales with $|p - p_c|$ with an exponent γ. The divergence of χ is very similar to that of magnetic susceptibility in the case of magnetic phase transition.

Beside the moments of the generating function, the linear size of the finite clusters, below and above p_c, is characterized by a correlation length ξ similar to the correlation length in thermodynamic phase transition. As $p \to p_c$, the correlation length ξ scales with $|p - p_c|$ as

$$\xi^2 = \frac{2 \sum_s' R_s^2 s^2 n_s(p)}{\sum_s' s^2 n_s(p)} \sim |p - p_c|^{-2\nu} \tag{1.20}$$

where R_s is the radius of gyration of a s-sited cluster and ν is an exponent. The singular behaviour of P_∞, χ and ξ are shown in Figure 1.7

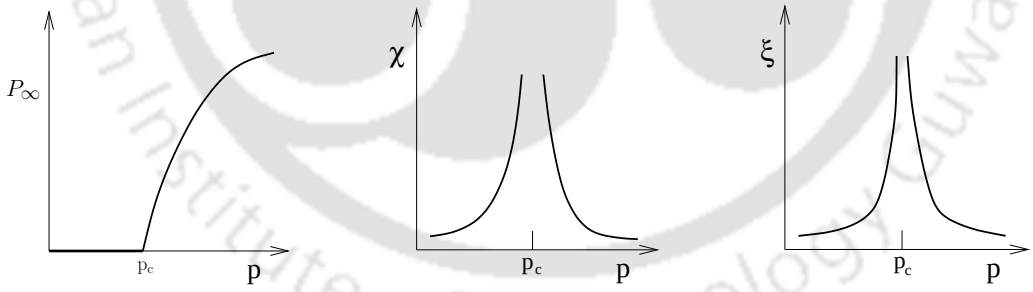

Figure 1.7: Plot of P_∞, χ and ξ against p around p_c.

Since geometrical quantities described above are just different moments of the cluster size distribution function $n_s(p)$, the critical exponents will not be all independent. The scaling relations among them can be obtained knowing the form of $n_s(p)$. As in thermodynamic phase transition, the free energy becomes a generalized homogeneous function in the critical regime, the cluster size distribution function $n_s(p)$ is then expected to be a generalized homogeneous function too in the critical

regime. The scaling function form of $n_s(p)$ is given by

$$n_s(p) = s^{-\tau}\mathsf{f}[s^{\sigma}(p - p_c)] \tag{1.21}$$

where τ and σ are two exponents. The kth moment of $n_s(p)$ then become singular as

$$\sum_s{}' s^k n_s(p) = (p - p_c)^{-(k-\tau+1)/\sigma}. \tag{1.22}$$

Choosing the appropriate values of k, the values of the critical exponents are possible to obtain in terms of τ and σ as $2-\alpha = (\tau-1)/\sigma$, $\beta = (\tau-2)/\sigma$ and $\gamma = (3-\tau)/\sigma$. The following scaling relation among them it can be easily obtained as

$$\alpha + 2\beta + \gamma = 2 \tag{1.23}$$

as it is known in thermal phase transition.

1.2.2 Fractal dimension of the spanning cluster

The spanning cluster at $p = p_c$ contains holes of all possible sizes and it is found to be self similar random object as fractal. The mass $M(L)$ of a fractal object scales with its lateral dimension L to the power of a fractional dimension d_f, $M(L) \approx L^{d_f}$, than an Euclidean dimension d. Thus, the size $S_{\max}$ of an infinite percolation cluster should scale with its radius of gyration R as

$$S_{\max} \sim R^{d_f}, \tag{1.24}$$

where d_f is the fractal dimension of the percolation cluster.

Since the probability that an arbitrary site to belong in the infinite cluster is P_∞, one has

$$P_\infty \approx \frac{R^{d_f}}{R^d} \approx \frac{\xi^{d_f}}{\xi^d}, \tag{1.25}$$

where d is the Euclidean dimension of the space. As $P_\infty \sim (p-p_c)^\beta$ and $\xi \sim |p-p_c|^{-\nu}$ in the vicinity of the critical point, for $p \neq p_c$ one has, $(p - p_c)^\beta = (p - p_c)^{\nu(d-d_f)}$ and hence a scaling relation

$$d_f = d - \beta/\nu, \tag{1.26}$$

called a hyper-scaling relation and valid for $d < 6$. Relation with τ and σ can be obtained incorporating the cluster size distribution and $R_s \sim s^{1/d_f}$ in the definition

of the correlation length ξ as

$$d_f = \frac{1}{\nu\sigma}, \tag{1.27}$$

a detailed derivation can be found in[11,40].

There are numerous analytical and numerical studies for estimating the values of the critical exponents of percolation transition[84–87]. The exact values of the critical exponents for 2d percolation model was obtained by mapping the model onto the $q \to 1$ Potts model[84,85]. The values of some of the exponents are listed below in Table 1.1. The values of the critical exponents are found the same on different lattices in the same space dimension. The critical exponents do not depend the site or the bond percolation on the same lattice in the same space dimension. This defines the universality class of the percolation model.

Order parameter exponent β	5/36
Average cluster size exponent γ	43/18
Correlation length exponent ν	4/3
Fractal dimension d_f	91/48

Table 1.1: Critical exponents of the ordinary percolation in 2d obtained by mapping it onto q-state Potts model in the limit $q \to 0$[84,85].

The ordinary percolation model thus exhibits a second-order continuous transition at a critical threshold $p = p_c$ and the critical behaviour can be described in the same fashion of a thermal phase transition.

1.3 Discontinuous percolation transition

Discontinuous percolation transition (DPT) was reported in the form of Explosive Percolation (EP) by Achlioptas *et al* in 2009[27] as already mentioned. To establish EP, Achlioptas process (AP), a correlated growth rule, was applied in generating a gain cluster on the Erdös-Rényi[88] random graph. Starting with a network of N vertices without edges, edges are added one at a time. In each time step, two unoccupied edges (say, e_1 and e_2) are chosen at random, each of which is supposed to connect two distinct clusters. The size of the cluster is defined as the number of connected nodes in it. Say, the edge e_1 connects two clusters of size s_1 and s_1' and the edge e_2 connects another two clusters of size s_2 and s_2'. An edge, e_1 or e_2 is selected following a product rule (PR). If $s_1 s_1' < s_2 s_s'$, e_1 is selected otherwise e_2 is selected for occupation and the other edge is discarded. This process led to a sharp jump in the largest cluster size at a significantly higher value of percolation threshold than that of the ordinary percolation. The situation is depicted in the

Figure.1.8. However, da Costa *et al.*[51] based on analytic and numerical analysis reported that the EP transition is actually continuous with unusual scaling.

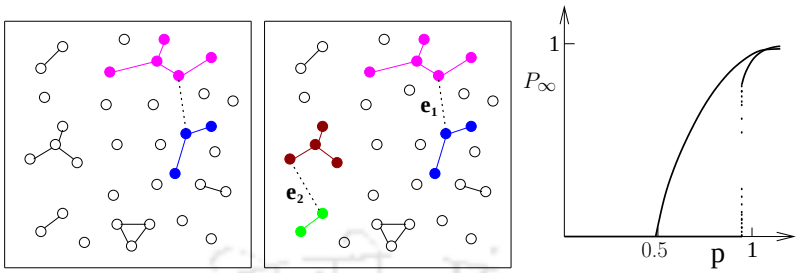

Figure 1.8: Plot of P_∞ vs p for continuous percolation transition (CPT) in regular percolation and for DPT. In EP, DPT is showing the delayed and explosive growth in the PR model.

Employing AP in the cluster growth process, a series of articles appeared in the literature that describe the EP transition and can be found in several review articles[18–20,54,89]. The study of those EP models have been carried out in various lattices and network configurations. A brief discussion on a few key models are given below.

Soon after the introduction of EP, Cho *et al.*[90] showed percolation transition in scale-free networks under AP. Almost at the same time, Radicchi and Fortunato[48,91] reported EP in scale-free networks, however in a slightly different model. Networks constructed via AP show continuous percolation transition for $\lambda \leq 3$ and discontinuous percolation transition for $\lambda > 3$ where λ is the degree distribution exponent of the scale-free network, $P(k) \sim k^{-\lambda}$. Cho *et al.* also reported existence of a tricritical point for λ in the range: $2.3 < \lambda < 2.4$. A discontinuous percolation transition on ER network was also reported by Cho and Kahng[92] designing dynamic growth rule to suppress the growth of all clusters. Another simple model of graph evolution was developed by D'Souza and Mitzenmacher[93] that exhibit discontinuous percolation transitions which can be analyzed via mathematical evolution equations. The underlying mechanism, the "powder keg", responsible for the first-order transitions in ER network was suggested by Friedman and Landsberg[94] and further developed by Hooyberghs and Schaeybroeck[95]. Explosive percolation with multiple giant clusters was studied by Chen and D'Souza[96], Yang *et al.*[97], Chen *et al.*[98,99], and Schrenk *et al.*[100] following random graph evolution process of Bohman, Frieze, and Wormald[101], known as BFW model.

Applying cooperative Achlioptas process to the growth of 2d bond percolation cluster, discontinuous transition was reported by Ziff[28,102] studying the critical properties of percolation probability, susceptibility and the second moment of finite

clusters. No power law scaling of the critical cluster size distribution found to appear for the system size used. A site percolation version of cluster growth via AP was also developed on a 2d square lattice by Bastas *et al.*[103]. It was observed that the order parameter changes more abruptly in comparison to ordinary percolation. Indications of different universality classes for the site and bond EP were obtained employing usual FSS analysis. Explosive site percolation studied by Choi *et al.*[104] was found to exhibit discontinuous transition supported by the existence of hysteresis loop. To establish bond-site duality of EP, the site and bond percolation was carefully defined on the square lattice and it was shown by Choi *et al.*[105] that duality exists and transition becomes discontinuous. Extension of such a problem to higher dimension was reported by Choi *et al.*[106]. A generalized product rule was proposed by Reis *et al.*[107] which reveals the effect of non-locality on the critical behaviour of the percolation process and a discontinuous transition form ordinary percolation to (nonlocal) EP was reported. Weakly EP on directed network was reported by Squires *et al.*[108] and Waagen *et al*[109]. An extensive FSS theory for the explosive percolation transition was developed by Cho *et al.*[110] on ER network and by Li and Östling[111] for different lattice as well as off lattice models.

Extended versions of Achlioptas process with PR and sum rule (SR) were developed and various growth models have been proposed. One of them is the best-of-m rule[45,112–114] in which at each time step m edges (m more than 2) are chosen to compete. Note that when $m = 1$ the best-of-m rule recovers the ordinary random percolation, which is continuous, whereas $m = 2$ corresponds to original AP. The models with higher m exhibited continuous transitions with a finite but very small order parameter exponent β. Discontinuous percolation could occur on networks if and only if m approaches infinite[115].

During the study of explosive percolation, however, there erupted a strong controversy in the literature over the order of transition in these model. In one hand, in certain cases because of slow convergence the transitions are found to be continuous in the thermodynamic limit. On the other hand, there are supporting evidence of discontinuous transition. The nature of transition, however, remains inconclusive in some of the EP models. Riordan and Warnke[52] showed all Achlioptas processes have continuous phase transitions, although related models in which the number of nodes sampled may grow with the network size can indeed exhibit explosive percolation. Studying several Achlioptas processes with explosive percolation transition Grassberger *et al*[53] showed that EP transition is continuous but with unusual finite size scaling. Lee *et al*[116] found continuity of the EP transition by investigating EP

on the complete graph by extensive numerical simulation. Continuous EP transition in PR processes on several networks was also reported by Tian and Shi[117]. A review on unusual transition in several EP models was provided by Basta *et al.*[54].

Apart from original Achlioptas processes, several other related models were developed that exhibit first-order discontinuous transition. Manna and Chatterjee[118] and later Manna[119], studied a new route to EP, where an edge between a pair of clusters of sizes s_i and s_j, say, is randomly occupied with a probability $(s_i s_j)^\alpha$, α is an exponent. For $\alpha < \alpha_c$, a critical value, the transitions were reported as first-order. A first-order EP transition was also observed in another probabilistic model introduced by Moreira *et al.*[120]. Controlling the growth of the largest cluster alone Araujo and Herrmann[42] and later Schrenk *et al.*[121] showed a first-order percolation transition via Gaussian distribution of cluster sizes in contrary to some of the EP models. A unified framework covering low-dimensional systems and the mean field limit for EP was proposed by Cho *et al.*[29] through a stochastic model in which formation of a spanning cluster is avoided. An upper critical dimension d_c had been identified below which the transitions are found to be first-order and above which the transitions are always continuous. Some of the previous contradictions were resolved by Cho *et al.*[29] and was further explained by Ziff[122]. Discontinuous percolation transition was also observed in the diffusion-limited cluster aggregation (DLCA) models of percolation[89,123,123,124].

Hybrid phase transition where properties of both second-order and first-order phase transitions occur at the same transition point is found to appear in percolation problems on complex networks, for instance, in k-core percolation[125–127], in the cascade failure model on multiplex networks[22,23], in Cluster Merging Processes[49,50,101,128,129].

There are several other model systems where first-order transitions were found to occur. A few of them are: nanotube based systems[130], social network[131,132], Human Protein Homology Network[133]. A first-order PT on the explosive electric breakdown due to conducting particle deposition on an insulating substrate was reported by Oliveira *et al.*[134]. First order transition was also observed in mechanical yield in amorphous solids[135], in the outbreak of coinfectious diseases[43], in structure formation in interconnected networks[136], in the failures in interdependent networks[30,137], failure and recovery in dynamical networks[138], in epidemic models of infectious diseases[44,139] and many others.

1.4 Equilibrium percolation models and first-order transition

We categorize some of the percolation models as equilibrium percolation model as the percolation transition in this models are characterized by the cluster properties of the final static or equilibrium cluster size distribution as in ordinary percolation[11]. However, the discontinuous transition reported in the above models are mostly non-equilibrium growth models as percolation transition can also be obtained occupying lattice sites dynamically when the concentration of occupied sites will achieve the percolation threshold[40]. Perhaps, bootstrap percolation introduced by Adler in 1991[140] is the oldest example that exhibits a discontinuous transition in the context of an equilibrium percolation model. In this model, the process will start from an original percolation configuration. The system is evolved by removing a site that has less than predefined number m of occupied nearest neighbour (NN) sites. The process will stop when every site has at least m_c number of occupied neighbours. A discontinuous jump in the largest cluster size is found to occur with larger values of p. The results of the model strongly depend on the type of lattice and the values of m. The disadvantage of bootstrap percolation is that removing of sites cannot be described by a statistical weight and the number of iteration depends on the initial configuration and can become very long close to the transition. However, much attention was not paid to bootstrap percolation in the literature. On the other hand, except the existence of a discontinuous jump, the other properties of a first-order transition such as phase coexistence, nucleation, bimodal distribution of the order parameter etc. are found to be absent in most of the explosive percolation models[53]. Motivated by these two aspects, absence of an equilibrium model of percolation that exhibits discontinuous transition and need to have phase coexistence and bimodal distribution of the order parameter, in this thesis an attempt has been made to construct models that would exhibit first-order transitions and develop a consistent theory of first-order transition in geometrical models.

A number of questions to be answered in order to recognize percolation as a first-order transition. Percolation is based on random processes and hence second order transition is a spontaneous outcome in the models of percolation. Thus, in the first place, the growth process has to be correlated. Moreover, in contrary to thermal phase transitions like liquid-gas or ferro to paramagnet, percolation has a single control parameter, the area fraction p. Due to lack of more than one parameter, the phase space becomes restricted and it becomes difficult to exhibit phase coexistence

or observe the presence of a tricritical point if any. Furthermore, nucleation and growth should lead to compact cluster and jump in the order parameter at the time of transition. In this thesis, a number of lattice models are developed incorporating the above essential ingredients and associating more than one parameter in order to realize percolation as a first-order transition. Staring with a simple two-parameter model with random processes and incorporating nucleation and coagulation it was possible to exhibit a crossover from continuous to discontinuous transition with a tricritical region in most of the models via extensive numerical simulation. Beside static equilibrium models, a non-equilibrium growth model is also developed incorporating the above ingredients. The dynamical model also found to have a crossover from continuous to discontinuous transition depending on the growth rate.

After this introductory chapter, we will present a two-parameter constant growth percolation model in chapter 2. In chapter 3, the model will be extended incorporating suppression in growing the clusters. In chapter 4, the model will be further modified and much stronger preferential growth will be incorporated which eventually will produce a discontinuous transition. In chapter 5, dynamical growth model will be developed keeping ingredients of nucleation and growth that will lead to a crossover from continuous to discontinuous transitions. A proper scaling theory for each model will be developed and numerically verified. Finally in chapter 6, a comprehensive summary of the whole thesis will be presented.

Chapter 2

Two parameter Constant growth percolation model

In this chapter, a new percolation model with nucleation and growth is developed involving two tunable parameters, the initial seed concentration ρ and a growth parameter g. Due to lack of more than one parameter in original percolation model, the phase space becomes restricted. It is difficult to locate the tricritical point if any and exhibit phase coexistence. Hence, this newly introduced two parameter percolation model (TPPM) is expected to exhibit non-trivial critical behaviour. As multiple clusters will grow simultaneously in this model, the growth of a cluster will encounter partial hindrance due to the presence of other clusters. Furthermore, nucleation and growth should lead to compact clusters and jump in the order parameter at the time of transition. Most importantly, unlike growth models, percolation transition (PT) in TPPM will be determined by the final equilibrium cluster properties as in original percolation model.

2.1 The model

The model, TPPM, is developed on a square lattice of size $L \times L$ in 2-dimensions (2d). In TPPM, the initial configuration is taken as a partially randomly populated lattice with an initial seed concentration ρ less than the threshold of original percolation (OP), $p_c \approx 0.5927$[11]. Hence, a number of small finite clusters of occupied sites are randomly distributed all over the lattice and the cluster size distribution

This chapter is based on the Ref.[38]; Bappaditya Roy and S. B. Santra, Croat. Chem. Acta **86**(4), 495 (2013).

is then obtained employing the Hoshen-Kopelman algorithm[141]. A cluster is a collection of occupied sites connected by nearest neighbour (NN) bonds. The process of nucleation and growth is then implemented by growing all these finite clusters simultaneously. Therefore, in each Monte Carlo (MC) time step, the empty NN perimeter sites of all the individual clusters are called once for occupation with a fixed but tunable growth probability $g \in [0, 1]$ following Leath algorithm[142]. Note that there are multiple growth centers instead of a single one as in Leath's OP[142]. In the MC algorithm, the clusters are grown sequentially starting from the smallest cluster. Once a site is rejected with probability $(1-g)$, it will remain empty forever, as in original percolation. As soon as all the clusters present at that time are allowed to grow one layer of NN perimeter sites, the cluster size distribution is updated and the MC time step is increased by one. A single MC step then consists of growth of the cluster taking the final configuration of the previous step as initial configuration and merging of the newly grown clusters. The process is then repeated. During the growth of these clusters, two clusters may come in contact. Two clusters with occupied perimeter sites separated by a single lattice spacing are considered to be a single cluster. The total number of clusters is then reduced by one and a cluster of larger size is incorporated in the cluster size distribution function. The growth of a cluster stops when there is no empty site on the cluster perimeter is available to occupy. As the process stops, the final cluster size distribution function $n_s(\rho, g)$ is obtained.

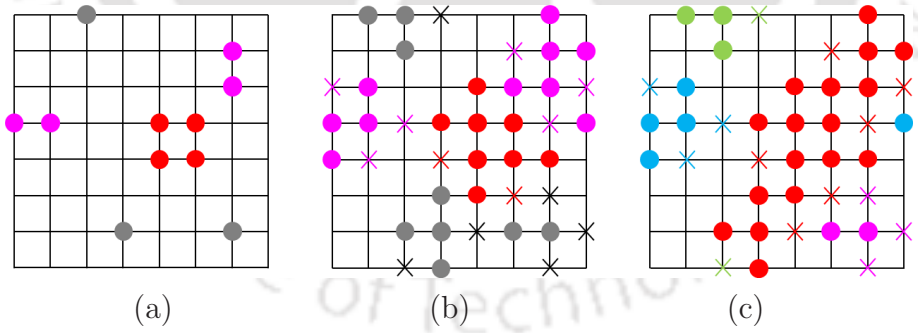

Figure 2.1: Presentation of one MC step of the growth process. Figure (a) represents the initial configuration, figure (b) represents the growth and figure (c) represents merging and relabeling. The occupied sites are presented by filled coloured circles. The largest cluster is shown in red and other smaller clusters are in different colors. The crosses represent the rejected sites. PBC is applied in both the directions in growing the clusters.

The growth process is demonstrated in Fig. 2.1 generating clusters on a 8×8 square lattice in two dimension. A random initial configuration is taken to demonstrate one MC time step. The initial configuration in Fig. 2.1(a) contains three

single-sited, two two-sited and one four-sited clusters shown in different colors. The largest cluster is always shown in red. The value of the growth parameter is taken as $g = 0.5$. The growth of the clusters are presented in Fig. 2.1(b). Periodic boundary conditions (PBC) are applied in both the directions. The newly occupied sites are shown in the same color of the respective cluster. The crosses on the perimeter of a cluster indicate the rejected sites. In Fig. 2.1(c), the merging of the clusters are shown and three clusters merge to generate a spanning cluster. It can be seen that the growth of a cluster is hindered by the presence of other clusters and their rejected neighbours during the growth process.

The model has two limiting situations. One is $\rho = p_c$, the critical site occupation probability of percolation and $g = 0$. The other one is $\rho = 1/L^2$, a single seed and $g = p_c$. Both the situations correspond to original percolation problem. The present model can be considered as a generalized random cluster growth model. It should be noted that the present model is substantially different from the "touch and stop" model[143–145]. In this model, the initial clusters also grow with a constant rate (with unit probability) however the growth stops as soon as two clusters come in contact. In the following, taking intermediate values of ρ and varying the growth probability g transitions from disconnected phase to fully connected phase are studied.

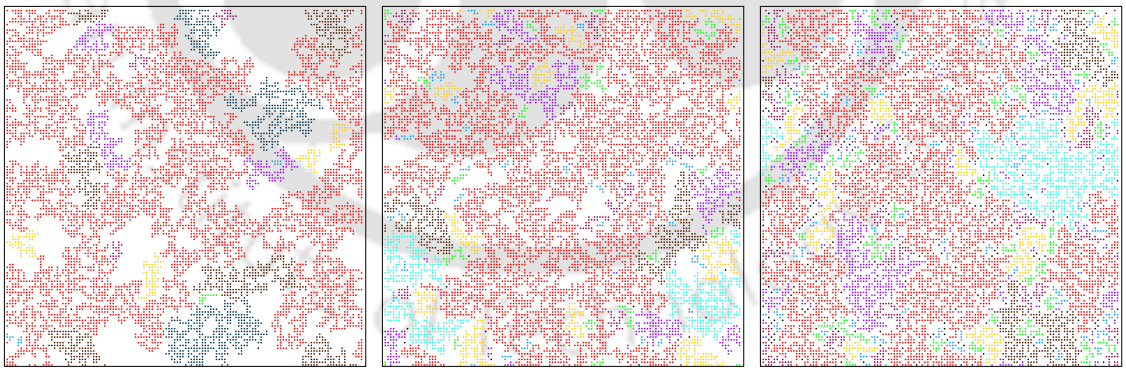

(a) $\rho = 0.005$, $g_c = 0.576$ (b) $\rho = 0.05$, $g_c = 0.556$ (c) $\rho = 0.5$,$g_c = 0.157$

Figure 2.2: Snapshots of cluster size distributions at the end of the growth process on a 2d square lattice of size $L = 128$ with initial seed concentration $\rho = 0.005, 0.05$ and 0.5 and their respective thresholds $g = 0.576, 0.556, 0.157$. In growing the clusters periodic boundary conditions are used. Solid line represents the lattice boundary. The different colors are indicating the all possible sizes of cluster. A spanning cluster appears in a red.

2.2 Spanning cluster morphology

Snapshots of the system morphology at the end of the growth process on a square lattice of size $L = 128$ with initial seed concentrations $\rho = 0.005, 0.05$ and 0.5 are shown in Fig. 2.2 at their respective thresholds $g_c(L) = 0.576, 0.556, 0.157$. In these snapshots, different colors indicate clusters of different sizes. White space corresponds to inaccessible lattice sites. It can be noticed that at the high ρ inaccessible area is less than that at small ρ at their respective thresholds. The spanning cluster is shown in red. It should also be noted that the critical growth parameter g_c increase as ρ decreases and also the number of small finite clusters decreases with ρ. Interestingly, irrespective of the values of ρ, it seems cluster of all possible sizes appear at their respective percolation thresholds indicating continuous phase transition for all values of ρ.

2.3 Percolation threshold

Identification of percolation threshold, a non-universal quantity, is one of the most important tasks in percolation theory. Here, the percolation threshold is identified as a critical growth probability g_c for a given ρ at which for the first time a spanning cluster connecting the opposite sides of the lattice appears in the system when g is increased from a smaller value. Though, there exist several approaches to determine the percolation threshold, here we calculate the threshold from the spanning cluster probability.

The probability to have a spanning cluster for a given ρ and system size L, is defined as

$$P_{sp}(\rho, g, L) = \frac{N_{sp}(\rho, g, L)}{N_{tot}} \tag{2.1}$$

where $N_{sp}(\rho, g, L)$ is the number of ensemble having spanning cluster out of the total number of ensemble N_{tot}. For a system size $L \ll \xi$, $P_{sp}(\rho, g, L)$ is expected to be

$$P_{sp}(\rho, g, L) = f[(g - g_c)L^{1/\nu}]. \tag{2.2}$$

In the $L \to \infty$, $P_{sp}(\rho, g, L)$ is expected to be a theta function at $g = g_c$. Its derivative with respect to g given by

$$\frac{dP_{sp}}{dg} = L^{1/\nu} f'[(g - g_c)L^{1/\nu}] \tag{2.3}$$

is a delta function in the $L \to \infty$ limit with its argument varying from $-\infty$ to $+\infty$. Therefore, for a given ρ and L, the value of $g_c(\rho, L)$ at which a spanning cluster appears for the first time is taken as the average g and can be defined as

$$g_c(\rho, L) = \int_0^1 g \frac{dP_{sp}}{dg} dg, \tag{2.4}$$

the average value of g for the distribution of dP_{sp}/dg. Substituting the value of dP_{sp}/dg from Eq.2.3, one may have

$$g_c(\rho, L) = g_c(\rho) \int_{-\infty}^{+\infty} f'(z)dz + L^{-1/\nu} \int_{-\infty}^{+\infty} z f'(z)dz \tag{2.5}$$

where $z = (g - g_c)L^{1/\nu}$. Since in the $L \to \infty$ limit the function $f(z)$ is a theta function, one has $f(+\infty) = 1$ and $f(-\infty) = 0$ and the integral $\int_{-\infty}^{+\infty} f'(z)dz = 1$. Assuming that $f'(z)$ is not a symmetric function, the integral $\int_{-\infty}^{+\infty} z f'(z)dz = c$ where c is a constant. Hence the value of percolation threshold for a system in

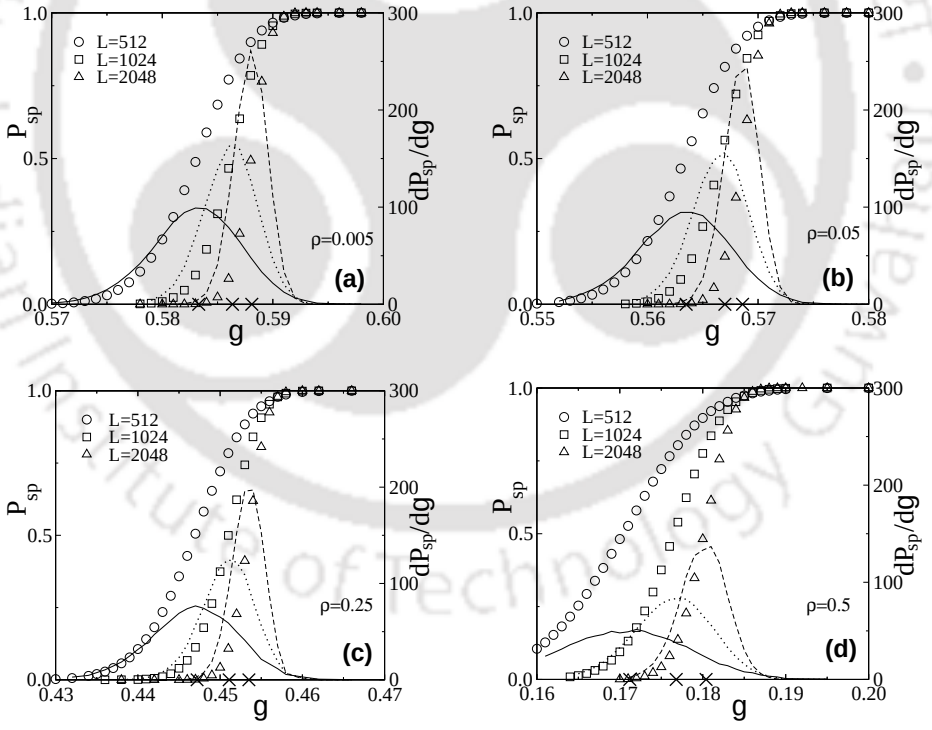

Figure 2.3: Plot of spanning probability P_{sp} and its derivative dP_{sp}/dg against g for system sizes $L = 512, 1024$ & 2048 and for four different distinct values of $\rho = 0.005$ in (a), 0.05 in (b), 0.25 in (c) and 0.5 in (d). The symbols are: circle for $L = 512$, squares for $L = 1024$ and triangles for $L = 2048$ and the derivatives are represented by a black solid line, a red dotted line and a blue discontinuous line respectively. The values of g corresponding to the maxima of the derivatives indicate $g_c(L)$ and marked by crosses.

thermodynamic limit i.e., $L \to \infty$ is given by

$$g_c(\rho, L) = g_c(\rho, \infty) + cL^{-1/\nu}. \tag{2.6}$$

After calculating $g_c(\rho, L)$ for different lattices and for given ρ from the distribution of dP_{sp}/dg in Eq.2.4, the percolation threshold $g_c(\rho)$ for $L \to \infty$ and for given ρ can be determined from the scaling relation Eq.2.6.

The values of P_{sp} are measured at different growth probabilities g in an interval of $\triangle g = 0.001$ on the square lattice of different sizes for given ρ. P_{sp} is then plotted against g for three different values of L, $L = 512$ (circles), $L = 1024$ (squares) and $L = 2048$ (triangles) and for four distinct ρ values in Figure 2.3 (a) for $\rho = 0.005$, (b) for $\rho = 0.05$, (c) for $\rho = 0.25$ and (d) for $\rho = 0.5$. Note that, P_{sp} is not going to zero sharply at a particular value of g. This is due to the finite size of the lattice chosen here. The percolation threshold $g_c(\rho, L)$ then can be determined from the value of g at which the maximum rate of change of P_{sp} occurs. The numerical derivative dP_{sp}/dg of the series of data points P_{sp} with respect to g is evaluated using the central difference method[146],

$$\frac{dP_{sp}(g)}{dg} = \frac{P_{sp}(g + \triangle g) - P_{sp}(g - \triangle g)}{2\triangle g} + O\{(\triangle g)^2\} \tag{2.7}$$

where $O\{(\triangle p)^2\}$ is the order of error. The derivative of P_{sp} is then plotted against g for lattice sizes $L = 512$ (solid line), $L = 1024$ (dotted line) and $L = 2048$ (dashed line) in Figure 2.3 (a), (b), (c) and (d) for their respective ρ values. Hence, the

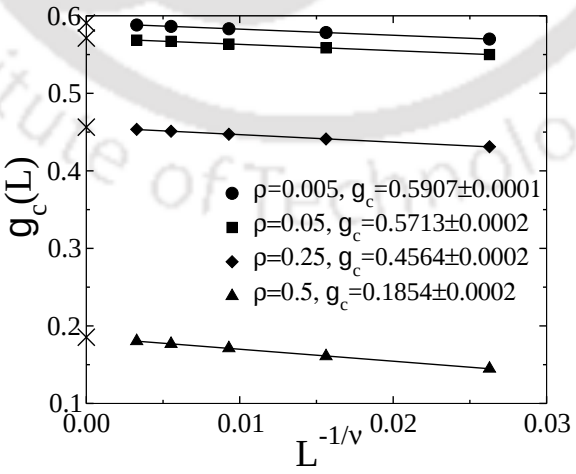

Figure 2.4: Plot of $g_c(L)$ versus $L^{-1/\nu}$ for $\rho = 0.005(\bigcirc), 0.05(\square), 0.25(\diamond)$ and $0.50(\triangle)$. The best straight line fit is found for $1/\nu = 0.75(\approx 3/4$ of OP). From the intercepts, $g_c(\rho)$ are obtained for respective ρ.

maximum of the dP_{sp}/dg represents the maximum slope of the P_{sp} versus g plot. A higher order non-linear curves is fitted to the each plot of dP_{sp}/dg vs g to make them smooth. The value of $g_c(\rho, L)$ is then identified as the value of g corresponding to the maximum of the derivatives and marked by crosses on the g-axis. The obtained values of the percolation threshold $g_c(\rho, L)$ are shown in table 2.1. The variation of $g_c(L)$ is plotted against $L^{-1/\nu}$ taking $1/\nu = 0.75$ as that of OP in Fig. 2.4. Hence, it is found that for all values of ρ, the scaling form in Eq.2.6 is well satisfied with $1/\nu = 0.75$. The thresholds $g_c(\infty)$ are obtained from the precise intersection value of g corresponding to $g_c(L)$ of respective ρ. The values of $g_c(\infty)$ are marked on y-axis by crosses.

L \ ρ	Percolation thresholds			
	0.005	0.05	0.25	0.5
512	0.5833	0.5635	0.4472	0.1712
1024	0.5864	0.5670	0.4511	0.1768
2048	0.5881	0.5686	0.4535	0.1804

Table 2.1: The value of $g_c(\rho, L)$ are measured from P_{sp} for different lattices L and for ρ.

2.4 Phase diagram

Finally a phase diagram of the percolating and non-percolating regions on the $\rho - g$ parameter space is suggested. Since the percolation has to occur at a well defined threshold value of area fraction p_c, the initial seed concentration ρ and the growth

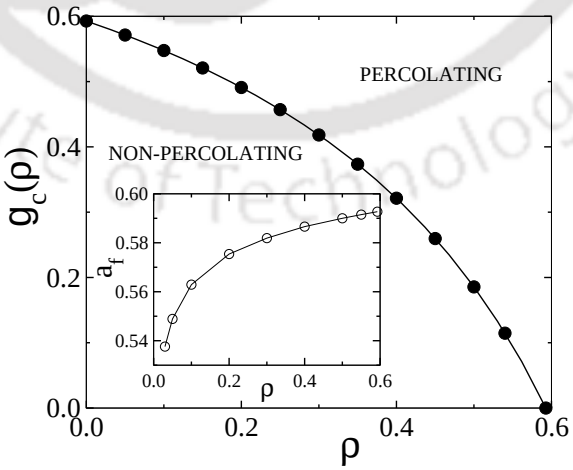

Figure 2.5: Plot of $g_c(\rho)$ against ρ. The circles represent the estimated threshold and the line represents the analytical value obtained from Eq.2.8. In the inset, plot of area fraction a_f against ρ at their respective thresholds.

probability g must satisfy the following equation

$$\rho + g_c(1-\rho) = p_c(OP) \approx 0.59247 \tag{2.8}$$

at the percolation transition. It means that there exists a well defined g_c value for every ρ in order to achieve the critical area fraction p_c at the percolation transition. The critical growth probabilities $g_c(\rho)$s are determined following the method described in the previous section for a series of ρ values. The values of $g_c(\rho)$ are plotted against ρ in Fig. 2.5. However, note that the actual area fraction, a_f not necessarily be equal to p_c(of OP) but a decreasing function of ρ as shown in the inset of Fig. 2.5. The solid line represents the Eq.2.8. It is essentially a line of second order phase transition points which terminates at two trivial percolation transition points and separates the percolating region from the non-percolating region. It will be shown later that the continuous percolation transitions, along this line belong to the same universality of original percolation.

2.5 Cluster properties and scaling relations

In original percolation[11,61], the geometrical quantities are defined in terms of cluster size distribution $n_s(p)$ at a given area fraction p in the critical regime is assumed to be a generalized homogeneous function of $(p-p_c)$ and the cluster size s as

$$n_s(p) = s^{-\tau} f[(p-p_c)s^{\sigma}] \tag{2.9}$$

where p_c is the percolation threshold and τ, σ are two critical exponents. The geometrical quantities are derived from the above distribution taking different moments of it (Eq.2.9) as given in Ref.[11]. The scaling behaviour of the geometrical quantities are then obtained in terms of $(p-p_c)$.

The scaling theory for the geometrical quantities that appear in TPPM is developed following the techniques of original percolation. In the present model, for a given system size L, one starts with an initial seed concentration ρ and with a constant growth probability g. At the critical value of the growth probability g_c, a percolation transition is found to occur for a given value of ρ. Hence the scaling form of the cluster size distribution function $n_s(\rho, g)$ should be obtained in terms of initial seed concentration ρ and growth probability g. For a given system of linear

size L, the cluster size distribution function $n_s(\rho, g)$ can be defined as,

$$n_s(\rho, g) = \frac{N_s(\rho, g)}{L^2} \tag{2.10}$$

where $N_s(\rho, g)$ is the number of s-sited clusters generated at the growth probability g at fixed ρ.

In TPPM, after populating the lattice sites with an initial seed concentration ρ, the empty sites around the clusters are occupied with a constant growth probability g. If all the remaining sites after populating the lattice with initial seed concentration ρ are called for occupation with probability g, the possible area fraction p at the end of the growth process is expected to be

$$p = \rho + g(1 - \rho) \tag{2.11}$$

for any system of size L. Though, in the reality case all the remaining sites could not be called for occupation as they would be surrounded by rejected sites. Note that for $g = 1$, the final area fraction would be always one irrespective of initial seed concentration. Therefore, for a fixed ρ, the difference in area fractions from the threshold value would be given by

$$p - p_c = (g - g_c)(1 - \rho). \tag{2.12}$$

It is expected that the cluster size distribution $n_s(\rho, g)$ becomes a generalized homogeneous function of two variables, namely inverse cluster size $1/s$ and $(g-g_c)(1-\rho)$, as the percolation threshold $g_c(\rho)$ is approached for a given ρ, like the thermodynamic functions in critical phenomena. The scaling function form of the cluster size distribution is then assumed to be

$$n_s(\rho, g) = s^{-\tau} \widetilde{n}_s \left[(g - g_c)(1 - \rho)s^{\sigma}\right], \tag{2.13}$$

where τ and σ are two new exponents and $\widetilde{n}_s$ is a universal scaling function. The scaling form of different geometrical quantities can be derived taking different moments of the cluster size distribution $n_s(\rho, g)$ in terms of ρ and g.

The kth moment of the cluster size distribution $n_s(\rho, g)$ is defined as

$$M_k = \sum_s{}' s^k n_s(\rho, g) \tag{2.14}$$

where k is an integer and the primed sum denotes summation of all finite clusters. In the thermodynamic limit, the summation can be replaced by an integration and the kth moment can be represented as

$$M_k = \int_0^\infty s^k n_s(\rho, g) ds = \int_0^\infty s^{k-\tau} \widetilde{n}_s \left[(g - g_c)(1-\rho)s^\sigma\right] ds. \tag{2.15}$$

Defining a scaled variable $z = s^\sigma (g - g_c)(1 - \rho)$, M_k can be obtained in terms of z as

$$M_k = \left[(g - g_c)(1-\rho)\right]^{-\frac{k+1-\tau}{\sigma}} \frac{1}{\sigma} \int z^{-1+\frac{k+1-\tau}{\sigma}} \widetilde{n}_s(z)\, dz. \tag{2.16}$$

Since the integral will contribute a constant, it is then possible to obtain M_k without knowing the exact form of $\widetilde{n}_s(z)$. Hence, the scaling form of M_k is obtained as

$$M_k = \sum_s{}' s^k n_s(\rho, g) \sim \left[(g - g_c)(1-\rho)\right]^{-\frac{k+1-\tau}{\sigma}}. \tag{2.17}$$

Scaling behaviour of different cluster properties can be obtained from Eq.2.17, assigning appropriate values of k. Several cluster properties and scaling behaviour are listed below where $p = \rho + g(1-\rho)$ and the third and fourth moments have no

Order parameter:	$P_\infty = p - \sum_s{}' s n_s(\rho, g)$	$\sim \left[(g - g_c)(1-\rho)\right]^\beta$,	$\beta = \frac{\tau-2}{\sigma}$
Average cluster size:	$\chi_2 = \sum_s{}' s^2 n_s(\rho, g)$	$\sim \left[(g - g_c)(1-\rho)\right]^\gamma$,	$\gamma = \frac{3-\tau}{\sigma}$
Third moment:	$\chi_3 = \sum_s{}' s^3 n_s(\rho, g)$	$\sim \left[(g - g_c)(1-\rho)\right]^\delta$,	$\delta = \frac{4-\tau}{\sigma}$
Fourth moment:	$\chi_4 = \sum_s{}' s^4 n_s(\rho, g)$	$\sim \left[(g - g_c)(1-\rho)\right]^\eta$,	$\eta = \frac{5-\tau}{\sigma}$

physical meaning. It can be noted that the critical exponents β, γ, δ and η satisfy certain scaling relations with τ and σ exactly same as those of original percolation. Hence, the critical exponents would satisfy certain scaling relations among them, such as:

$$\delta = 2\gamma + \beta \quad \text{and} \quad \eta = 2\delta - \gamma. \tag{2.18}$$

Below we present numerical estimates of these cluster properties and verify the scaling relations.

2.6 Order parameter

In the percolation transition, the order parameter P_∞, the probability that a site belongs to an infinite (spanning) cluster, is given by

$$P_\infty = \frac{S_{\max}}{L^2} \tag{2.19}$$

where $S_{\max}$ is the size of the spanning cluster and L is the system size. As given in the previous section, it can also be obtained in terms of the first moment of the cluster size distribution function $n_s(\rho, g)$. The definition of P_∞ and its scaling for $g \geq g_c$ is given as

$$P_\infty = \rho + g(1-\rho) - \sum_s{}' s n_s(\rho, g) \sim [(g - g_c)(1-\rho)]^\beta \tag{2.20}$$

where the primed sum indicates that the spanning cluster is excluded from the sum and β is the order parameter exponent.

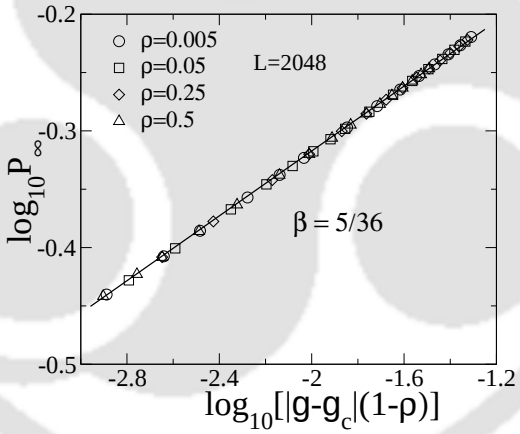

Figure 2.6: Plot of P_∞ versus $[|g - g_c|(1-\rho)]$ for $g > g_c(\rho)$ for four different ρ values 0.005(◯), 0.05(□), 0.25(◇) and 0.5(△) and for $L = 2048$. The solid lines represent the best fits through the data points.

For the system size $L = 2048$, P_∞ is estimated for several values of g above $g_c(\rho)$ respectively for different values of ρ. In Fig. 2.6, P_∞ is plotted against $[|g-g_c|(1-\rho)]$ for $g > g_c(\rho)$ for $\rho = 0.005$ (circles), 0.05 (squares), 0.25 (diamonds), 0.5 (triangles) for lattice size $L = 2048$. It can be seen that P_∞ obeys the power law scaling as in Eq.2.20. Hence the order parameter exponent β can be estimated independently. The exponent β is determined by linear least square fit through the data points and it is found to be $\beta \approx 0.1398 \pm 0.0003$ as that of percolation (5/36). The solid line is drawn guide to eye with slope 5/36 in these figures. It can be also seen that all

the curve for different ρ collapses into a single curve. Therefore, the scaling of P_∞ in terms of ρ and g in Fig. 2.6 shows almost same magnitudes. The existence of power law scaling and finite value of $\beta > 0$ indicate that the transition studied here continuous or second order rather than discontinuous or first-order.

2.7 Moments of cluster size distribution and Correlation length

The average cluster size χ_2, the second moment of the cluster size distribution $n_s(\rho, g)$, is the average number of occupied lattice sites in a cluster, generated at a given site occupation probability g. The definition of χ_2 and two other higher moments χ_3 and χ_4 are given below

$$\chi_2 = \sum_s{}' s^2 n_s(\rho, g) \sim |(g - g_c)(1 - \rho)|^{-\gamma} \tag{2.21}$$

$$\chi_3 = \sum_s{}' s^3 n_s(\rho, g) \sim |(g - g_c)(1 - \rho)|^{-\delta} \tag{2.22}$$

$$\chi_4 = \sum_s{}' s^4 n_s(\rho, g) \sim |(g - g_c)(1 - \rho)|^{-\eta} \tag{2.23}$$

which are also given in section 2.5, γ, δ and η are corresponding exponents.

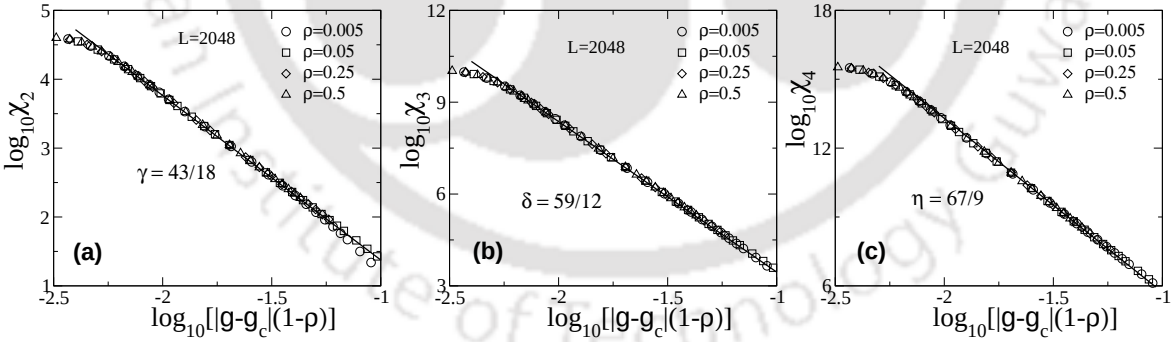

Figure 2.7: Plot of second, third and fourth moments, χ_2 in (a), χ_3 in (b) and χ_4 in (c) against $[|g - g_c|(1 - \rho)]$ for $g < g_c(\rho)$ for four different ρ values $0.005(\bigcirc), 0.05(\square), 0.25(\diamond)$ and $0.5(\triangle)$ for $L = 2048$. The solid lines represent the best fits through the data points.

The values of the critical exponents γ, δ and η are estimated studying the scaling behaviour of χ_2, χ_3 and χ_4 on the square lattice of linear size $L = 2048$ at different values of g. In Fig. 2.7(a) for χ_2, Fig. 2.7(b) for χ_3 and Fig. 2.7(c) for χ_4 are plotted against $[|g - g_c(\rho)|(1 - \rho)]$ for $g < g_c(\rho)$ and for $\rho = 0.005$ (circles), 0.05 (squares), 0.25 (diamonds), 0.5 (triangles). It can be seen that χ_2 and the other moments of

average cluster size obey power law scaling as in Eq.2.21, Eq.2.22 and Eq.2.23. The exponent values are then obtained from the respective linear least square fit slopes as $\gamma = 2.379 \pm 0.003$, $\delta = 4.878 \pm 0.004$ and $\eta = 7.385 \pm 0.004$ as that of percolation ($\gamma = 43/18$, $\delta = 59/12$ and $\eta = 67/9$ respectively). The solid lines are drawn guide to eye with slope 43/18 in Fig. 2.7 (a), 59/12 in Fig. 2.7 (b) and 67/9 in Fig. 2.7 (c) as that of original percolation of these figures. The magnitudes of χ_2, χ_3 and χ_4 are independent on ρ for given L according to the scaling in terms of ρ and g in Fig. 2.7(a), (b) and (c).

In percolation, system has clusters of all possible sizes, starting from single sited cluster to system size at critical point g_c. The linear size of the finite clusters, below and above p_c, is characterized by correlation length ξ. Here ξ is defined as the root mean square distance between two sites on the same finite cluster and averaged over all finite clusters and given by

$$\xi^2 = \frac{2\sum_s{}' R_s^2 s^2 n_s(p)}{\sum_s{}' s^2 n_s(p)}, \tag{2.24}$$

where R_s is the radius of gyration of a cluster. Due to the appearance of large finite clusters at the critical point, the correlation length diverges as $g \to g_c$ with an exponent ν given by

$$\xi \sim [(g - g_c)(1 - \rho)|^{-\nu}. \tag{2.25}$$

Using the scaling relation in Eq.2.6, we determined the value of $1/\nu$ for different ρ as 0.75, shown in Fig. 2.4. Therefore, the value of $\nu \approx 1.33$ as that of OP (4/3). However, the values of ν obtained following the scaling in Eq.2.25 are found to be slightly lesser than expected.

2.8 Fractal dimension and hyper-scaling

Since the clusters are grown here applying PBC, the horizontal and vertical extensions of the largest cluster is kept stored. If either the horizontal or the vertical extension of the largest cluster is found to be $\geq L$, it is identified as a spanning cluster. The percolation spanning cluster is a random object with all possible holes in it and is expected to be fractal. For system size $L \ll \xi$, the mass of the spanning cluster varies with the system size L as

$$S_{\max} \approx L^{d_f} \tag{2.26}$$

where d_f is the fractal dimension of the spanning cluster. The values of $S_{\max}$ are noted at the estimated thresholds $g = g_c(\rho)$ for several lattice sizes L as well as for different values of ρ and they are scaled with L according to the Eq.2.26. The percolation spanning cluster is a random object with all possible sizes of holes in it and is expected to be fractal $d_f < d$ for a continuous percolation transition whereas it becomes compact $d_f = d$ in the case of a discontinuous transition, where d is the space dimension. Hence, the values of $S_{\max}$ are plotted against L in double logarithmic scales in Fig. 2.8(a) for four different $\rho = 0.005$(circles), 0.05 (squares), 0.25 (diamonds) and 0.5 (triangles). The values of d_f are estimated by linear least square fit through the data points. It is found that $d_f = 1.896 \pm 0.002$[38]. The value of d_f agrees well with the value for original 2d percolation, *i.e.*, $d_f = 91/48$[11]. It is also interesting to note that the absolute values of these quantities are independent of the initial seed concentration ρ.

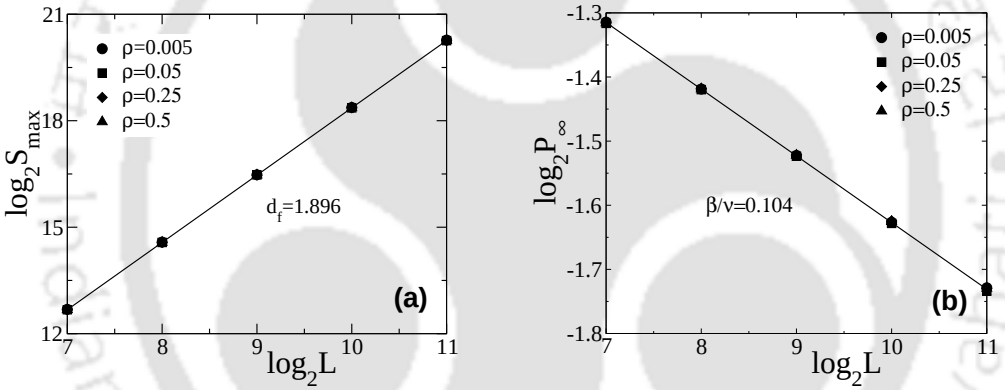

Figure 2.8: Plot of $S_{\max}$ in (a) and P_∞ in (b) against lattice sizes L at their respective thresholds $g_c(\rho)$ for four different values of $\rho = 0.005(\bigcirc)$, $0.05(\square)$, $0.25(\diamond)$ and $0.5(\triangle)$. The fractal dimension d_f= 1.896 and the ratio of critical exponents $\beta/\nu = 0.104$ are estimated from the slope of the straight line and found to be independent of ρ.

P_∞ are also measured at $g = g_c(\rho)$ for different values of the system size L. At $g = g_c(\rho)$, the scaling form of P_∞ is expected to be $P_\infty(\rho, g, L) \approx L^{-\beta/\nu}$. P_∞ is plotted against L for same set of ρ values in Fig. 2.8(b). It can be seen that it follows the respective scaling behaviour with exponent $\beta/\nu = 0.104$. The ratio of the exponents again confirms the percolation exponents. It is also interesting to note that the absolute values of P_∞ are independent of the initial seed concentration ρ.

A scaling relation between d_f and the order parameter exponent can be obtained via the correlation length exponent ν. In a d-dimensional lattice, the order parameter is given by

$$P_\infty = \frac{S_{\max}}{L^d} = L^{-(d-d_f)}, \tag{2.27}$$

as $S_{\max} \approx L^{d_f}$. Since as the criticality is approached, the order parameter P_∞ and the correlation length ξ, which is of the order of L at $g = g_c$, scales as

$$P_\infty \sim [(g - g_c)(1 - \rho)]^\beta \quad \text{and} \quad L = \xi \sim [(g - g_c)(1 - \rho)]^{-\nu}, \tag{2.28}$$

one obtains a scaling relation

$$d - d_f = \beta/\nu. \tag{2.29}$$

The scaling relation is exactly satisfied here from the measured values of fractal dimension $d_f = 1.896$ and the critical exponents $\beta/\nu = 0.104$.

2.9 Verification of Cluster size distribution

For a given ρ, the cluster size distribution $n_s(\rho, g)$ is expected to obey a power law scaling behaviour at $g = g_c$. As per Eq.2.13 in section 2.5, it is given by

$$n_s(\rho, g_c) \approx s^{-\tau} \tag{2.30}$$

where τ is an exponent and it is assumed that $\widetilde{n}_s(0)$ is a constant. For a system size $L = 2048$, $n_s(\rho, g_c)$s are obtained for four different values of $\rho = 0.005$ (circles), 0.05 (squares), 0.25 (diamonds), 0.50 (triangles). The distributions are plotted in Fig. 2.9(a). The distributions are found to obey power law scaling with an exponent $\tau = 2.055$ ($\approx 187/91$) as that of original percolation as indicated by the solid line. It is also interesting to note that the probability of occurrence of a cluster size at the respective threshold values for different ρ are almost same. Therefore, the existence of power law scaling of the cluster size distribution with percolation exponents indicate that the transition studied here continuous or second order percolation transitions.

The scaling function form of $n_s(\rho, g)$ can be verified by plotting $n_s(\rho, g)/n_s(\rho, g_c)$ against the scaled variable $[(g - g_c)(1 - \rho)s^\sigma]$. In Fig. 2.9(b), data for two different values of $\rho = 0.05$ (in red) and for $\rho = 0.25$ (in blue) at different growth probabilities $g < g_c$ and $g > g_c$ on a lattice of size $L = 2048$. If $\widetilde{n}_s(0)$ is a constant, it is expected that the plot of $n_s(\rho, g)/n_s(\rho, g_c)$ against the scaled variable $[(g - g_c)(1 - \rho)s^\sigma]$ for different values of g, ρ and s should collapse onto a single curve for the right value of the exponent σ. For $\sigma = 0.4$, it can be seen that a good data collapse is observed irrespective of the values of g, ρ or s. Thus the value of σ taken here (approximately the same value of σ of percolation) is right and the scaling form assumed for $n_s(\rho, g)$ is a correct one.

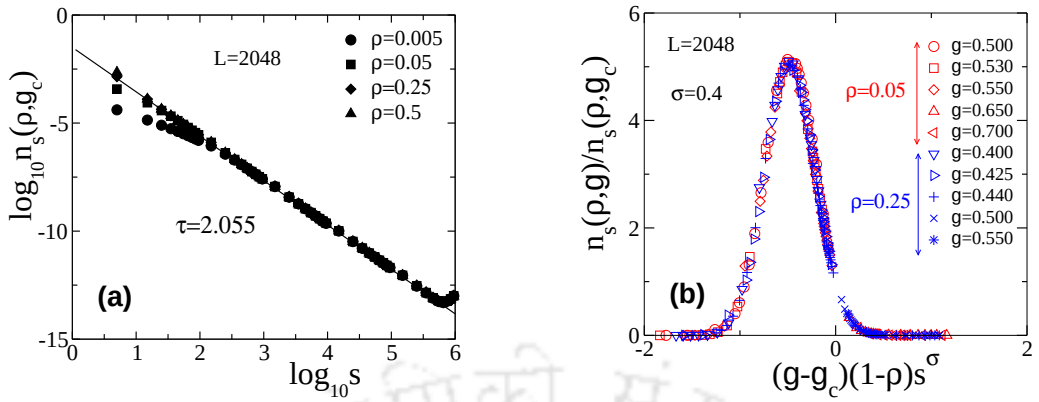

Figure 2.9: (a) Plot of cluster size distribution per lattice site $n_s(\rho, g)$ against s at g_c for four different values of ρ: $0.005(\bigcirc), 0.05(\square), 0.25(\diamond), 0.50(\triangle)$ for the lattice size $L = 2048$. The exponent τ is found to be 2.055. (b) Plot of $n_s(\rho, g)/n_s(\rho, g_c)$ against $[(g - g_c)(1 - \rho)s^{\sigma}]$ taking $g = 0.500(\bigcirc)$, $0.530(\square)$, $0.550(\diamond)$, $0.650(\triangle)$, $0.700(\triangleright)$ in red for $\rho = 0.05$ and taking $g = 0.400(\triangledown)$, $0.425(\triangleleft)$, $0.440(+)$, $0.500(\times)$, $0.550(*)$ in blue for $\rho = 0.25$ on a lattice size $L = 2048$. For $\sigma = 0.4$, a good data collapse is obtained for both the ρ values.

2.10 Conclusion

A new two-parameter percolation model (TPPM) of simultaneous multiple cluster growth is developed. The model would have extended parameter space than that of the original percolation model. The TPPM is studied extensively numerically on several finite lattices. In this model, two tunable parameters are the initial seed concentration ρ and the cluster growth probability g. It is found that for each ρ there exists a critical growth probability g_c at which a continuous percolation transition occurs. A scaling theory for such percolation transition involving ρ and g is proposed and verified numerically. It is found that the values of the critical exponents describing the scaling functions at the criticality are that of the original percolation for all values of ρ. Hence, all such transitions belong to the same universality class of percolation. A phase line consisting of second order phase transition points is found to separate the connected region from the disconnected region in the $\rho - g$ parameter space. No discontinuous percolation transition is found may be because of the fact that the partial hindrance remains a weak effect in comparison to an overall random growth process.

Chapter 3

Suppressed growth percolation model: A finite size scaling theory

As no discontinuous transition is found to occur in the case of the constant growth two parameter percolation model (TPPM), it is worth introducing a suppression mechanism to control the growth of the larger clusters over the smaller clusters. In this chapter, the constant growth TPPM is then modified to a suppressed cluster growth model in which smaller clusters will have higher growth probability than larger clusters present at a given time. The model incorporates nucleation and growth of multiple finite clusters simultaneously under two tunable parameters, the initial seed concentration ρ and a growth parameter g as in TPPM. In one hand, the introduction of an extra parameter will enhance the parameter space of the percolation model and could be useful in locating the tricritical point if any. On the other hand, the dynamic growth probability which prefers growth of clusters of smaller sizes over the clusters of larger sizes would lead to a correlated cluster growth beside partial hindrance by simultaneous growth of other clusters as in constant growth model. As in original percolation (OP) and unlike any growth models, the percolation transition (PT) in this model is determined by the final static or equilibrium spanning cluster configurations. It is intriguing to study the effect of the suppression of the growth of the larger clusters on the critical properties as well as on the nature of percolation transitions in the enhanced parameter space of the model.

The details of the model will be described below. A finite size scaling (FSS)

This chapter is based on the Ref.[147]; Bappaditya Roy and S. B. Santra, Physica A: Statistical Mechanics and its Applications, to appear.

theory will be developed and will be verified numerically. Since the model is an extension of the constant growth model, the FSS properties of suppressed growth model will always be compared with that the constant growth model.

3.1 Model and simulation

The model, TPPM, is developed on a square lattice of size $L \times L$ in 2-dimensions (2d). The initial configuration is taken as a partially randomly populated lattice with an initial seed concentration ρ less than the site percolation threshold on the square lattice, ≈ 0.592746 [11] and the cluster size distribution is obtained employing the Hoshen-Kopelman algorithm [141]. The process of nucleation and growth is then implemented by growing all these finite clusters simultaneously with an instantaneous cluster size s dependent growth probability $g_s(t)$. Note that there are now multiple growth centers instead of a single one as in Leath's [142] algorithm of generating percolation clusters. Time is equivalent to a Monte Carlo (MC) step in which perimeter sites of all individual clusters are called once for occupation with an appropriate probability. At any instant t, $g_s(t)$ for a cluster of size s_t is given by

$$g_s(t) = g \exp\left[-\frac{(s_t - 1)}{a(t)}\right]; \quad a(t) = \sum_{i=1}^{N(t)} s_t^{(i)} \tag{3.1}$$

where $N(t)$ is the number of clusters present, $a(t)$ is the the total number of occupied sites at time t and g is the growth parameter, a constant between $[0, 1]$. In this algorithm, the smaller clusters have higher growth probability than the larger cluster at any Monte Carlo (MC) step. In a MC step, the clusters are grown sequentially, starting from the smallest cluster. Once a site is rejected with probability $[1 - g_s(t)]$, the site remains unoccupied throughout the growth process, as in the original percolation model. As soon as all the clusters present at that time are allowed to grow one layer of nearest neighbour (NN) perimeter sites, the MC time step is increased by one and the cluster size distribution is updated. During the growth of these clusters, two clusters may come in contact. Two clusters with occupied perimeter sites separated by a single lattice spacing are considered to be a single cluster. The total number of clusters is then reduced by one and a cluster of larger size is incorporated in the cluster size distribution. The growth probability $g_s(t)$ is recalculated as per the new cluster size distribution. As the growth process seized due to unavailability of empty NN perimeter sites of any cluster for occupation, the

final static cluster size distribution is obtained to analyze PT, unlike the process of collecting cluster size distributions during the growth process as in the explosive percolation (EP)[27,103]. Hence, the final cluster size distribution function $n_s(\rho, g)$ is obtained.

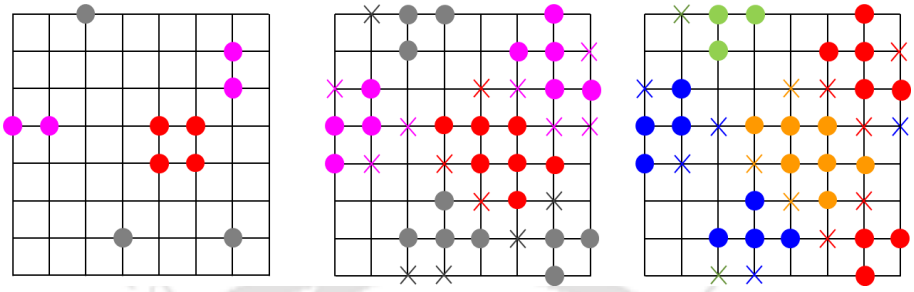

Figure 3.1: Presentation of one MC step of the suppressed growth process. Figure (a) represents the initial configuration, figure (b) represents the growth and figure (c) represents merging and relabeling. The occupied sites are presented by filled coloured circles. The largest cluster is shown in red and other smaller clusters are in different colours. The crosses represent the rejected sites. PBC is applied in both the directions in growing the clusters.

The growth process is demonstrated in Fig. 3.1 generating clusters on a 8×8 square lattice in 2d. A random initial configuration is taken to demonstrate one MC step. The initial configuration in Fig. 3.1(a) contains three single-sited, two two-sited and one four-sited clusters and are shown in different colors. The largest cluster is always shown in red. The value of the growth parameter g is taken to be 0.5. The growth of the clusters are presented in Fig. 3.1(b). Periodic boundary conditions (PBC) are applied in both the directions. The growth probability $g_s(t)$ is estimated for each cluster according to their sizes. Note that in the case of constant growth, the growth probability remains same (g) for all the clusters. The newly occupied sites are shown in the same color of the respective cluster. The crosses on the perimeter of a cluster indicate the rejected sites. In Fig. 3.1(c), the merging of the clusters are shown. Here, two small clusters (magenta and grey) merged to a single largest cluster (in red) without generating any spanning cluster yet. Beside, suppression of growth, it can be seen that the growth of a cluster is also hindered by the presence of the other clusters and their rejected neighbours as in the constant growth model.

The model has two limiting situations equivalent to OP as in the constant growth model. The present model can be considered as a generalized multiple cluster growth model of percolation with varying growth probability. In the following, taking in-

termediate values of ρ and varying the growth parameter g, transition from disconnected phase to fully connected phase is studied following an FSS theory.

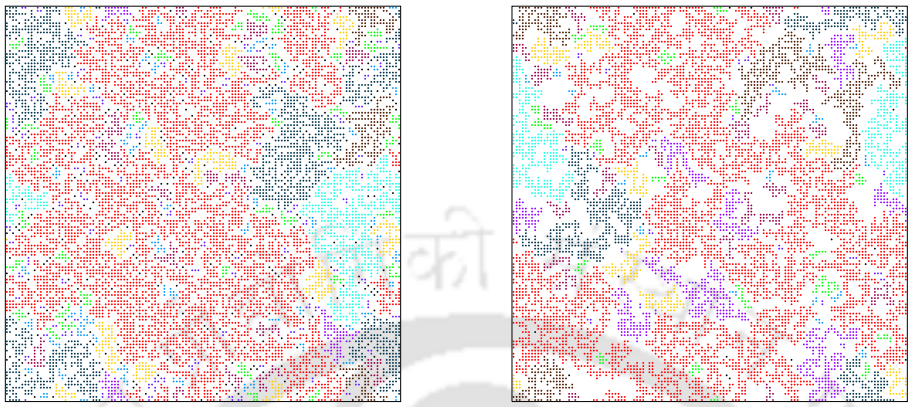

(a) $\rho = 0.5$, $g_c = 0.158$ (b) $\rho = 0.05$, $g_c = 0.565$

Figure 3.2: Snapshots of cluster configurations at the end of the growth process on a 2d square lattice of size $L = 128$ with initial seed concentration $\rho = 0.5$ (a) and 0.05 (b) at their respective percolation thresholds $g_{0c}(L) = 0.158$ & 0.565. Solid line represents the lattice boundary. The different colors indicate clusters of different sizes. The spanning clusters are shown in red.

3.2 Cluster morphology

Snapshots of the system morphology at the end of the growth process on a 2d square lattice of size $L = 128$ with initial seed concentrations $\rho = 0.5$ and 0.05 are shown in Figs. 3.2(a), (b) for their respective thresholds $g_c(L) = 0.158$ & 0.565. In these snapshots, the spanning clusters are shown in red, other clusters of different sizes are indicated in various different colors. White space corresponds to the inaccessible lattice sites. It can be noticed that at the high ρ inaccessible area is less than that at small ρ. Besides, the inaccessible area becomes more prominent than the previous constant growth model for $\rho = 0.05$ in 3.2(b). It should also be noted that the critical growth probability $g_c(L)$ increase as ρ decreases, in which smaller clusters grow with higher probability than the larger clusters. In both the ρ, enclave of smaller clusters inside larger clusters is an increasingly rare event at smaller values of ρ which seems to be an indication of departure from continuous transition[49]. At smaller ρ, the finite clusters are grown with higher growth probability that leads to more compact clusters than the higher values of ρ. It is then intriguing to characterize the PT especially at smaller values of ρ.

3.3 Finite size scaling

The singularities of cluster related quantities that occur at the critical point in the second order phase transitions are generally described by power laws and characterized by well defined critical exponents in the thermodynamic limit of the system size ($L \to \infty$). In a finite system, there is rounding off and shifting of critical singularities depending on the ratio of correlation length ξ to the linear size L of the system. Since in numerical simulation only lattices of finite sizes are used, it might happen that the values of the critical exponents are not free from finite size effect. An FSS theory for TPPM is developed following the techniques of original percolation[11,148,149]. A system is said to be finite if its size L is less than the correlation length ξ. As the growth parameter g is the control parameter here, a geometrical quantity Q is expected to scale as

$$Q \sim |(g - g_c(\rho))|^{-q} \tag{3.2}$$

for a system of size $L \gg \xi$, then the finite size scaling form of Q for the system size $L \ll \xi$ is expected to be

$$Q(\rho, g, L) = L^{q/\nu} \widetilde{Q}[\{g - g_c(\rho)\} L^{1/\nu}] \tag{3.3}$$

where q is an exponent, $\widetilde{Q}$ is a scaling function and ν is the correlation length exponent. Below we develop the FSS forms of the order parameter P_∞, its distribution $P(P_\infty)$ and fluctuation in order parameter χ_∞.

The order parameter, the probability to find a lattice site in the spanning cluster, is given by

$$P_\infty = S_{\max}/L^2, \tag{3.4}$$

where $S_{\max}$ is the size of the spanning cluster. As per Eq.3.3, the FSS form of P_∞ is expected to be

$$P_\infty = L^{-\beta/\nu} \widetilde{P}_\infty[(g - g_c) L^{1/\nu}], \tag{3.5}$$

where $\widetilde{P}_\infty$ is a scaling function, β is the order parameter exponent, ν is the correlation length exponent, and g_c is the critical value of g at which a spanning cluster connecting the opposite sides of the lattice appears for the first time and below which no percolation transition occurs. At the threshold, the size of the spanning

cluster $S_{\max}$ scales with lattice size L as

$$\langle S_{\max} \rangle \approx L^{d_f}, \tag{3.6}$$

where $d_f = d - \beta/\nu$ is the fractal dimension of the spanning cluster. Following the formalism of thermal critical phenomena[150], the distribution of P_∞ is taken as

$$P(P_\infty) = L^{\beta/\nu} \widetilde{P}[P_\infty L^{\beta/\nu}], \tag{3.7}$$

where $\widetilde{P}$ is a scaling function. Such a distribution was also used recently in the context of EP[53]. With such a scaling form of $P(P_\infty)$, one could obtain $\langle P_\infty \rangle$ and $\langle P_\infty^2 \rangle$ as

$$\begin{aligned} \langle P_\infty \rangle &= \int P_\infty P(P_\infty) dP_\infty = \int P_\infty L^{\beta/\nu} \widetilde{P}[P_\infty L^{\beta/\nu}] dP_\infty \\ &= L^{-\beta/\nu} \int z \widetilde{P}[z] dz \end{aligned} \tag{3.8}$$

and

$$\begin{aligned} \langle P_\infty^2 \rangle &= \int P_\infty^2 P(P_\infty) dP_\infty = \int P_\infty^2 L^{\beta/\nu} \widetilde{P}[P_\infty L^{\beta/\nu}] dP_\infty \\ &= L^{-2\beta/\nu} \int z^2 \widetilde{P}[z] dz \end{aligned} \tag{3.9}$$

where $z = P_\infty L^{\beta/\nu}$ is a scaled variable. As the integrals in both the cases would contribute certain constants, one has

$$\langle P_\infty \rangle \sim L^{-\beta/\nu} \quad \text{and} \quad \langle P_\infty^2 \rangle \sim L^{-2\beta/\nu}. \tag{3.10}$$

The fluctuation in P_∞ is defined as

$$\chi_\infty = \frac{1}{L^2}[\langle S_{max}^2 \rangle - \langle S_{max} \rangle^2] = L^2[\langle P_\infty^2 \rangle - \langle P_\infty \rangle^2] \sim L^{2-2\beta/\nu}, \tag{3.11}$$

on a 2d lattice. Hence, at the threshold, the fluctuation χ_∞ would scale as

$$\chi_\infty \sim L^{d-2\beta/\nu}, \tag{3.12}$$

on a d-dimensional lattice. AS $\gamma/\nu = d - 2\beta/\nu$, the FSS form of χ_∞ is then given by

$$\chi_\infty = L^{\gamma/\nu} \widetilde{\chi}[(g - g_c) L^{1/\nu}], \tag{3.13}$$

where γ is the exponent that describes the singularity of average size of the finite clusters and $\widetilde{\chi}$ is a scaling function. Studying the FSS form of χ_∞, the values of the critical thresholds $g_c(L)$ and that of γ/ν are now estimated.

3.4 Results and discussions

An extensive computer simulation has been performed on 2d square lattices of size $L \times L$ varying L from 2^7 to 2^{11}, in multiple of 2. For a given L, the initial seed concentration ρ is varied from 0.025 to 0.59, close to percolation threshold of OP, whereas the growth parameter g vary from 0 to 1 for each ρ. In growing the clusters, PBC is applied in both the directions. Data are averaged over 5×10^4 to 10^6 ensembles for each parameter set. The fluctuation in order parameter will be considered first to identify the percolation thresholds, then the scaling of the spanning cluster and the order parameter will be studied. The order of transition will be verified by the estimates of Binder cumulant, cluster size distribution, and distribution of the order parameter.

3.4.1 FSS of χ_∞

Percolation threshold: The percolation threshold is estimated from the variation of fluctuation of order parameter χ_∞ as a function of growth parameter g for the different values of L and ρ. In Figs. 3.3, χ_∞/L^2 is plotted against the growth parameter g for different values of L and for $\rho = 0.5$, $\rho = 0.05$ for the constant growth [Fig. 3.3(a) and Fig. 3.3(b)] and for the correlated growth [Fig. 3.3(c) and Fig. 3.3(d)]. For each L, the plot has a maximum corresponding to a critical growth parameter g_c at which the percolating spanning cluster appears for the first time. The values of the g_c are marked on g axis by crosses. The critical growth parameter $g_c(L)$ of a finite system of size L is expected to scale with the system size L as

$$g_c(L) - g_c(\rho) \approx L^{-1/\nu} \tag{3.14}$$

where $g_c(\rho)$ is the critical threshold of the system in the limit $L \to \infty$ and ν is the correlation length exponent. In the inset of each plot of Figures 3.3, variation of $g_c(L)$ is plotted against $L^{-1/\nu}$ taking $1/\nu = 0.75$ as that of OP. A definite $g_c(\rho)$ is identified as 0.1855 ± 0.0001 for $\rho = 0.5$ [Fig. 3.3(a)], 0.5713 ± 0.0001 for $\rho = 0.05$ [Fig. 3.3(b)] for constant growth and 0.1856 ± 0.0002 for $\rho = 0.5$ [Fig. 3.3(c)] for correlated growth. Whereas for $\rho < 0.2$, no definite $g_c(\rho)$ is found in the correlated

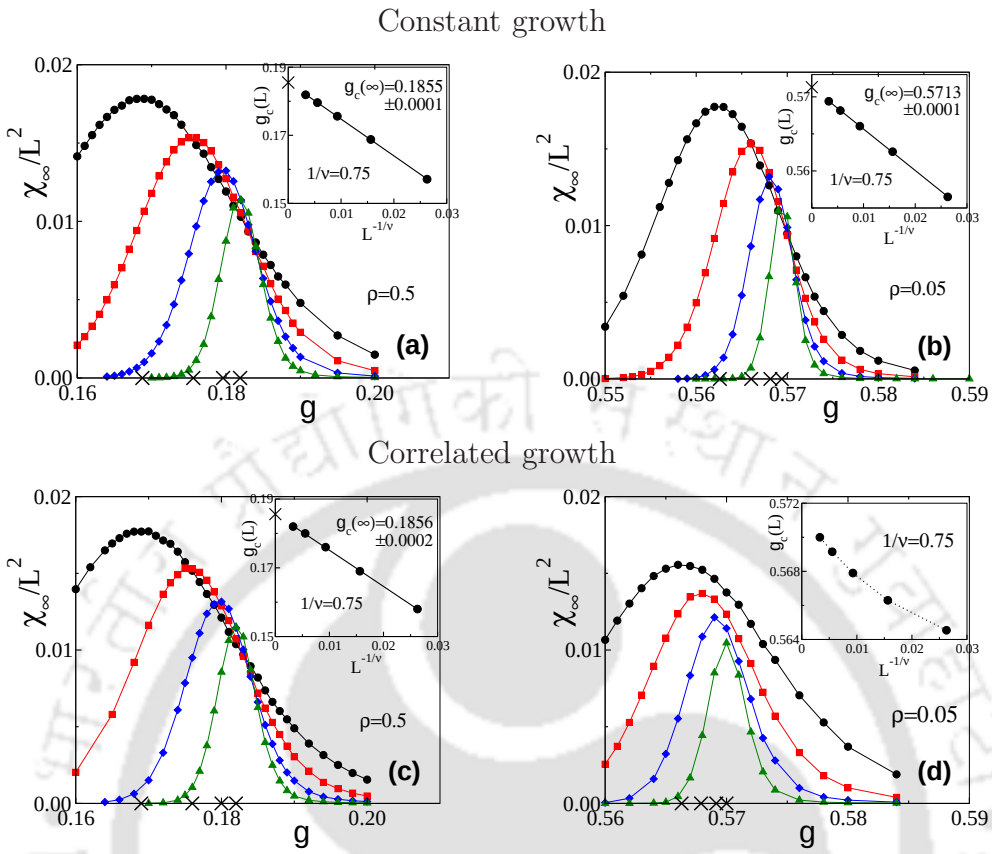

Figure 3.3: Plot of χ_∞/L^2 against g for $\rho = 0.5$ & 0.05 in (a) & (b) for the constant growth and in (c) & (d) for the correlated growth. Different lattice sizes taken are $L = 256(\bigcirc)$ in black, $512(\square)$ in red, $1024(\diamond)$ in blue and $2048(\triangle)$ in green. Crosses on the g-axis represents the thresholds $g_c(L)$. In the inset of each plot, $g_c(L)$s are plotted against $L^{-1/\nu}$ taking $1/\nu = 0.75$.

growth model at the limit $L \to \infty$, as shown in the inset of Fig. 3.3(d) for $\rho = 0.05$ taking $1/\nu = 0.75$. The value of $1/\nu$ agrees well with the value of original 2d percolation, *i.e.*, $1/\nu = 3/4$ for the constant growth as well as for the correlated growth with higher ρ.

Phase diagram: The thresholds $g_c(\rho)$ (or $g_c(L)$) are obtained for several other values of ρ. A phase diagram in the $\rho - g$ parameter space is constructed by plotting the values of g_c against ρ in Fig. 3.4(a) for the correlated growth model. The black circles represent $g_c(\rho)$ for $\rho \geq 0.2$ and red squares are $g_c(L)$ for $\rho < 0.2$ of $L = 2048$, as there are not any definite $g_c(\rho)$. The points constitute a phase line that separates the phase space into percolating and non-percolating regions. The line of continuous phase transitions terminates at two trivial critical points as indicated in the model. The phase line does not follow the Eq.2.8, which is implemented in the previous

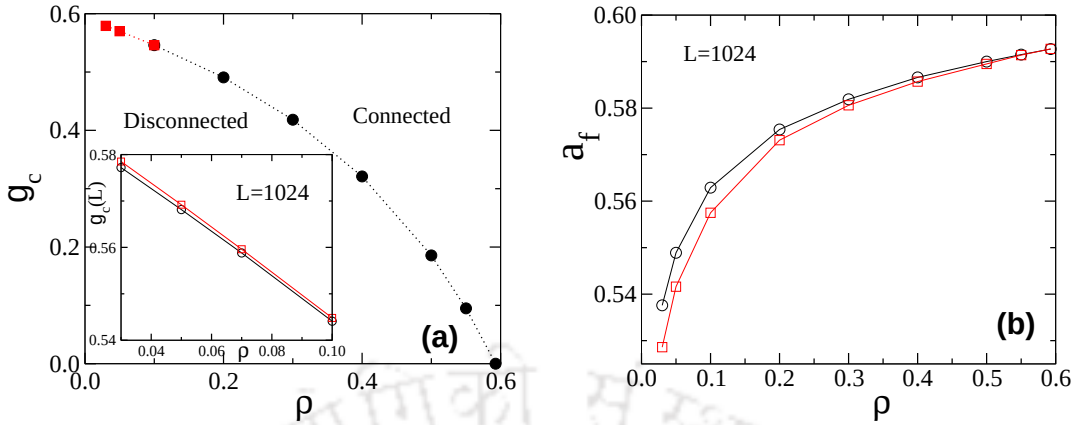

Figure 3.4: (a) Plot of g_c against ρ for the correlated growth. The black circles represent $g_c(\rho)$ and red squares are $g_c(L)$ of $L = 2048$, as there are not any definite $g_c(\rho)$. The phase line separates the connected phase from the disconnected phase. In the inset of Fig. (a), plot of $g_c(L)$ against ρ and in Fig. (b) plot of the area fraction, a_f against ρ for the constant growth (◯) (black solid line) and for the correlated growth (□) (red solid line) at their respective thresholds for $L = 1024$.

chapter in the $\rho \to 0$ limit. In the inset of Fig. 3.4(a), the deviation in $g_c(L)$ from that of the constant growth is shown for $\rho \leq 0.1$ for a system of size $L = 1024$. It can be seen that $g_c(L)$ is slightly higher in the correlated growth (red squares) than that of constant growth model (black circles). For $L = 1024$, the variation of actual area fraction a_f with ρ at their respective thesholds, is shown in Fig. 3.4(b) for both the models. Not only a_f decreases from OP critical threshold as ρ decreases from ≈ 0.59274 but also it is always lower for the correlated growth (red squares) than that of the constant growth (black circles).

Exponent γ/ν: The maximum values of fluctuation, $\chi_\infty(\max)$, are estimated at $g_c(L)$ for several systems sizes L as well as for different values of ρ and they are plotted against L in double logarithmic scales in Fig. 3.5(a) and Fig. 3.5(b) for the constant growth and for the correlated growth respectively. It can be seen that they follow the scaling behavior in Eq.3.13: $\chi_\infty(\max) \sim L^{\gamma/\nu}$. The values of γ/ν are estimated by linear least square fit through the data points. For the constant growth, it is found that $\gamma/\nu = 1.79 \pm 0.01$. Not only the absolute values of $\chi_\infty(\max)$ are independent of the initial seed concentration ρ but also the value of the exponent γ/ν in the case of constant growth remain same as that of OP, 43/24, as well as that of the random multi-cluster growth model by Melchert *et al.*[151]. Hence, the transitions under constant growth are continuous and belong to the same universality class of OP. Therefore the partial hindrance due to the presence of other clusters in

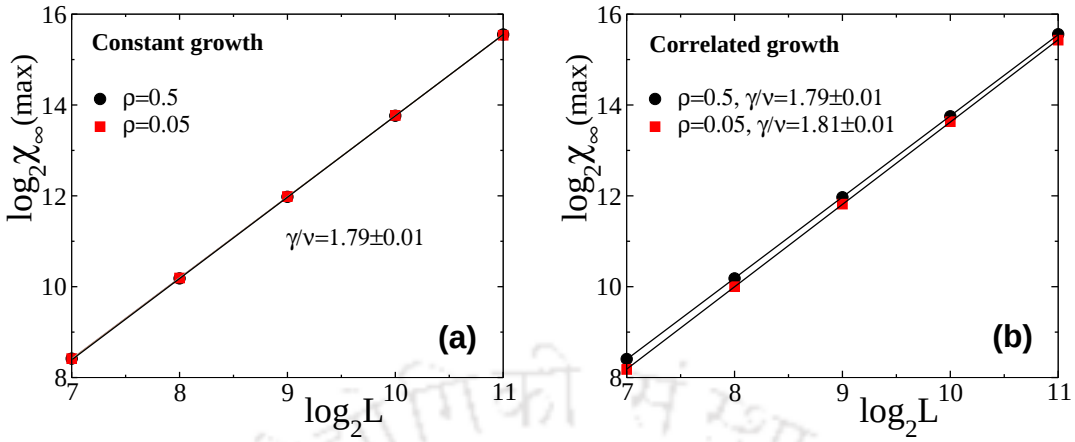

Figure 3.5: Plot of $\chi_\infty(\max)$ against L at their respective thresholds $g_c(L)$ for two different values of $\rho = 0.5(\bigcirc)$ in black and $0.05(\square)$ in red for the constant growth in (a) and for the correlated growth in (b). Solid lines correspond to linear least square fit through the data points.

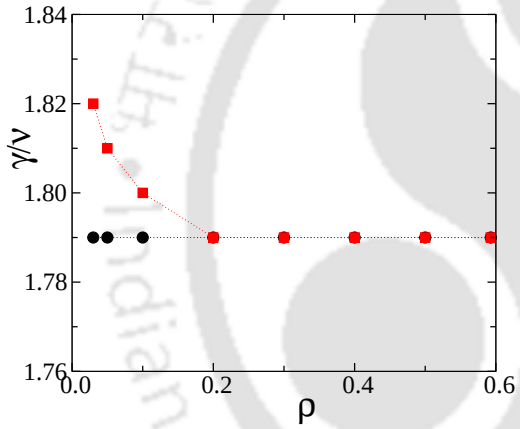

Figure 3.6: Plot of the variation of critical exponents γ/ν against ρ. Black circles represent the percolation exponents and red squares are obtained values of exponents for given ρs.

the system plays no role on the critical properties of the system. On the other hand, for the correlated growth, shown in Fig. 3.5(b), it is found that $\gamma/\nu = 1.79 \pm 0.01$ for $\rho = 0.5$ as that of OP and $\gamma/\nu = 1.81 \pm 0.01$ for $\rho = 0.05$. Not only the values of the exponents but also the absolute values of $\chi_\infty(\max)$ are found to depend on the initial seed concentration ρ. The values of γ/ν are deviated continuously from the percolation value 1.79 as the initial seed concentration decreases from $\rho = 0.2$. The variation of γ/ν for both the models over a wide range of ρ is shown in Fig. 3.6. The suppression of the growth of the larger clusters then has a weak effect on the critical properties of the system in the dilute limit of ρ but not strong enough to change the order of transition.

Verification of FSS form: The FSS form of χ_∞ from, Eq.3.13, is verified in Fig. 3.7(a) and Fig. 3.7(c) for the constant growth and the correlated growth respectively

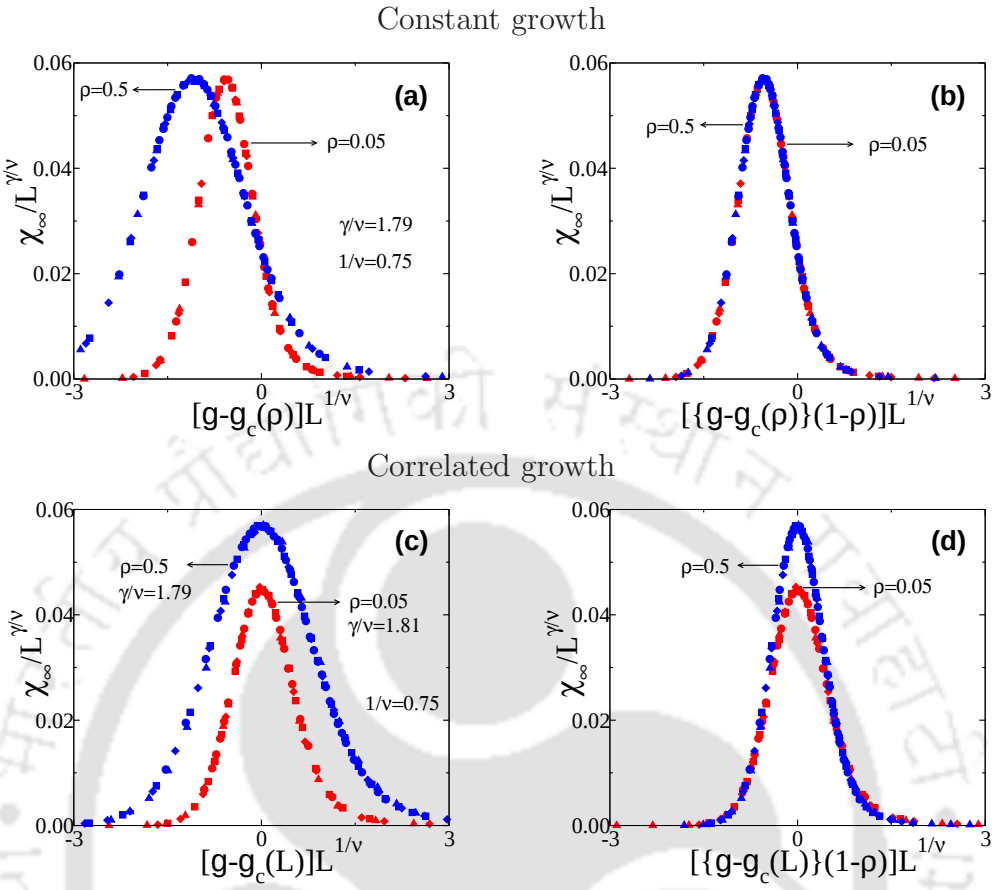

Figure 3.7: Plot of $\chi_\infty/L^{\gamma/\nu}$ against $[g-g_c(\rho)]L^{1/\nu}$ in (a) for the constant growth and $[g-g_c(L)]L^{1/\nu}$ in (c) for the correlated growth for $\rho = 0.5$ (blue) and 0.05 (red) for the same set of L of Fig. 3.3. A good data collapse is obtained for the respective values of γ/ν taking $1/\nu = 0.75$ for both the growth processes. Plot of $\chi_\infty/L^{\gamma/\nu}$ against $[\{g-g_c(\rho)\}(1-\rho)]L^{1/\nu}$ in Fig. (b) for the constant growth and against $[\{g-g_c(L)\}(1-\rho)]L^{1/\nu}$ in Fig. (d) for the correlated growth. A good data collapse is obtained for the constant growth (b) whereas no such collapse is obtained for the correlated growth (d).

for two different values of $\rho = 0.5$ (blue) and 0.05 (red). For the constant growth, in Fig. 3.7(a), $\chi_\infty/L^{\gamma/\nu}$ is plotted against the scale variable $[g-g_c(\rho)]L^{1/\nu}$ whereas for the correlated growth, in Fig. 3.7(c), it is plotted against $[g-g_c(L)]L^{1/\nu}$ taking the respective values of γ/ν and $1/\nu = 0.75$ for both the cases. The collapses of data are found to be good for all values of ρ and that confirm the values of the critical exponents. Furthermore, incorporating the relation of ρ and g in Eq.2.8, the modified FSS form of χ_∞ in terms of L, g and ρ is given by

$$\chi_\infty = L^{\gamma/\nu}\widetilde{\chi}_\infty[\{g-g_c(\rho)\}(1-\rho)L^{1/\nu}]. \tag{3.15}$$

In order to verify the ρ dependent FSS form, $\chi_\infty/L^{\gamma/\nu}$ are plotted against $[\{g-$

$g_c(\rho)\}(1-\rho)]L^{1/\nu}$ in Fig. 3.7(b) for the constant growth and against $[\{g-g_c(L)\}(1-\rho)]L^{1/\nu}$ in Fig. 3.7(d) for the correlated growth for the same set of data in Fig. 3.7(a) and (c). For the constant growth, a good data collapse is obtained irrespective of different values of ρ whereas for the correlated growth, no such collapse is found to occur.

Though the partial hindrance plays no role on the critical properties, the suppression of the growth of the larger clusters has a weak effect on the critical properties of the system in the dilute limit of ρ but not strong enough to change the order of transition.

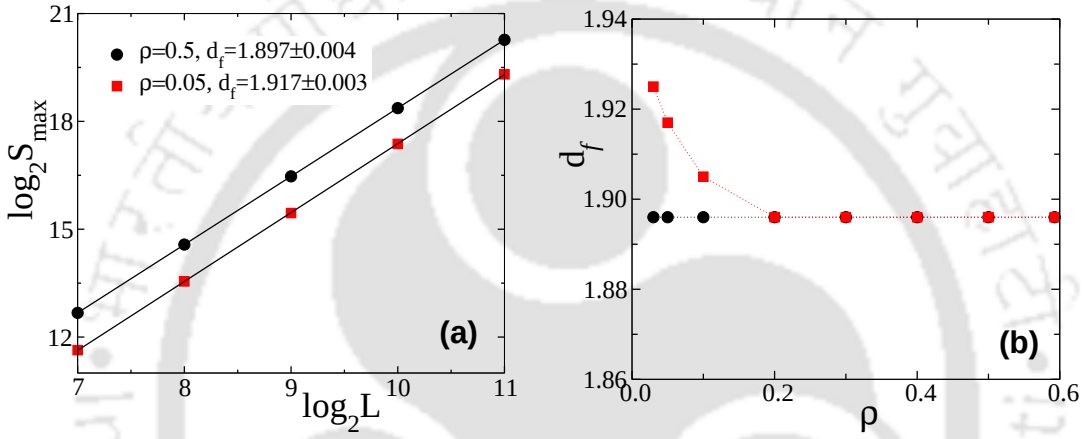

Figure 3.8: (a) Plot of $S_{\max}$ against lattice sizes L at the thresholds $g_c(\rho)$ for $\rho = 0.5(\bigcirc)$ in black and at $g_c(L)$ for $0.05(\square)$ in red. The values of fractal dimension $d_f = 1.897 \pm 0.004$ & 1.917 ± 0.003 are obtained from linear least square fit through the data points for their respective ρs. (b) Plot of the fractal dimension d_f against ρ. Black circles represent the percolation exponents and red squares are obtained values of exponents for given ρs.

3.4.2 Spanning cluster dimension

Since the clusters are grown here applying PBC, the horizontal and vertical extensions of the largest cluster is kept stored. If either the horizontal or the vertical extension of the largest cluster is found to be greater than or equal to the lattice size L, it is identified as a spanning cluster. In the constant growth, the values of $S_{\max}$ are noted at the respective thresholds for all values of ρ. Whereas $S_{\max}$ is estimated at $g_c(\rho)$ for $\rho \geq 0.2$ and at $g_c(L)$ for $\rho < 0.2$. The percolation spanning cluster is known to be a random object with all possible sizes of holes in it and is fractal with a fractal dimension $d_f < d$ (d, space dimension) for a continuous PT. However, it becomes compact with a dimension $d_f = d$ in the case of a discontinuous transition[39,42]. The values of $S_{\max}$ are plotted against L in double logarithmic scale

in Fig. 3.8(a) for $\rho = 0.5$ (black circles) and $\rho = 0.05$ (red squares). The values of d_f are estimated by linear least square fit through the data points. It is found that $d_f = 1.897 \pm 0.004$ for $\rho = 0.5$ and agrees well with the fractal dimension $d_f = 91/48$ that of original 2d percolation[11]. For $\rho = 0.05$, it is found that $d_f = 1.917 \pm 0.003$. In fact, in this model, the value of d_f is found to be that of OP for $\rho \geq 2$ and it increases for $\rho < 2$ as $g_c(L)$ is slightly higher than the constant growth. The variations of fractal dimension d_f with the initial seeds concentration ρ are presented in Fig. 3.8(b). The values of the critical exponents clearly distinguishes the two classes of PT for $\rho \geq 0.2$ the scaling and exponents are same class of percolation universality and for $\rho < 0.2$ the values of the critical exponents are deviated from OP (belongs to different universality class) as it is observed in several models with unusual finite size behavior[54]. Moreover, the absolute values of $S_{\max}$ depend on the initial seed concentration ρ. The values of $d_f < 2$ shows that the phase transitions are continuous for all values of ρ. The partial hindrance and suppression on the growth of the clusters show a weak effect at the dilute limit of ρ, where slightly compact clusters (because of slightly high growth probability) merge together to form the spanning cluster. As d_f remains less than 2, the space dimension for all values of ρ in the model, the nature of transition seems to be always continuous. Though, for the smaller ρ values, the exponents are expected to be different from those of OP as it is observed in several hybrid models[50,128].

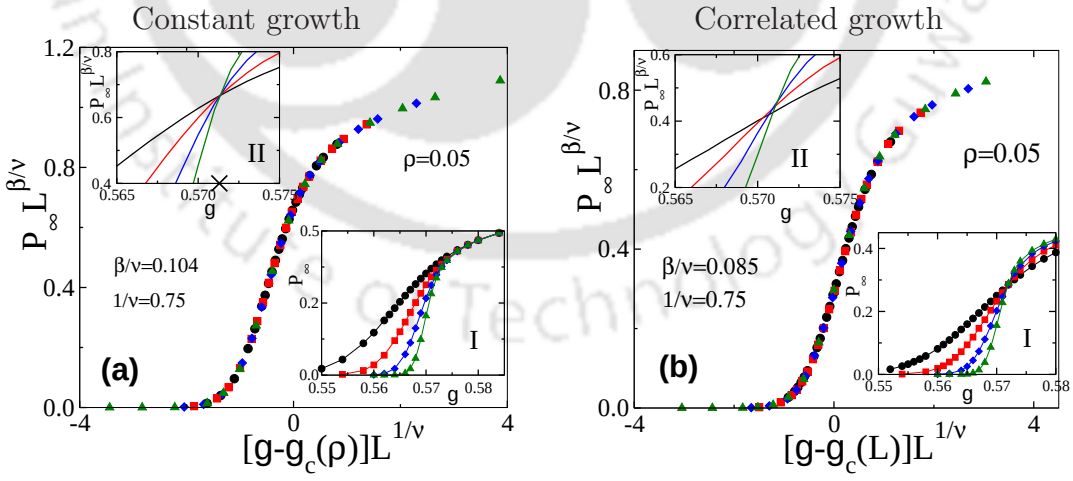

Figure 3.9: Plot of $P_\infty L^{\beta/\nu}$ against $[g - g_c(\rho)]L^{1/\nu}$ in Fig. (a) for the constant growth and against $[g - g_c(L)]L^{1/\nu}$ in Fig. (b) for the correlated growth taking $\rho = 0.05$ for both the processes for the same set of L of Fig. 3.3. A good data collapse is obtained for the respective values of β/ν taking $1/\nu = 0.75$ for both the cases. P_∞ and $P_\infty L^{\beta/\nu}$ are plotted against g in the inset-I and inset-II of the figures respectively.

3.4.3 FSS of P_∞

The variation of P_∞ against g is studied for the constant growth as well as for the correlated growth for $\rho = 0.05$ and are shown in Fig. 3.9(a) and Fig. 3.9(b) respectively. In the inset-I of Figs. 3.9(a) & 3.9(b), P_∞ is plotted against the growth parameter g for different system sizes L. The transition becomes sharper and sharper as $L \to \infty$ in both the cases. In the inset-II of Figs. 3.9(a) & 3.9(b), the scaled order parameter $P_\infty L^{\beta/\nu}$ is plotted against the growth parameter g for the same values of L. For $\beta/\nu = 0.104$, the curves of different L cross at a particular value of g that corresponds to the critical threshold $g_c(\rho) = 0.5713$ for the constant growth. Whereas for the correlated growth, no such precise crossing point is found for $\rho < 0.2$. Finally, the scaled order parameter $P_\infty L^{\beta/\nu}$ is plotted against the scaled variable $[g - g_c(\rho)]L^{1/\nu}$ for the constant growth in Fig. 3.9(a) and against $[g - g_c(L)]L^{1/\nu}$ for the correlated growth in Fig. 3.9(b) for different system sizes L. A good collapse of data are observed for the critical exponents $\beta/\nu = 0.104$ and $1/\nu = 0.75$ for the constant growth and $\beta/\nu = 0.085$ and $1/\nu = 0.75$ for the correlated growth. The scaling relation $\beta/\nu = 2 - d_f$ is satisfied within the error bars for both the models. As it appears, the value of β/ν and $1/\nu$ agrees well with the value for original 2d percolation, *i.e.*, $\beta/\nu = 5/48$ and $1/\nu = 3/4$ for the constant growth as well for $\rho \geq 0.2$ in the correlated growth. But the values of exponent β/ν are deviated from the percolation exponents for $\rho < 0.2$ in the correlated growth model.

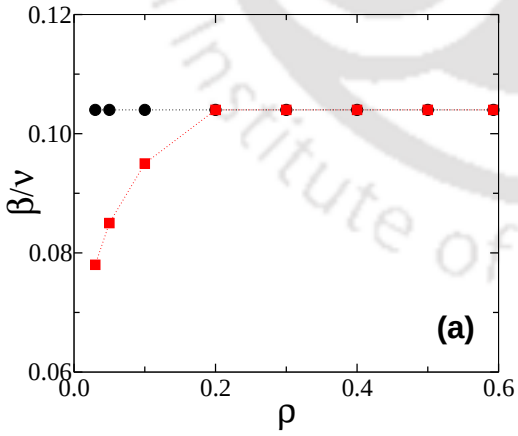

Figure 3.10: Plot of the variation of ratios of critical exponents β/ν against ρ. Black circles represent the percolation exponents and red squares are obtained values of exponents for given ρs.

The variations of the critical exponents β/ν (red squares), obtained from FSS of P_∞ with the initial seeds concentration ρ are presented in Fig. 3.10. The values of the critical exponents clearly distinguish the two classes of PT, for $\rho \geq 0.2$, the scaling and exponents are the same class of percolation universality whereas

for $\rho < 0.2$, the values of the critical exponents are deviated from OP (belongs to different universality class).

3.4.4 Binder cumulant

The values of the critical exponents and the scaling forms of different geometrical quantities suggest that the PT in TPPM for both the constant and the correlated growth processes are of continuous second order transition at all values of ρ. In order to confirm the nature of the transition in TPPM, the 4th order Binder cumulant (BC) [152],

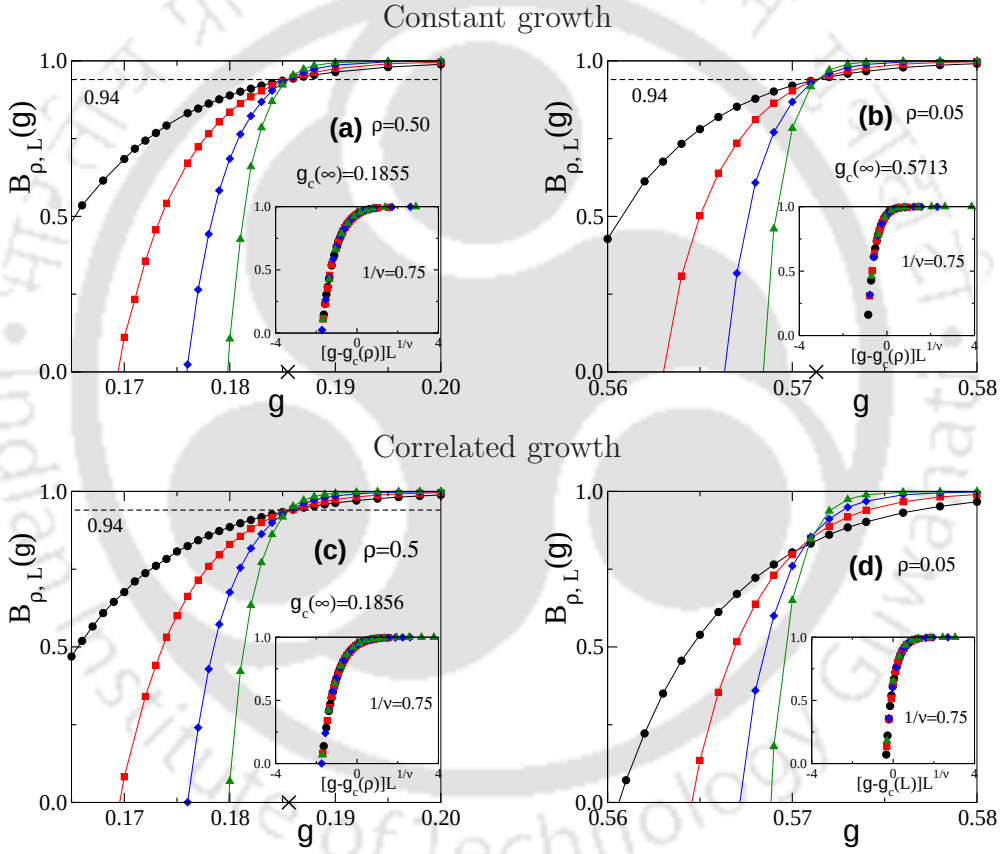

Figure 3.11: Plot of $B_{\rho,L}(g)$ versus g for $\rho = 0.5$ & 0.05 in (a) & (b) for the constant growth and in (c) & (d) for the correlated growth. The same set of color symbols of Fig. 3.3 for different L are used. The cross on the g axis corresponds to $g_c(\rho)$ at which the plots of $B_{\rho,L}$ for different L intersect. In a case of correlated growth for $\rho = 0.05$ in Fig. (d), the plots cross over a wide range of g. In the insets, $B_{\rho,L}(g)$ are plotted against $[g - g_c(\rho)]L^{1/\nu}$ in (a), (b) & (c) and against $[g - g_c(L)]L^{1/\nu}$ in (d). A good data collapse is obtained taking $1/\nu = 0.75$. The value of BCs (≈ 0.94) at the percolation thresholds are shown by dotted line.

$$B_{\rho,L}(g) = \frac{3}{2}\left[1 - \frac{\langle S^4_{\max}\rangle}{3\langle S^2_{\max}\rangle^2}\right] \tag{3.16}$$

is studied. $B_{\rho,L}(g)$ is plotted against g for different values of L for $\rho = 0.5$, $\rho = 0.05$ for constant growth in Fig. 3.11(a) and 3.11(b) and for the correlated growth in Fig. 3.11(c) and 3.11(d) respectively. For both the values of ρ in the constant growth the plots of $B_{\rho,L}(g)$ for different L intersect at a point corresponding to the critical percolation threshold $g_c(\rho)$ of the respective values of ρ as it occurs for a continuous PT. Whereas in the correlated growth, a definite crossing point is found to exist for $\rho \geq 0.2$ but for $\rho < 0.2$ the plots cross each other over a range of g and no precise point of crossing is found. The value of BC at their respective thresholds are shown by a dotted line at 0.94, which is similar to that of the site percolation in $2D$.

The FSS form of BC is given by,

$$B_{\rho,L}(g) = \widetilde{B}[\{g - g_c(\rho)\}L^{1/\nu}] \tag{3.17}$$

where $\widetilde{B}$ is a scaling function. The FSS scaling form is verified in the insets of each plot in Figs. 3.11, plotting BC against $[g - g_c(\rho)]L^{1/\nu}$ for both the values of ρ in the case of constant growth but only for $\rho = 0.5$ in the case of correlated growth. For $\rho = 0.05$ in the case of correlated growth BC is plotted against $[g - g_c(L)]L^{1/\nu}$ for different system sizes L. A good data collapse is observed taking $1/\nu = 0.75$ as that of OP for the both the model for all the values of ρ. Therefore, both the models represent second order PTs over a wide range of ρ.

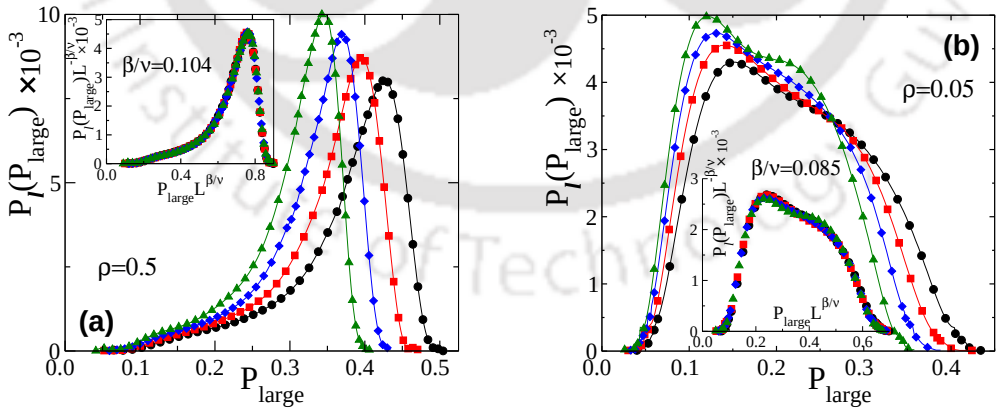

Figure 3.12: Plot of $P_\ell(P_{\text{large}})$ against P_{large} for $\rho = 0.5$ & 0.05 in (a) & (b). Same set of color symbol of Fig. 3.3 for different lattice sizes are used. In inset, $P_\ell(P_{\text{large}})L^{-\beta/\nu}$ are plotted $P_{\text{large}}L^{\beta/\nu}$ in Figs. (a) and (b). A good data collapse is obtained for the expected critical exponents $\beta/\nu = 0.104$ in (a) and $\beta/\nu = 0.085$ in (b).

3.4.5 Order parameter distributions

To realize the presence of co-existing phases, an ensemble of the spanning or the largest cluster, if no spanning cluster appears, at g_c for a given ρ and L are generated. The distribution of probability $P_{\text{large}} = S_{\text{large}}/L^2$ to find a lattice site in a spanning/largest cluster of size S_{large} is expected to be

$$P_\ell(P_{\text{large}}) \approx L^{\beta/\nu} \widetilde{P}_\ell[P_{\text{large}} L^{\beta/\nu}] \tag{3.18}$$

where $\widetilde{P}_\ell$ is a scaling function. In Figs. 3.12, the distributions $P_\ell(P_{\text{large}})$, each interpolated through 1000 equally spaced bins of data points, are plotted against P_{large} for $\rho = 0.5$ at $g_c(\rho)$ and for $\rho = 0.05$ at $g_c(L)$ in Figs. 3.12(a) & 3.12(b) respectively. For $\rho = 0.5$ in Fig. 3.12(a), the distributions are found to be single-humped and the scaled distributions collapse onto a single curve for $\beta/\nu = 0.104$. For $\rho = 0.05$, a broader distributions are found for different L as shown in Fig. 3.12(b). However, for $\rho = 0.05$ the scaled distributions are found to collapse onto a single curve for $\beta/\nu = 0.085$, smaller than that of OP. No double-humped bimodal distribution is found to occur as it appears in thermal first-order phase transitions[153,154] and as well as in some of the EP models[39,53,117,119]. Thus, no first order transition is found to occur over a wide range of ρ in this correlated growth models. Though the partial hindrance in the constant growth has no effect on the order parameter distribution, the broadening of the distribution in the dilute limit of ρ under correlated growth indicates a possibility of obtaining a bimodal distribution of the order parameter under stronger suppression of the growth of the larger clusters[39].

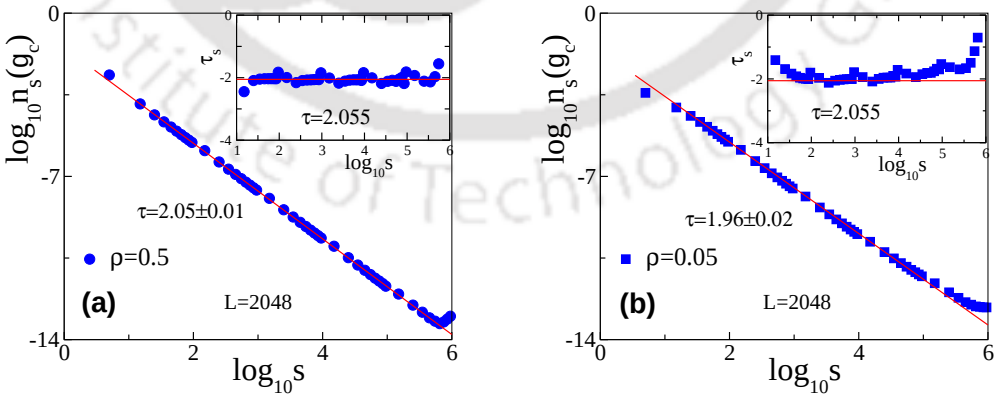

Figure 3.13: Plot of $n_s(g_c)$ against s at their respective thresholds for $\rho = 0.5$ (circles) and $\rho = 0.05$ (squares) in (a) & (b) for the lattice of size $L = 2048$. The red solid lines are drawn from the linear least square fit through the data points with slope 2.05 ± 0.01 and 1.96 ± 0.02 for the respective ρs. The slope of τ_s *vs* s plots are shown in inset of figures for the same set of ρ values.

3.4.6 Cluster size distributions

Though a detailed FSS theory is developed and numerical verified, the cluster size distribution per lattice site $n_s(g,\rho) = N_s(g,\rho)/L^2$ on a single large lattice needs to be verified for different values of g and ρ. The scaling form of the cluster size distribution in terms of growth parameter g is given as

$$n_s(\rho, g) = s^{-\tau}\widetilde{n}_s[\{g - g_c(\rho)\}s^{\sigma}] \tag{3.19}$$

where $\widetilde{n}_s$ is a new scaling function and τ, σ are two new scaling exponents. As the PT in this model is found to be continuous, a power law distribution of cluster sizes at the critical threshold $g_c(\rho)$ is expected to occur and can be given by

$$n_s(g_c) \approx s^{-\tau} \tag{3.20}$$

where τ is the scaling exponent. The cluster size distributions $n_s(g_c)$ are determined for different values of ρ at their respective thresholds for a lattice of size $L = 2048$. The data are binned of varying widths and finally normalized by the respective bin width. The critical distributions $n_s(g_c)$ are plotted against s in double logarithmic scale for $\rho = 0.5$ (circles) in Fig. 3.13(a) and $\rho = 0.05$ (squares) in Fig. 3.13(b). It can be seen that the distributions describe power law scaling. For $\rho \geq 0.2$, the distribution scales with an exponent $\tau \approx 2.05$ within the error bar of ± 0.01. Such a value of τ is comparable with the value of $\tau = 187/91$ of OP[11]. Whereas for lower values of ρ, the distributions develop curvature and the exponent deviates from the percolation value. In Fig. 3.13(b), for $\rho = 0.05$, the value of τ is found to be 1.96 ± 0.02. In order to visualize such deviation, the measured local slope of the distribution in double logarithmic scale

$$\tau_s = \frac{\partial \log_{10} n_s(g_c)}{\partial \log_{10} s} \tag{3.21}$$

is plotted against $\log_{10} s$ in the insets of the the respective plots. The exact value of $\tau = 187/91$ of OP is shown by solid lines. For $\rho \geq 0.2$, the value of τ_s found to be close to the exact value as that of OP over a wide range of s whereas for $\rho < 0.2$ τ_s varies with s and deviates from the OP value. It can again be emphasized that the suppression of growth of larger clusters leads the model to new universality classes with a new set of critical exponents that OP in the dilute limit of the initial seed concentration.

3.5 Conclusion

A two-parameter suppressed cluster growth percolation model with multiple cluster growth is developed and studied extensively following finite size scaling hypothesis. In this model, two tunable parameters are the initial seed concentration ρ and the cluster growth probability g as in the previous model. There exists a critical growth probability g_c at which a continuous percolation transition occurs for each ρ. It is found that the values of the critical exponents describing the scaling functions at the criticality in this model are that of original percolation for $\rho \geq 0.2$. Hence, for $\rho \geq 0.2$, all such transitions belong to the same universality class of percolation. On the other hand, for $\rho < 0.2$, suppression of the growth of larger clusters seems to have a weak effect on the critical properties. The values of the critical exponents found to deviate from those of the OP and the model is found to belong in new universality classes. However, such an effect is not found to be strong enough to change the order of transition apart from the fact that the cluster size distribution develops curvature and the order parameter distribution broadens in the limit $\rho \to 0$. A phase line consisting of second order phase transition points is found to separate the connected region from the disconnected region in the $\rho - g$ parameter space. As no discontinuous percolation transition is found in this model, the suppression in growing the larger clusters does not give any effect on the order of transition. The FSS theory proposed here is found to be well satisfied by the critical exponents obtained in these models. The broadening of the order parameter distribution in the correlated growth model in the dilute limit of ρ indicates a possibility of obtaining a bimodal distribution of the order parameter under stronger suppression of the growth of the larger clusters corresponding to a first-order transition. A tricritical point as well may exist in the enhanced parameter space.

Chapter 4

First-order percolation transition in a preferential growth model

In the previous two chapters, A two-parameter percolation model (TPPM) was developed and studied once under constant growth and then under suppressive growth of clusters. Though the constant growth model belongs to the same universality class of original percolation (OP), the suppressed cluster growth model exhibits a departure from the OP universality class in the dilute regime of initial seed concentration. It is then intriguing to study the model under more drastic suppression or more complicated correlated growth and see whether that could lead to discontinuous transition. There is then still a possibility of observing a first-order discontinuous transition in an equilibrium model of percolation. As already mentioned in the Introduction, the bootstrap percolation model[140,155,156] perhaps is the only model that exhibits non-universal first-order percolation transition in the context of equilibrium percolation model. Instead of such an example, a first-order transition in the final static (or equilibrium) spanning cluster properties of a percolation model is rarely reported in the literature. On the other hand, the nature of discontinuous transitions in several growth models of explosive percolation (EP) remain inconclusive due to the slow convergence of cluster properties[51,52,94]. In most of the EP models, except for a jump in the order parameter, the other aspects of first-order transitions, such as phase coexistence, nucleation, etc., are found to be absent[43,53], which are essential features of a first-order thermal phase transition[157].

In this chapter, the two-parameter percolation model with the initial seed concen-

This chapter is based on the Ref.[39]; Bappaditya Roy and S. B. Santra, Phys. Rev. E **95**, 010101(R) (2017).

tration ρ and a growth parameter g_0 as two tunable parameters are further modified incorporating stronger suppression of the growth of larger clusters in comparison to the smaller clusters. Except the preferential growth of smaller clusters with a size-dependent growth probability of amplitude g_0, the model preserves all other criteria of the original percolation model. Though the clusters are grown following a nonequilibrium growth process, the percolation transition in this model is always determined by the final equilibrium spanning cluster properties, as in OP. The equilibrium spanning cluster properties of the percolation model is found to exhibit a first-order transition in the dilute limit of the initial seed concentration and a continuous percolation transition for the higher values of initial seed concentration. Such crossover from continuous to discontinuous transition is separated by a tricritical region. The coexistence of two different phases is found to be enclosed within lines of first-order transitions.

4.1 The model

In this model, the initial configuration is taken as a partially randomly populated lattice with an initial seed concentration ρ less than $p_c(\approx 0.5927)$, the threshold of OP, and the cluster size distribution is obtained by employing the Hoshen-Kopelman algorithm[141]. The process of nucleation and growth is then implemented by growing all these finite clusters simultaneously with a size-dependent growth probability $g_s(t)$, and allowing them to merge as soon as two clusters are separated by the nearest-neighbor (NN) distance. Note that there are multiple growth centers instead of a single one as in the Leath's OP model[142]. At any time, $g_s(t)$ of a cluster of size s_t is given by

$$g_s(t) = g_0 \exp\left[-\frac{(s_t - 1)}{s_{t,\text{large}}}\right], \tag{4.1}$$

where the growth parameter g_0 is a constant between $[0, 1]$ and $s_{t,\text{large}}$ is the size of the largest cluster present at that time. In this preferential growth, the largest cluster grows with the smallest probability (g_0/e) and the smallest cluster grows with the highest probability (g_0). In the Monte Carlo (MC) algorithm of preferential growth, the clusters are grown sequentially, starting from the smallest cluster. Once a site is rejected with probability $[1-g_s(t)]$, the site remains unoccupied throughout the growth process, as in the Leath algorithm. Since the empty sites of the smallest cluster are occupied first, the status of occupation or rejection of such sites cannot be altered in the future at the time of the growth of other clusters of higher sizes if they

are encountered as their neighbors. As soon as all the clusters present at that time are allowed to grow one layer of NN perimeter sites, the MC time step is increased by one and the cluster size distribution is updated. The growth probability $g_s(t)$ is recalculated as per the new cluster size distribution. As the growth process seized due to a decrease in the average growth probability as well as the unavailability of empty NN perimeter sites of any cluster for occupation, the final static cluster size distribution is obtained to analyze percolation transition, unlike the process of collecting cluster size distributions during the growth process as in the EP models.

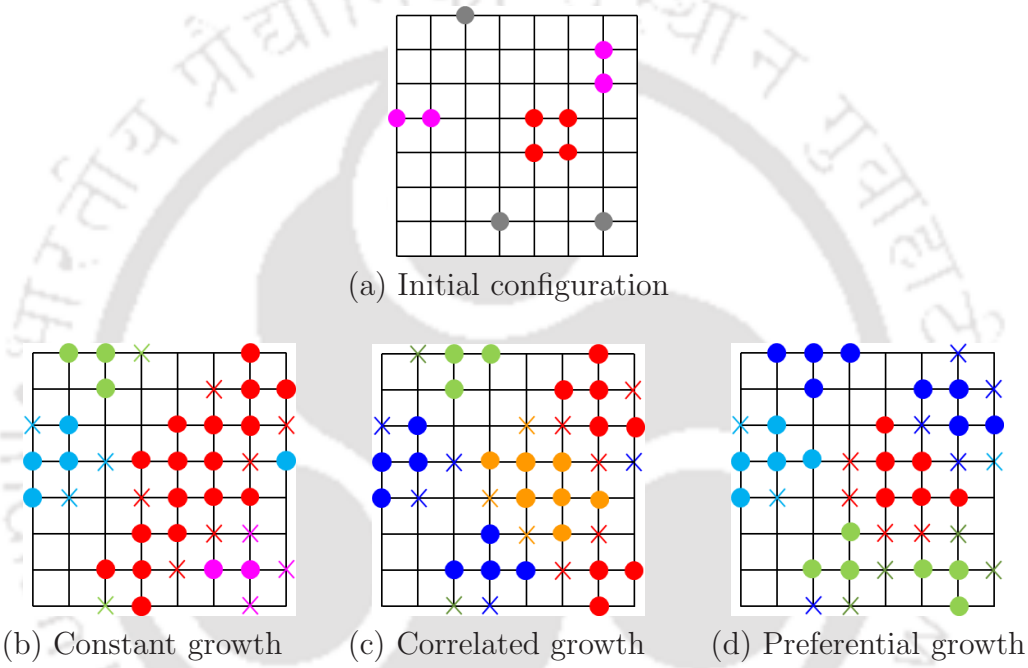

(a) Initial configuration

(b) Constant growth (c) Correlated growth (d) Preferential growth

Figure 4.1: Cluster configurations on a 8×8 square lattice in different growth models after one MC step starting from the same initial concentration. (a) Represents the initial configuration. Cluster configurations of the constant growth (b) and of the correlated growth (c) and that of the preferential growth (d). The occupied sites are presented by filled coloured circles. The largest cluster is shown in red and other smaller clusters are in different colors. The crosses represent the rejected sites. PBC is applied in both the directions in growing the clusters.

A comparison of cluster configuration generated on a 8×8 square lattice at the end of one MC step is given in Fig. 4.1 for constant growth, correlated growth and preferential growth models. The same initial configuration (shown in Fig. 4.1(a)) is taken for all three growth models. The largest cluster is shown in red. The value of the growth parameter (g or g_0) is kept fixed at 0.5. Though a spanning cluster appears in the case of constant growth, no such cluster appears in either of the correlated or preferential growth models. Moreover, the size of the largest cluster in

the preferential growth model is found to be lowest. The largest cluster size in the correlated growth model is lesser than that of the constant growth model but larger than that of the preferential growth model. Hence under preferential growth, the growth of the larger clusters are substantially suppressed and that of the smaller clusters are enhanced.

As $\rho \to p_c$ of OP, the initial configuration itself consists of clusters of many possible sizes which are grown with a small value of $g_0(\ll p_c)$ to achieve percolation transition. Hence, the final configuration should remain the same as the initial one, but a spanning cluster appears due to the minimal growth of some finite clusters and merging with the largest cluster. The transition is expected to be a continuous percolation transition. On the other hand, as $\rho \to 0$, the initial configuration will consist of a few small clusters which will be grown with a high value of $g_0(\gg p_c)$. Hence, the final configuration will consist of a few large compact clusters along with a spanning cluster leading to a discontinuous percolation transition due to the lack of clusters of all possible sizes. Note that this is neither the case in Bootstrap percolation nor the case for most of the EP models. Two distinct regimes of ρ are expected to appear in TPPM corresponding to continuous and discontinuous percolation transitions. It is important to note that if all the clusters were grown with a constant probability g_0, it would lead to a continuous percolation transition at all values of ρ[38].

4.2 Numerical simulation and Cluster morphology

Extensive computer simulations have been performed on the square lattices in two dimensions (2d) for different system sizes L. The system size is varied from $L = 128$ to $L = 2048$ in multiple of 2. The initial seed concentration ρ is varied from a small value upto the percolation threshold ≈ 0.59 and the growth parameter g_0 is varied from 0 to 1 for every system. Note that though there is a trivial upper limit of $\rho \approx 0.59$, the lower limit of ρ should be such that the system initially should have a sufficient number of growth centers. Clusters are grown by applying a periodic boundary condition in both the horizontal and vertical directions. An ensemble average is made over 10^5 random initial configurations for each ρ and g_0 on a given L.

A few typical final static cluster configurations on a square lattice of size $L = 128$ are shown in Figs.4.2. The final configuration for $\rho = 0.50$ and $g_0 = 0.169$ is given in Fig. 4.2(a), for $\rho = 0.40$ and $g_0 = 0.320$ is given in Fig. 4.2(b), for $\rho = 0.20$ and

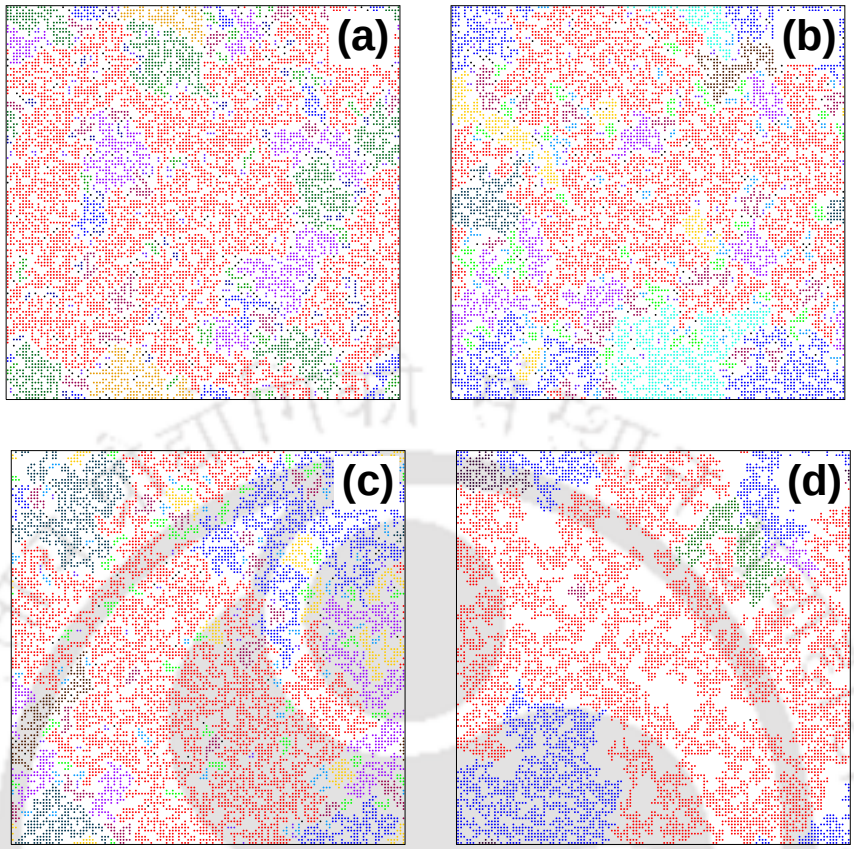

Figure 4.2: The final static cluster configurations on a square lattice of size $L = 128$ (a) for $\rho = 0.50$ at $g_{0c}(L) = 0.169$, (b) for $\rho = 0.40$ at $g_{0c}(L) = 0.320$, (c) for $\rho = 0.20$ at $g_{0c}(L) = 0.520$ and (d) for $\rho = 0.02$ at $g_{0c}(L) = 0.751$. The spanning clusters are shown in red and finite clusters are in different colors depending on their size. The white space represents the inaccessible lattice sites.

$g_0 = 0.520$ is given in Fig. 4.2(c), and for $\rho = 0.02$ and $g_0 = 0.751$ is given in Fig. 4.2(d). The growth probabilities taken correspond to the percolation thresholds of the respective systems. The spanning clusters are shown in red and the finite clusters are in different colors as per their size. As the initial seed concentration, ρ decreases the system becomes more and more rarefied. For $\rho = 0.50$, besides the spanning cluster, finite clusters of all possible sizes exist in the system (Fig. 4.2(a)) and smaller clusters are also found to be enclaved inside the larger clusters and the largest cluster becomes fractal[11,49], as in OP. On the other hand, for $\rho = 0.02$, as the threshold value of $g_0 = 0.751$ for $L = 128$ is found high, the clusters of smaller sizes are merged with the fast-growing other finite smaller clusters. Therefore, a few large clusters appear along with the spanning cluster, as expected. Enclave of smaller clusters within the largest cluster have almost disappeared. Hence, the fractal spanning cluster as in OP becomes a compact. It can also be noted that

for $\rho = 0.02$ a large number of lattice sites remain unoccupied as the excluded area. The appearance of compact spanning cluster corresponds to a discontinuous transition[29,42,100]. In the intermediate region of ρ, it is clearly observed from Fig. 4.2(b) for $\rho = 0.40$ and Fig. 4.2(c) for $\rho = 0.20$ that number of all possible sizes of clusters are decreasing with ρ whereas the inaccessible lattice space is increasing.

4.3 Finite size scaling relations

Since a detailed Finite-Size Scaling (FSS) theory has been developed in the previous chapter, only the essential definitions, and a few FSS relations will be given here. The order parameter, the probability to find a lattice site in the spanning cluster, is given by

$$P_\infty = S_{\max}/L^2, \tag{4.2}$$

where $S_{\max}$ is the size of the spanning cluster. The FSS form of P_∞ is expected to be

$$P_\infty = L^{-\beta/\nu}\widetilde{P}_\infty[(g_0 - g_{0c})L^{1/\nu}], \tag{4.3}$$

where $\widetilde{P}_\infty$ is a scaling function, β is the order parameter exponent, ν is the correlated length exponent, and g_{0c} is the critical value of g_0 at which a spanning cluster connecting the opposite sides of the lattice appears for the first time and below which no percolation transition occurs. At the threshold, the size of the spanning cluster $S_{\max}$ scales with lattice size L as

$$\langle S_{\max}\rangle \approx L^{d_f}, \tag{4.4}$$

where $d_f = d - \beta/\nu$ is the fractal dimension of the spanning cluster. Following the formalism of thermal critical phenomena[150], the distribution of P_∞ is taken as

$$P(P_\infty) = L^{\beta/\nu}\widetilde{P}[P_\infty L^{\beta/\nu}], \tag{4.5}$$

where $\widetilde{P}$ is a scaling function. Such a distribution was also used recently in the context of EP[53]. With such a scaling form of $P(P_\infty)$, one could show that $\langle P_\infty\rangle$ and $\langle P_\infty^2\rangle$ scale as

$$\langle P_\infty\rangle \sim L^{-\beta/\nu} \quad \text{and} \quad \langle P_\infty^2\rangle \sim L^{-2\beta/\nu}. \tag{4.6}$$

The fluctuation in P_∞ is defined as

$$\chi_\infty = \frac{1}{L^2}[\langle S_{max}^2\rangle - \langle S_{max}\rangle^2] = L^2[\langle P_\infty^2\rangle - \langle P_\infty\rangle^2], \tag{4.7}$$

on a 2d lattice. The FSS form of χ_∞ is then given by

$$\chi_\infty = L^{\gamma/\nu}\widetilde{\chi}[(g_0 - g_{0c})L^{1/\nu}], \tag{4.8}$$

where $\gamma/\nu = d - 2\beta/\nu$ on a d-dimensional lattice, γ is the average finite cluster size exponent and $\widetilde{\chi}$ is a scaling function. Studying the FSS of χ_∞, the values of the critical thresholds $g_{0c}(L)$ and that of γ/ν are now estimated. The formalism above describes a continuous transition as ν corresponds to the diverging correlation length. However, discontinuous transitions are expected to occur in this model at the dilute limit of ρ and in such situations ν would not correspond to the correlation length exponent as already observed in several explosive percolation models[111,119]. The same notation for the exponent ν is, however, kept throughout the range of ρ to avoid another notation.

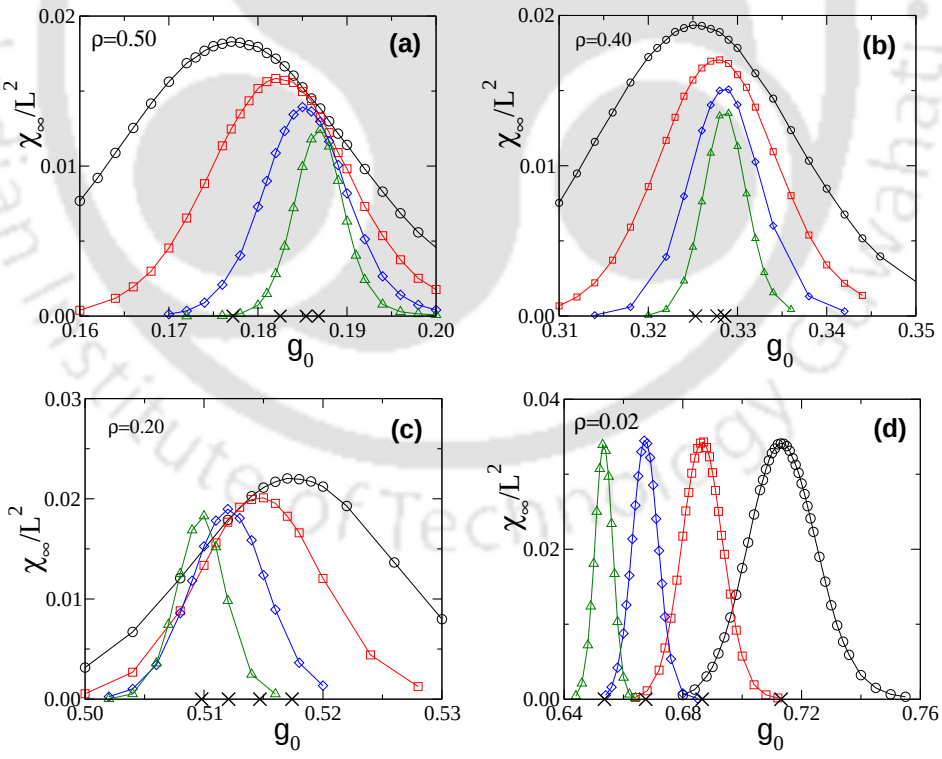

Figure 4.3: Plot of χ_∞/L^2 *vs* g_0 for $\rho = 0.50$ (a), $\rho = 0.40$ (b), $\rho = 0.20$ (c) and $\rho = 0.02$ (d) for different lattice sizes $L = 256[\bigcirc]$, $512[\square]$, $1024[\diamond]$, $2048[\triangle]$. Crosses on the g_0-axis represent the thresholds $g_{0c}(L)$.

4.4 FSS study of χ_∞

The fluctuation χ_∞ has been measured on lattices of several sizes for a wide range of ρ varying the growth parameter g_0. The variation of fluctuation per lattice site χ_∞/L^2 against g_0 is shown in Figs. 4.3 for lattice sizes $L = 256[\bigcirc]$, $512[\square]$, $1024[\diamond]$, $2048[\triangle]$. It is shown for $\rho = 0.50$ in Fig. 4.3(a), for $\rho = 0.40$ in Fig. 4.3(b), for $\rho = 0.20$ in Fig. 4.3(c) and for $\rho = 0.02$ in Fig. 4.3(d). As expected, the plots are found to have a maximum for a particular value of g_0, the percolation threshold $g_{0c}(L)$, for a given L and ρ. The values of $g_{0c}(L)$ are marked by crosses on the g_0 axis. For the system sizes $L = 128$ to 2048, the critical growth probabilities $g_{0c}(L)$ remain within 0.169 and 0.187 for $\rho = 0.50$, within 0.320 and 0.329 for $\rho = 0.40$, within 0.520 and 0.510 for $\rho = 0.20$, which all are less than the threshold of OP, whereas for $\rho = 0.02$ they are found to be within 0.751 and 0.654, which are greater than the threshold of OP, as it happens in EP transitions[27,28,45]. For $\rho \lesssim 0.4$, the values of $g_{0c}(L)$ are found to decrease with increasing L as seen in the dielectric breakdown model[134]. A phase diagram in the $\rho - g_0$ parameter space separating the disconnected and connected phases is obtained plotting $g_{0c}(L)$ against ρ for a lattice of size $L = 2048$ in Fig. 4.4. However, the nature of transitions along the phase line needs to be determined. It is intriguing to locate the tricritical point if any where the line of continuous transitions will meet the line of discontinuous transitions.

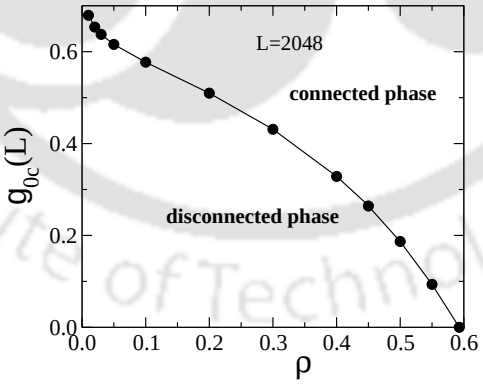

Figure 4.4: Plot of $g_{0c}(L)$ against ρ for $L = 2048$.

Below we determine the critical exponent γ/ν and verify the scaling form assumed for χ_∞.

Exponent γ/ν: At the threshold, the scaling function $\widetilde{\chi}(0)$ in Eq.4.8 is constant.

Hence, the fluctuation χ_∞ scales with lattice size L as

$$\chi_\infty \sim L^{\gamma/\nu}. \tag{4.9}$$

The peak values of the fluctuation $\chi_\infty(\max)$ for different L at their respective $g_{0c}(L)$ are estimated and plotted against L in Fig. 4.5(a) for $\rho = 0.02$ (circles), 0.20 (squares), 0.40 (diamonds) and 0.50 (triangles). The values of γ/ν are extracted by a linear least squares fit to the data points. For $\rho = 0.50$, γ/ν is found to be 1.80 ± 0.01, that of the OP (≈ 1.792[11]) within the error bar. The values of γ/ν are found to remain within 2% of that of the OP value for all $\rho \geq 0.45$, whereas for $\rho = 0.02$, γ/ν is found to be 2.00 ± 0.01, as expected in a first-order transition[42,100]. The value of $\gamma/\nu \approx 2$ is also found to occur for $\rho \leq 0.05$ within the error bar. In the intermediate region $0.05 < \rho < 0.45$, the value of γ/ν is found to decrease continuously from 2.0 to 1.80 as ρ increases from 0.05 to 0.45. Here, the values of γ/ν for two intermediate values of $\rho = 0.40$ and for $\rho = 0.20$ in Fig. 4.5(a) are shown and found to be 1.83 ± 0.01 and 1.90 ± 0.01 respectively. The variations of the critical exponents γ/ν (black circles) with the initial seed concentration ρ are presented in Fig. 4.5(b). The values of the critical exponents clearly distinguishes the discontinuous transitions for $\rho \leq 0.05$ from the continuous transitions with percolation exponents for $\rho \geq 0.45$. Such continuously varying exponents are also observed in hybrid percolation models[50,128].

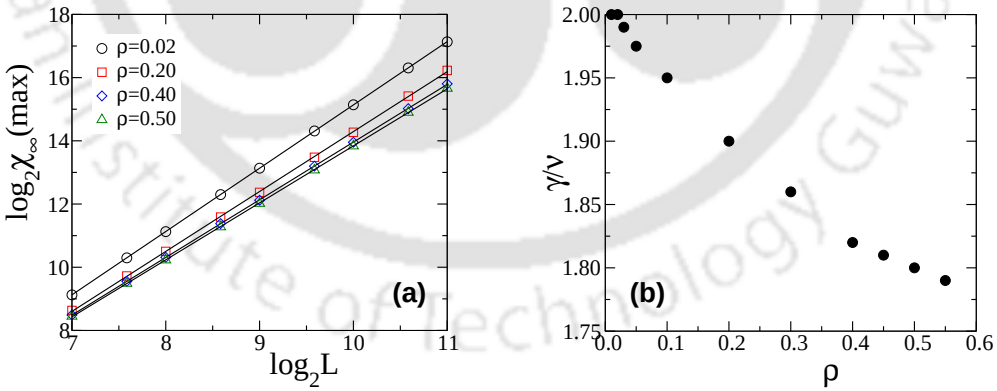

Figure 4.5: (a) Plot of $\chi_\infty(\max)$ against lattice sizes L for $\rho = 0.02[\bigcirc]$, $0.20[\square]$, $0.40[\diamond]$ and $0.50[\triangle]$, taking different lattice sizes. Solid lines are drawn by a linear least squares fit to the data points. (b) The ratios of critical exponents, γ/ν is plotted against ρ.

Scaling verification: The FSS form of χ_∞ as given in Eq.4.8

$$\chi_\infty = L^{\gamma/\nu}\widetilde{\chi}[(g_0 - g_{0c})L^{1/\nu}],$$

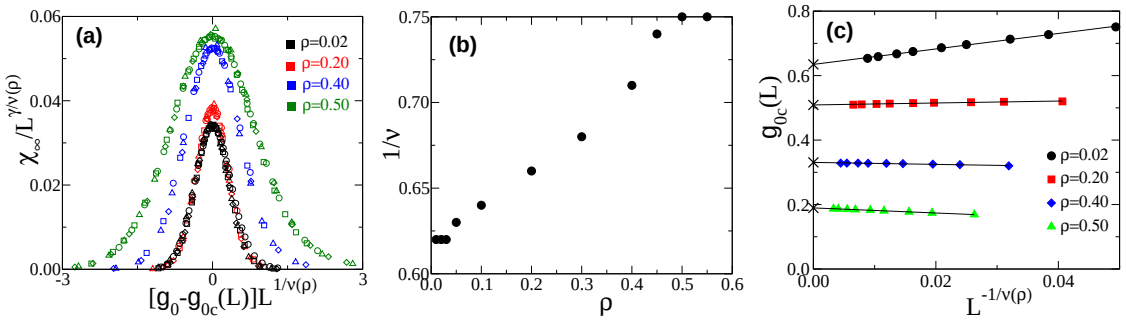

Figure 4.6: (a) Plot of $\chi_\infty/L^{\beta/\nu(\rho)}$ against $[g_0 - g_{0c}(L)]L^{1/\nu(\rho)}$ for $\rho = 0.02$ (black), 0.20 (red), 0.40 (blue) and $\rho = 0.50$ (green) using the same symbols for different L as in Fig. 4.3. (b) Plot of $1/\nu$ against ρ. (c) Plot of $g_{0c}(L)$ against $L^{-1/\nu(\rho)}$. Solid lines represent the linear least square fit through the data points.

where $\widetilde{\chi}$ is the scaling function. As the value of the exponent γ/ν is known for each ρ, the scaling form can be now verified by tuning the value of $1/\nu$. The scaled fluctuation $\chi_\infty/L^{\gamma/\nu(\rho)}$ is plotted against the scaled variable $[g_0 - g_{0c}(L)]L^{1/\nu(\rho)}$ in Fig. 4.6(a) for several values of ρ. The best collapses of data are obtained by tuning the value of $1/\nu$ and taking the exponent $\gamma/\nu = 1.80$, 1.83, 1.90 and 2.00 for $\rho = 0.50$, 0.40, 0.20 and 0.02 respectively. It is found that $1/\nu = 0.75$ for $\rho = 0.50$ (green), $1/\nu = 0.71$ for $\rho = 0.40$ (blue), $1/\nu = 0.66$ for $\rho = 0.20$ (red) and $1/\nu = 0.62$ for 0.02 (black). The value of $1/\nu(\rho)$ is found to decrease from 0.75, that of OP, to 0.62, as ρ decreases from 0.50 to 0.02. The variation of $1/\nu(\rho)$ with ρ is shown in Fig. 4.6(b). It can be noted that the FSS form is found to be valid through out the range of ρ.

In case of continuous percolation transition as in OP[11], the critical growth probability $g_{0c}(L)$ is expected to scale with the system size L as

$$g_{0c}(L) - g_{0c}(\rho) \approx L^{-1/\nu}, \tag{4.10}$$

where ν is the correlation length exponent and in the limit $L \to \infty$, the value of $g_{0c}(L)$ should correspond to $g_{0c}(\rho)$, the percolation threshold of the model for a given ρ. Knowing the values of $1/\nu(\rho)$, the above scaling can be verified. In the Fig. 4.6(c), $g_{0c}(L)$ is plotted against $L^{-1/\nu(\rho)}$ for $\rho = 0.02$ (circles), 0.20 (squares), 0.40 (diamonds) and 0.50 (triangles). The scaling form given in Eq.4.10 is found to be well satisfied for each ρ with the respective values of $1/\nu(\rho)$. Linear least square fitting through the data points for each ρ is performed using the estimated values of $1/\nu(\rho)$ and shown by solid straight lines. The intercepts of the fitted lines on the $g_{0c}(L)$ axis correspond to $g_{0c}(\infty)$ in the limit $L \to \infty$ for each ρ. It can be noted

that the value of $1/\nu(\rho)$ is consistent with scaling form throughout the range of ρ irrespective of the nature of transitions.

Though it is known in the case of equilibrium thermal first-order phase transition that the difference of the system size dependent critical point $[g_{0c}(L)]$ from the true critical point $[g_{0c}(\rho)]$ scales with the system size as $1/L^d$ where d is the space dimension[59,157], it is rarely observed in first-order percolation transitions. Rather, it is found to vary from model to model[50,100,121,128].

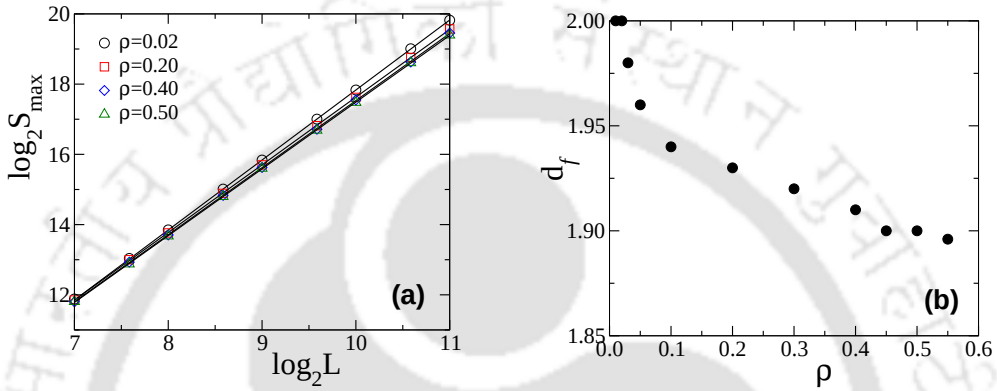

Figure 4.7: (a) Plot of $s_{\max}$ against L at their respective thresholds for $\rho = 0.02[\bigcirc]$, $0.20[\square]$, $0.40[\diamond]$ and $0.50[\triangle]$ and for different lattice sizes. Solid lines are drawn by a linear least square fit to the data points. (b) Plot of fractal dimension d_f against ρ.

4.5 Compactness of spanning cluster

For the system size $L \ll \xi$, the size of the spanning cluster $S_{\max}$ at the criticality varies with the system size L as in Eq.4.4

$$\langle S_{\max} \rangle \approx L^{d_f},$$

where d_f is the fractal dimension of the spanning cluster. Therefore, the value of $S_{\max}$ are collected at the respective thresholds for several lattice sizes L for a given ρ. For continuous transitions, the spanning cluster is a random object with all possible sizes of holes in it and is expected to be fractal *i.e.,* the fractal dimension always $d_f < 2.0$ whereas in the case of a first-order discontinuous transition it becomes a compact cluster whose size is expected to scale with the system size as L^d where d is the space dimension[39,119,158]. Hence, $S_{\max}$ is plotted against L for $\rho = 0.02$ (circles), 0.20 (squares), 0.40 (diamonds) and 0.50 (triangles) in Fig. 4.7(a). By a linear least squares fit, the values of d_f are obtained as $d_f = 1.90 \pm 0.01$, as that of OP ($\approx 91/48$)

within the error bar, for $\rho = 0.50$. The values of d_f are found to remain within 2% of that of the OP value for all $\rho \geq 0.45$. For $\rho = 0.40$ & 0.20, the values of fractal dimension $d_f = 1.91 \pm 0.01$ & 1.93 ± 0.01 respectively. It can be seen that the value of d_f is deviated from percolation value for intermediate values of ρ. Whereas for $\rho = 0.02$, $d_f = 1.99 \pm 0.01$, as that of the space dimension d. The values of d_f are found to be $d \approx 2$ for all $\rho \leq 0.05$, as expected in a discontinuous transition. Since $g_{0c} \gg p_c$ for $\rho \leq 0.05$, the initial small finite clusters grow as compact clusters. As already pointed out, a compact spanning cluster at smaller values of ρ emerges due to the merging of these compact finite clusters. In the intermediate region $0.05 < \rho < 0.45$, the value of d_f is found to increase continuously with decreasing ρ, as shown in Fig. 4.7(b). The variation of d_f with ρ is shown in Fig. 4.7(b). It can be noted here that the hyper-scaling relation is satisfied within error bars for $\rho \geq 0.45$, whereas for $\rho < 0.45$ it is slightly out of the error bars.

ρ	0.01	0.02	0.03	0.05	0.10	0.20	0.30	0.40	0.45	0.50	0.55
γ/ν	2.00	2.00	1.99	1.97	1.95	1.90	1.86	1.82	1.81	1.80	1.79
$1/\nu$	0.62	0.62	0.62	0.63	0.64	0.66	0.68	0.71	0.74	0.75	0.75
d_f	2.00	2.00	1.98	1.96	1.94	1.93	1.92	1.91	1.90	1.90	1.896
β/ν	0.00	0.00	0.02	0.04	0.06	0.07	0.08	0.09	0.10	0.10	0.104

Table 4.1: Values of the exponent γ/ν and $1/\nu$, fractal dimension d_f, and β/ν obtained from the scaling relation $\beta/\nu = 2 - d_f$.

4.6 FSS study of P_∞

As given in the section 4.3, the order parameter P_∞ is the probability to find a lattice site in the spanning cluster *i.e*; $P_\infty = S_{\max}/L^2$, where $S_{\max}$ is the size of the spanning cluster and its FSS form is given by

$$P_\infty = L^{-\beta/\nu} \widetilde{P}_\infty[(g_0 - g_{0c})L^{1/\nu}]$$

where the exponent β/ν satisfy the following scaling relations

$$\beta/\nu = d - d_f \quad \text{or} \quad \beta/\nu = \frac{1}{2}(d - \gamma/\nu). \tag{4.11}$$

As the values of both γ/ν and the fractal dimension d_f are estimated in the previous sections, the values of β/ν can be obtained using one of the scaling relations above.

The estimated values of β/ν are given in table 4.1. Knowing the value of β/ν, the FSS form of P_∞ is verified instead of measuring the value of β/ν directly from the variation of P_∞. FSS form of P_∞ given above is verified for $\rho = 0.50$, 0.40, 0.20 and 0.02 by plotting $P_\infty L^{\beta/\nu(\rho)}$ vs $[g_0 - g_{0c}(L)]L^{1/\nu(\rho)}$ in Figs. 4.8 with their respective values of β/ν and $1/\nu$. A good collapse of the data is observed. Thus, P_∞ follows the usual FSS of OP for $\rho \geq 0.45$, whereas P_∞ becomes L independent ($\beta \approx 0$) for $\rho \leq 0.05$. As the exponent $\beta \to 0$ for $\rho \leq 0.05$, a jump in the order parameter is expected to occur during percolation transition in the thermodynamic limit, as in the case of a first-order transition. In the intermediate region $0.05 < \rho < 0.45$, the transitions follow the usual FSS form with the different critical exponents than original percolation and the transitions are found to belong to different universality classes.

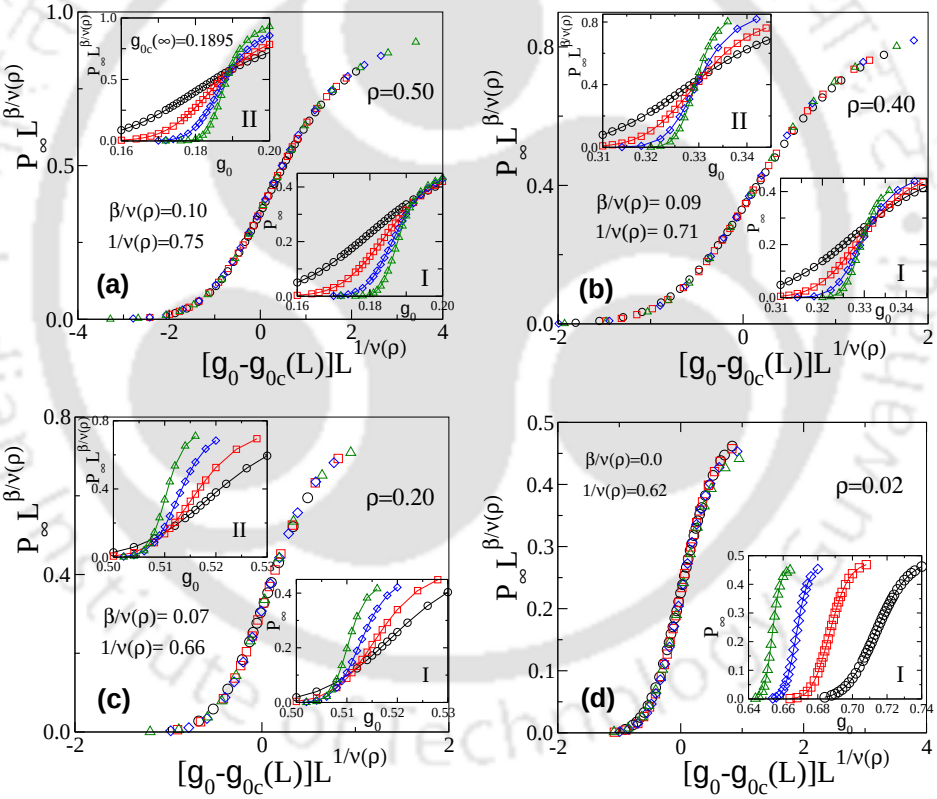

Figure 4.8: P_∞ *vs* g_0 in inset-I, $P_\infty L^{\beta/\nu(\rho)}$ *vs* g_0 in inset-II and $P_\infty L^{\beta/\nu(\rho)}$ *vs* $[g_0 - g_{0c}(L)]L^{1/\nu(\rho)}$ are plotted in each figure of $\rho = 0.50$ (a), $\rho = 0.40$ (b), $\rho = 0.20$ (c) and $\rho = 0.02$ (d) for different lattice sizes $L = 256[\bigcirc]$, $512[\square]$, $1024[\diamond]$, $2048[\triangle]$. Good data collapses are found by taking the respective critical exponents β/ν and $1/\nu$ respectively.

Beside the verification of the FSS form, variation of P_∞ against the growth parameter g_0 for different system sizes L are shown in the inset-I of of the plots for each ρ. The variation of P_∞ against g_0 becomes steeper and steeper with L

as ρ decreases and finally for $\rho = 0.02$ it is found to be the steepest. Such steep variation of the order parameter is also noted in several EP models[100]. In the inset-II of Fig. 4.8(a), (b) and (c), the scaled order parameter $P_\infty L^{\beta/\nu(\rho)}$ is plotted against the growth parameter g_0 taking respective values of β/ν for the same set of system size L. For $\rho = 0.50$, the plots for different L intersect at a particular point corresponding to $g_{0c}(\infty) \approx 0.1895$, whereas for $\rho = 0.02$ (and for $\rho \leq 0.05$ as well) no such intersection point can be observed as $\beta/\nu = 0$. In the intermediate region $0.05 < \rho < 0.45$, the plots of different L intercept over a range of g_0 values, indicating no precise crossover value, as shown in the inset-II of Fig. 4.8(b) for $\rho = 0.40$ and Fig. 4.8(c) for $\rho = 0.20$.

4.7 Binder cumulant

To confirm the nature of percolation transition in this model, the Binder cumulant (BC), fourth moment of order parameter[152],

$$B_{\rho,L}(g_0) = \frac{3}{2}\left[1 - \langle S^4_{\max}\rangle / 3\langle S^2_{\max}\rangle^2\right] \tag{4.12}$$

is studied. $B_{\rho,L}(g_0)$ is plotted against g_0 for different L for $\rho = 0.50$ [Fig. 4.9(a)], $\rho = 0.40$ [Fig. 4.9(b)], $\rho = 0.20$ [Fig. 4.9(c)] and for $\rho = 0.02$ [Fig. 4.9(d)]. For $\rho = 0.50$ (as well for $\rho \geq 0.45$), the plots of $B_{\rho,L}(g_0)$ for different L intersect at a point corresponding to $g_{0c}(\infty)$, as it occurs for a continuous percolation transition. At $g_{0c}(\infty)$, the value of BC is 0.894, as shown by a dotted line, which is similar to that of the random site percolation[159]. For $\rho = 0.02$ (as well as for $\rho \leq 0.05$), however, no such crossing of BCs for different L is found to occur, as expected in first-order transitions. In the intermediate region $0.05 < \rho < 0.45$, BCs intercept over a range of g_0 values, indicating no precise crossover value, as shown in Fig. 4.9(b) for $\rho = 0.40$ and Fig. 4.9(c) for $\rho = 0.20$. Discontinuous percolation transitions in this intermediate region are not necessarily first-order transitions. The FSS form of BC, $B_{\rho,L}(g_0) = \widetilde{B}[\{g_0 - g_{0c}(L)\}L^{1/\nu(\rho)}]$, where $\widetilde{B}$ is a scaling function, is verified in the insets of Figs. 4.9, by plotting BC against $[g_0 - g_{0c}(L)]L^{1/\nu(\rho)}$. A good collapse of data is observed for different values of ρ taking the respective values of $1/\nu(\rho)$. Thus, inclusion of nucleation and preferential growth in obtaining the final static cluster configuration in this model is able to exhibit first-order transitions for $\rho \leq 0.05$ and continuous percolation transitions for $\rho \geq 0.45$ that belong to the same universality class of OP.

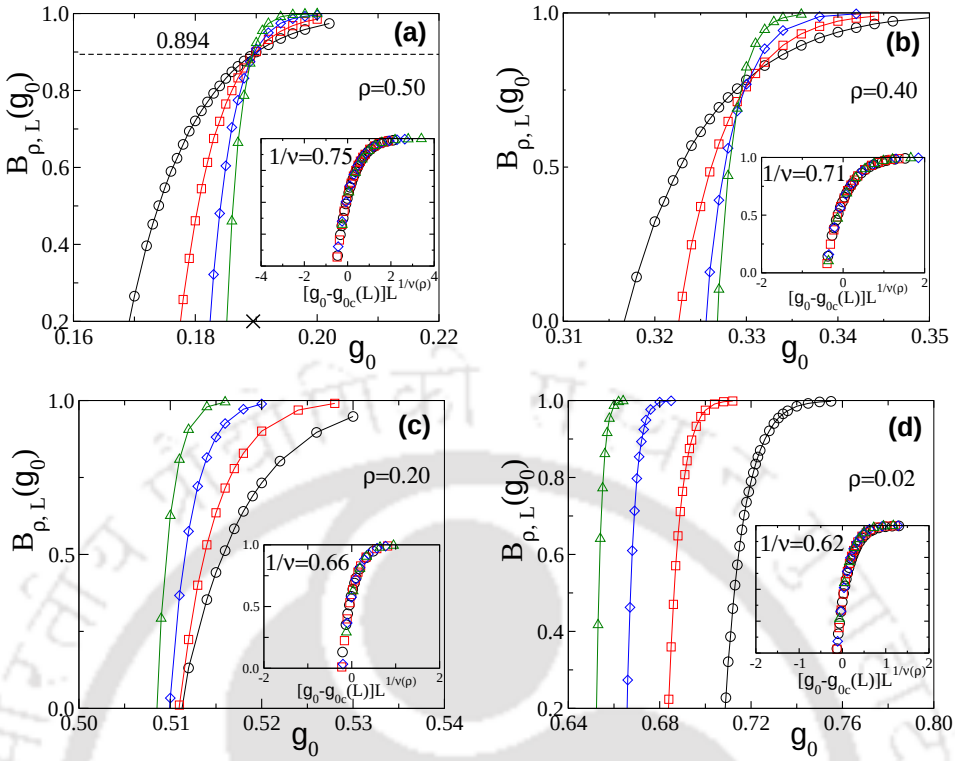

Figure 4.9: Plot of $B_{\rho,L}(g_0)$ *vs* g_0 for $\rho = 0.50$ (a), $\rho = 0.40$ (b), $\rho = 0.20$ (c) and $\rho = 0.02$ (d) for different L using the same symbol set of Fig. 4.3. In the insets, $B_{\rho,L}(g_0)$ is plotted against $[g_0 - g_{0c}(L)]L^{1/\nu(\rho)}$.

4.8 Order parameter distribution

To realize the presence of coexisting phases, an ensemble of the spanning or the largest clusters, if no spanning cluster appears, at g_{0c} for a given ρ and L, are generated. The distribution of probability $P_{\rm large} = S_{\rm large}/L^2$ to find a lattice site in a spanning/largest cluster of size $S_{\rm large}$ is expected to be

$$P_\ell(P_{\rm large}) \approx L^{\beta/\nu}\widetilde{P}_\ell[P_{\rm large}L^{\beta/\nu}], \tag{4.13}$$

where $\widetilde{P}_\ell$ is a scaling function. In Fig. 4.10(a), the distributions $P_\ell(P_{\rm large})$, each interpolated through 1000 equally spaced bins of data points, are plotted against $P_{\rm large}$ for a wide range of ρ. For $\rho \geq 0.45$, the distributions are not only found to be single humped but also the scaled distributions $P_\ell L^{-\beta/\nu}$ collapse onto a single curve when plotted against $P_{\rm large}L^{\beta/\nu}$ at the percolation thresholds $g_{0c}(\rho)$. The transitions in this region are thus continuous transitions which follow usual percolation scaling. On the other hand, for $\rho \leq 0.05$, the distributions are found to be double-humped bimodal distributions at $g_{0c}(L)$, as it appears in thermal first-order phase transi-

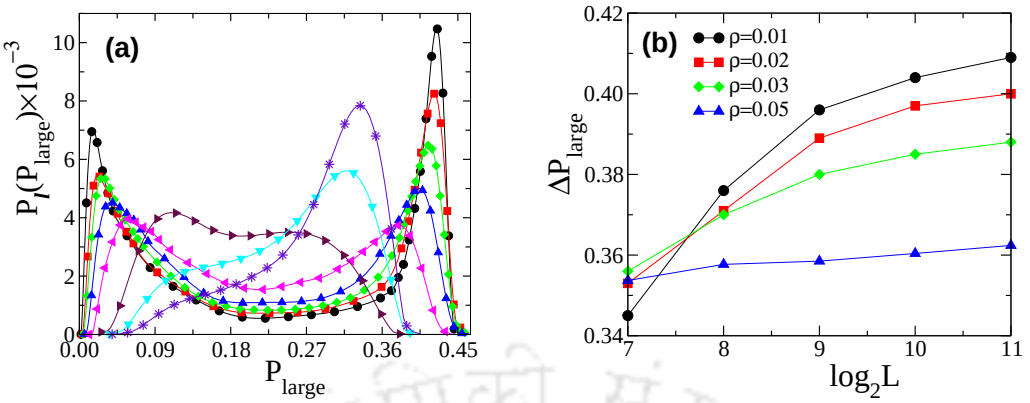

Figure 4.10: (a) Plot of $P_\ell(P_{\rm large})$ against $P_{\rm large}$ for $L = 2048$ for $\rho = 0.01$[●], 0.02[■], 0.03[♦], 0.05[▲], 0.10[◀], 0.42[▶], 0.45[▼] and 0.50[∗]. (b) Plot of $\Delta P_{\rm large}$ against L for $\rho = 0.01$[●], 0.02[■], 0.03[♦], 0.05[▲]

tions[153,154] and as well as in some of the EP models[53,117,119]. The appearance of bimodal distributions indicates the coexistence of percolative and nonpercolative clusters of sizes of the order of the system size. No suitable scaling exponent is found to collapse either of the humps of these bimodal distributions of different L. The heights of the humps are found to increase with L for a given ρ.

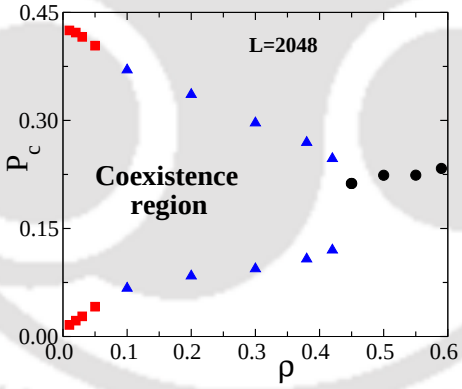

Figure 4.11: Plot of P_c against ρ. Black circles represent the continuous percolation transition with universality class of OP, blue triangles represent a mixed discontinuous percolation transition with nonuniversal critical behaviour accompanied by a finite jump in the order parameter and red squares are for the first-order transition.

Though the distributions shift leftward as L increases, the hump-to-hump separation $\Delta P_{\rm large}$ (or, the jump in the order parameter at the threshold) is found to be either constant or increasing with L, as shown in the Fig. 4.10 (b) for different values of $\rho \leq 0.05$, as in some of the EP models[119,134]. It is important to note that $\Delta P_{\rm large}$ is also increasing with decreasing ρ for large L, indicating a more drastic jump in the dilute limit of ρ. The process of nucleation and preferential growth then

produces compact spanning clusters, a jump in the order parameter at transition and the coexistence of two phases, which are features of true first-order transition. In the intermediate region of ρ, $P_\ell(P_{\text{large}})$ becomes broader as ρ decreases and the double humps start developing as ρ decreases further. Thus, in this region, the model exhibits nonuniversal critical behaviour accompanied by the unusual FSS besides a finite jump in the order parameter, such as a mixed discontinuous percolation transition in some of the EP models[29,49,50,129]. However, discontinuous percolation transition in this region may disappear in the $L \to \infty$ limit and one may find the line of the continuous transition is extended further down to lower values of ρ. In Fig. 4.11, another phase diagram of TPPM is presented in the $P_c - \rho$ parameter plane for $L = 2048$, where P_c is the critical area fraction of the largest/spanning cluster, the hump positions of the distributions. A line of second-order transitions (for $\rho \geq 0.45$) is found to bifurcate, though not sharply, at a tricritical point into two lines of the first-order transitions (for $\rho < 0.45$) enclosing a region of coexistence. The existence of a tricritical point is also observed in a growth model with a modified product rule incorporating a dilution parameter[45].

4.9 Conclusion

A two-parameter percolation model with nucleation and preferential growth in cluster generation is developed and studied numerically. Following usual spanning cluster approach of original percolation, the model is found to exhibit distinctly a first-order transition as well as a continuous percolation transition at different regimes of initial seed concentration ρ. The continuous transitions are found to belong to the same universality class of OP. The first-order transitions, however, are characterized by a discontinuous jump in the order parameter, the coexistence of spanning and non-spanning large clusters, and the appearance of compact spanning clusters. A compact spanning cluster in this region is an outcome of the merging of the compact finite clusters that were grown with probability $g_0 \gg p_c$. The region of coexistence is found to be confined within a double-humped bimodal distribution of the order parameter. In the intermediate range of ρ, the nature of percolation transition still remains inconclusive as the characteristic features of both continuous and discontinuous percolation transitions appear concurrently and can only be resolved in the true thermodynamic limit. After Bootstrap percolation, TPPM with preferential growth is another percolation model where first-order transitions occur. The model is expected to shine a light on abrupt connectivity problems in nature as well as on

the growth processes such as EP.

Chapter 5

Random growth lattice filling model of percolation

In the previous chapters, different types of equilibrium percolation models were developed incorporating different cluster growth techniques and the percolation transitions were characterized at the equilibrium (or static) state at the end of the growth process. Though the constant growth and suppressed cluster growth models unable to exhibit discontinuous transition, the preferential cluster growth model is able to display discontinuous transition in the dilute limit of the initial seed concentration.

In this chapter, a novel non-equilibrium growth model of percolation namely "random growth lattice filling" (RGLF) model is developed. In this model nucleation centers are added continuously to the lattice sites as long as a site is available and clusters are grown from these randomly implanted nucleation centers with a constant but tunable growth probability g. RGLF can be considered as a discrete version of the continuum space filling model (SFM)[161] with the touch and stop rule in the growth process as that of the growing cluster model (GCM)[144,145]. However, RGLF displays a crossover from continuous to discontinuous transitions as the value of g is tuned continuously from 0 to 1 in contrast to both SFM and GCM which display a second order continuous transition. Below we present the model and analyze data that are obtained from extensive numerical computations.

This chapter is based on the Ref.[160]; Bappaditya Roy and S. B. Santra, arxiv:cond-mat: 1705.03780 (2017), and communication.

5.1 The Model

A Monte Carlo (MC) algorithm is developed to study percolation transition (PT) in RGLF defined on a 2-dimensional (2d) square lattice. Initially, the lattice was empty except one nucleation center placed randomly to an empty site. In the next time step, besides adding a new nucleation center randomly to another empty site, one layer of perimeter sites of all the existing active clusters including the nucleation center implanted in the previous time step are occupied with a constant growth probability g following the Leath algorithm [142]. The process is then repeated. A cluster is called an active cluster as long as it remains isolated from any other cluster or nucleation center at least by a layer of empty nearest neighbours (NN). Each cluster (active or dead) are marked with a unique label. At the end of an MC step, if an active cluster is found separated by the NN bond from another cluster (active or dead), they are merged into a single cluster and marked as a single dead cluster. The growth of a dead cluster is seized forever as in GCM. If a peripheral site is rejected during the growth of an active cluster, it will be not available for occupation by any other growing cluster as in original percolation (OP). However, such a site can be occupied by a new nucleation center added externally. The growth of a cluster stops due to the fact that either it becomes a dead cluster by merging with another cluster or all its peripheral sites become forbidden sites for occupation. The process of lattice filling stops when no lattice site is available to add a nucleation center. Time in this model is equal to the number of nucleation centers added. Therefore, for any given value of g, there will always be a PT during the evolution. The model with $g = 0$ naturally corresponds to the Hoshen-Kopelman percolation as the instantaneous area fraction $p(t)$ reaches the OP threshold $p_c(\text{OP}) \approx 0.5927$. It can be noted here that in SFM with growth rate tending to 0, PT occurs only at unit area fraction [161]. The area fraction $p(t)$ in this model at time t for $g = 0$ is nothing but the number of nucleation centers added per lattice site up to time t whereas, for $g > 0$, it is the total number of occupied sites per lattice site at time t.

Below we present the details of the MC time step used for the implementation of growing the cluster model. The details of the algorithm are following accordingly to the Fig. 5.1.

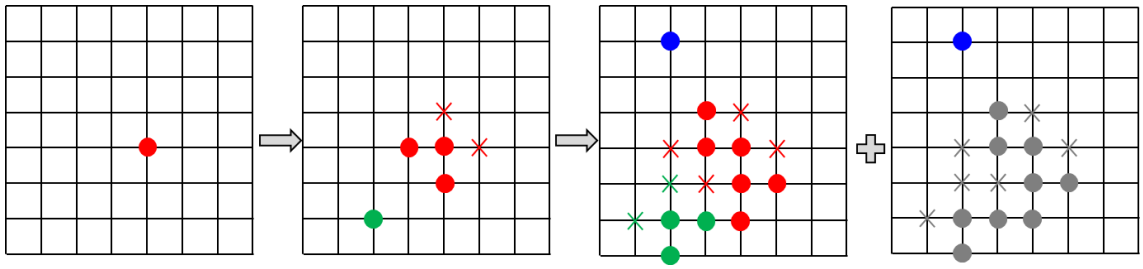

Figure 5.1: The growth process is demonstrated on a 8×8 square lattice. Figure (a) represents MC step $t = 1$, figure (b) represents MC step $t = 2$ and Figures (c) & (d) represent MC step $t = 3$. The crosses are rejected sites.

Algorithm:

A step-wise algorithm of the cluster growth process on a $L \times L$ square lattice is given below. Each lattice site has three states, occupied, unoccupied and rejected. There are two lists. *list1* consists of unoccupied sites including rejected sites and *list2* consists of empty nearest neighbour sites excluding rejected sites of active clusters.

Step 1: A site is chosen randomly from the list *list1* of the unoccupied sites including rejected sites. At $t = 1$, it would be the first growth or nucleation center to grow a cluster. A unique label is given to it as shown in red in Fig. 5.1(a). This will be considered as a single sited active cluster in the next time step. The *list1*, list of unoccupied sites, is modified and the *list2* of the empty perimeter sites is generated.

Step 2: A new growth center is implanted randomly from *list1* and will be labeled (shown in green in Fig. 5.1(b)). The empty NN sites of the active cluster(s) of the previous step in *list2* are now called for occupation with a fixed probability g. A random number $r \in [0, 1]$ is drawn from a uniform distribution for each member of *list2* and compared with g. If $r \leq g$ it is occupied otherwise it is rejected. Once a site is rejected with probability $(1 - g)$, it will not be called again for occupation as a neighbour of the same or another active cluster. However, a growth center can be implanted on a rejected site. Both the lists, *list1* and *list2*, are updated. In Fig. 5.1(b), at $t = 2$, two NN sites of the active cluster are occupied, whether another two sites are rejected, marked by red crosses.

Step 3: At the end of the growth process in each time step, the cluster size distribution is identified and a unique label is given to each cluster. There are now two situations: (1) If all clusters are separated by more than one lattice spacing from each other, the step 2 repeats. (2) If two or more clusters are found separated

by a single lattice spacing from each other, they are merged into a single cluster and marked as a dead cluster. In Fig. 5.1(c), at $t = 3$, two different clusters (grown from the red and the green clusters) separated by a single lattice spacing are now merged and shown in grey in Fig. 5.1(d) at the same time step. Then, step 2 repeats.

The model is studied at several different values of g ranging from 0 to 1 and the nature of PT at each g value is characterized. The model with $g = 0$ naturally corresponds to the Hoshen-Kopelman percolation as the instantaneous area fraction $p(t)$ reaches the OP threshold $p_c(\mathrm{OP}) \approx 0.5927$ and system exhibits a percolation transition. For $g = 0$, the area fraction $p(t)$ at time t is nothing but the number of nucleation centers added per lattice site up to time t whereas for $g \neq 0$, it is the number of occupied sites per lattice site at time t. At smaller values of g (close to 0), small fractal clusters will grow here and there and by coagulation of these small clusters a large spanning cluster is expected to appear that would lead to a continuous transition. On the other hand for higher values of g (close to 1), a large cluster will appear due to the coagulation of compact finite clusters originated from continuously added nucleation centers that would lead to a discontinuous transition with a discrete jump in the spanning cluster size. A smooth crossover from continuous to discontinuous transition is expected to occur as g varies from 0 to 1.

5.2 Results and discussion

Extensive computer simulation of the above model is performed on 2d square lattices of size $L \times L$. The size L of the lattice is varied from $L = 64$ to 1024 in multiple of 2. Clusters are grown applying periodic boundary condition (PBC) in both the horizontal and the vertical directions. All dynamical quantities are stored as function time t, the MC step or the number of nucleation centers added. As there is no control parameter in the system for a given g, time evolution of the cluster properties are finally studied as a function of the corresponding instantaneous area fraction $p(t)$ instead of time t directly in order to compare the results with that of the other models. Averages are made over 2×10^5 to 5×10^3 ensembles as the system size is varied from $L = 64$ to 1024.

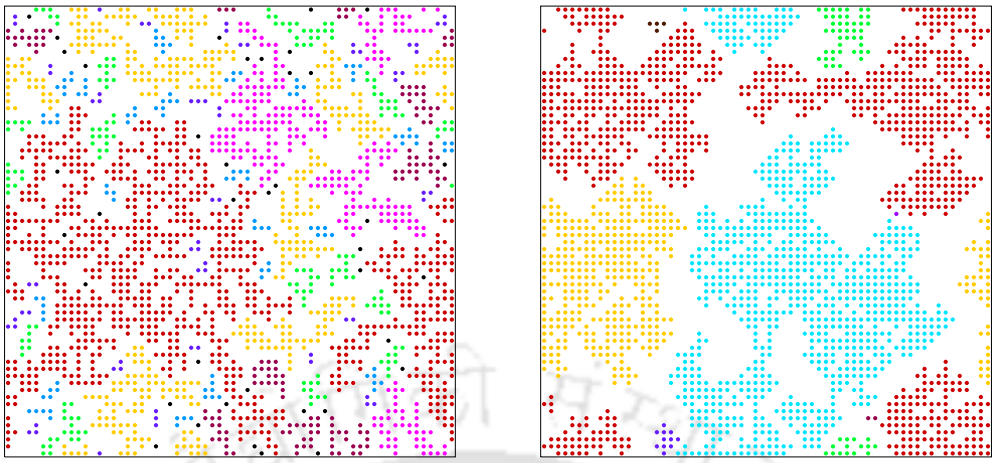

(a) $g = 0.4$, $t = 859$ (b) $g = 0.8$, $t = 75$

Figure 5.2: Snapshots of cluster configurations just before the appearance of a spanning cluster: (a) for $g = 0.4$ at $t = 859$ and (b) for $g = 0.8$ at $t = 75$ on a 2d square lattice of size $L = 64$. The red color shows the largest cluster and other different colors represent the presence of clusters of different sizes. Periodic boundary condition is applied in both horizontal and vertical directions during cluster growth.

5.2.1 Cluster morphology and time evolution of the largest cluster

Snapshots of cluster configurations generated on a 2d square lattice of size $L = 64$ are taken just prior to the appearance of the spanning cluster in the system. The cluster configurations are shown for $g = 0.4$ in Fig. 5.2(a) and for $g = 0.8$ in Fig. 5.2(b). The largest cluster is shown in red and the other smaller clusters of different sizes are depicted in other different colors. At a lower growth probability $g = 0.4$, clusters of many different sizes exist along with a large finite cluster (Fig. 5.2(a)). Several smaller clusters are found to be enclaved inside the larger clusters and the largest cluster becomes fractal. PT occurs in the next step with no significant change in the largest cluster size as the largest cluster in the present step is about to span the lattice. Such continuous change in the size of the largest fractal cluster is found to appear in continuous transition[11,49,162]. On the other hand, as the growth probability is taken to be high $g = 0.8$, clusters of smaller sizes are merged with the fast growing other finite clusters. As a result, only a few large compact clusters are found to exist beside newly planted nucleation centers (Fig. 5.2(b)). Clusters of intermediate sizes are found to be absent. An enclave of smaller clusters within the larger clusters have almost disappeared. The clusters in cyan and red are merged in the next step and generate a compact spanning cluster with a significant increase

in the largest cluster size which might lead discontinuity in the order parameter. The appearance of compact spanning cluster corresponds to discontinuous transitions[42,134,158] and the compactness will be determined by estimating the fractal dimension of the spanning cluster.

The variations of the size of the largest clusters $S_{\text{large}}(t)$ of three different samples are shown against $p(t)$ at $g = 0.4$ in Fig. 5.3(a) and at $g = 0.8$ in Fig. 5.3(b) for a system of size $L = 512$. The average area fractions corresponding to the thresholds at which PT occur in these systems with a given g are marked by the crosses on the respective $p(t)$-axis. Around the respective thresholds, the evolution of the size of

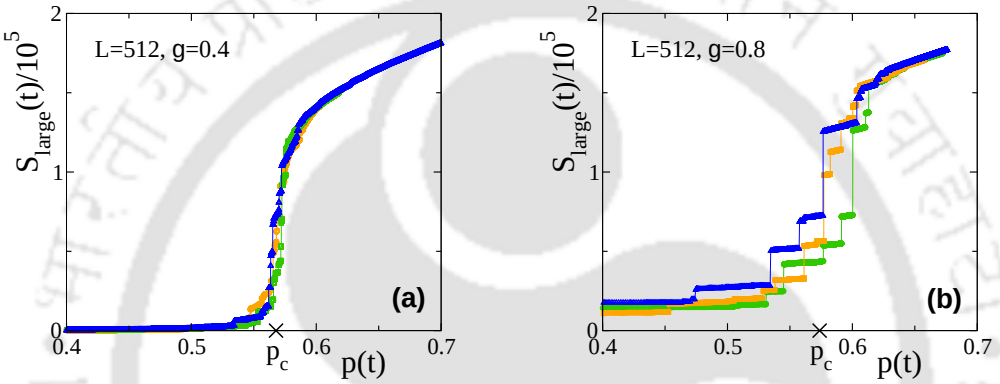

Figure 5.3: Plot of time evolution of the size of the largest cluster $S_{\text{large}}(t)$ for a few samples against the area fraction $p(t)$ for $g = 0.4$ (a) and for $g = 0.8$ (b) for a system of size $L = 512$.

the largest clusters for $g = 0.4$ and $g = 0.8$ are drastically different. For $g = 0.4$, the size of the largest cluster in different samples are found to increase almost continuously with the instantaneous area fraction $p(t)$ around the threshold as it happens in a continuous PT. However, for $g = 0.8$, S_{large} grows with discontinuous jumps and increases drastically with the largest possible jump of the order of 10^5 ($\gg L$) at the threshold. The effect would be more prominent at higher values of g in the systems of higher sizes as expected in a discontinuous PT. However, such drastic jump in S_{large} occurring in individual samples would not be visible if it is averaged over a number of samples on a finite lattice as the jumps since different samples are not occurring exactly at the same $p(t)$. The finite jump in every single sample will make the ensemble averaged order parameter sharper and sharper at the transition point which eventually will lead to a jump like a singularity in the order parameter. Whether the process leads to a discontinuous PT or not for $g \geq 0.8$ then should be identified by determining the critical singularity associated with the order parameter at the transition point as well as by the nature of distribution of

the order parameter. It is then intriguing to study the model varying the growth probability g and characterize the nature of transitions at different regimes of g.

5.2.2 Dynamical finite size scaling

Detailed finite size scaling (FSS) theory is developed in the previous chapters for the static models. The dynamical version of FSS is very similar to the static version. Only the definitions of the dynamical quantities and their scaling relations are kept here. The dynamical order parameter $P_\infty(t)$, the probability to find a lattice site in the spanning cluster at time t, is defined as

$$P_\infty(t) = \frac{S_{\max}(t)}{L^2} \tag{5.1}$$

where $S_{\max}(t)$ is the size of the spanning cluster at time t. Expecting a PT at a critical area fraction $p_c(g)$ for a given growth probability g, the FSS form of $P_\infty(t)$, following the usual continuous percolation theory[11,40], is assumed to be

$$P_\infty(t) = L^{-\beta/\nu}\widetilde{P}_\infty[\{p(t) - p_c(g)\}L^{1/\nu}] \tag{5.2}$$

where $\beta/\nu = d - d_f$, β is the order parameter exponent, ν is the correlation length exponent, d is the space dimension, d_f is the fractal dimension of the spanning cluster and $\widetilde{P}_\infty$ is a scaling function. The distribution of P_∞ is taken as

$$P[P_\infty(t)] = L^{\beta/\nu}\widetilde{P}[P_\infty(t)L^{\beta/\nu}] \tag{5.3}$$

where $\widetilde{P}$ is a scaling function following the formalism of thermal critical phenomena[153] as well as recent models of percolation[39,53]. With such a scaling form of $P[P_\infty(t)]$, one could easily show that

$$\langle P_\infty^2(t)\rangle \sim L^{-2\beta/\nu} \quad \text{and} \quad \langle P_\infty(t)\rangle^2 \sim L^{-2\beta/\nu}. \tag{5.4}$$

The fluctuation in $P_\infty(t)$ at an area fraction $p(t)$ is defined as

$$\chi_\infty(t) = \frac{1}{L^2}\left[\langle S_{\max}^2(t)\rangle - \langle S_{\max}(t)\rangle^2\right]. \tag{5.5}$$

The FSS form of $\chi_\infty(t)$ is given by

$$\chi_\infty(t) = L^{\gamma/\nu}\widetilde{\chi}[\{p(t) - p_c(g)\}L^{1/\nu}] \tag{5.6}$$

where $\gamma/\nu = d - 2\beta/\nu$, γ is the average cluster size exponent and $\widetilde{\chi}$ is a scaling function. The formalism above describes a continuous transition as ν corresponds to the diverging correlation length. However, discontinuous transitions are expected to occur in this model at higher values of g and in such situations ν does not correspond to the correlation length exponent as already observed in several explosive percolation models[111,119]. The same exponent ν is, however, kept throughout the range of g to avoid another notation.

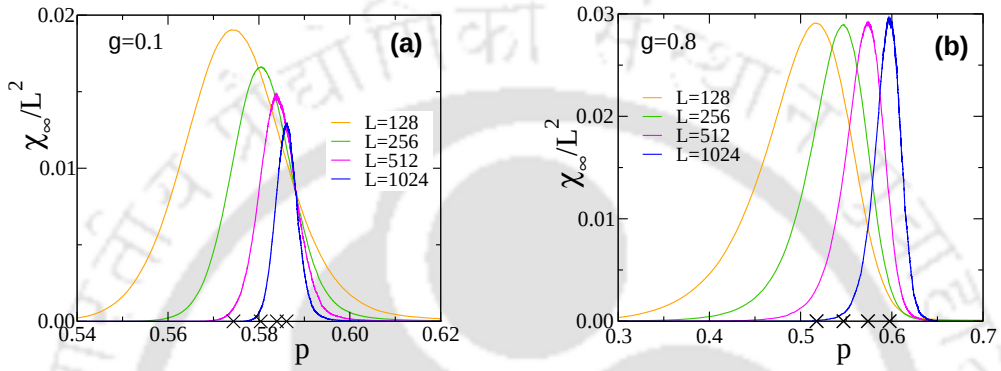

Figure 5.4: Plot of $\chi_\infty(t)/L^2$ against $p(t)$ for $g = 0.1$ (a) and $g = 0.8$ (b) for different lattice sizes L= 128 (orange solid line), 256 (green solid line), 512 (magenta solid line) and 1024 (blue solid line). Crosses on the $p(t)$-axis represent the thresholds $p_c(L)$.

5.2.3 Fluctuation in order parameter

The values of $\chi_\infty(t)$ are obtained for several values of g on lattices of different sizes. In Fig. 5.4, $\chi_\infty(t)/L^2$ is plotted against $p(t)$ for different lattice sizes at two extreme values of g: for $g = 0.1$, it is shown in Fig. 5.4(a) and for $g = 0.8$, it is shown in Fig. 5.4(b). Each plot has a maximum at a certain value of $p(t)$ for a given g and L. The locations of the peaks correspond to the critical thresholds $p_c(L)$ (marked by crosses on the $p(t)$-axis) at which a spanning cluster appears for the first time in the system. The peak values on the other hand varies with L and that would lead to the determination of the exponent γ/ν. First we estimate the values of the exponent γ/ν, then a phase diagram on the percolation threshold $p_c(L)$ and the growth parameter g will be presented. Finally the FSS form will be verified.

Exponent γ/ν: At the threshold, the scaling function $\widetilde{\chi}(0)$ in Eq.5.6 is a constant. Hence, the fluctuation χ_∞ would scale with lattice size L as

$$\chi_\infty(\max) \sim \mathrm{L}^{\gamma/\nu}. \tag{5.7}$$

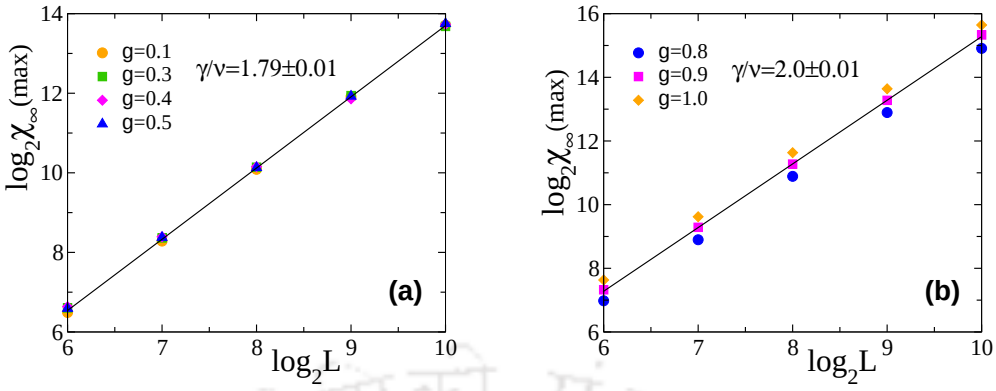

Figure 5.5: Plot of $\chi_\infty(\max)$ against L for $g \leq 0.5$ (a) and for $g \geq 0.8$ (b). The straight lines of slope $\gamma/\nu = 1.79$ and $\gamma/\nu = 2.0$ in (a) and (b) respectively are guide to eye.

In order to extract the exponent γ/ν at a given value of g, the peak values of the fluctuation $\chi_\infty(\max)$ are plotted against L for $g \leq 0.5$ in Fig. 5.5(a) and for $g \geq 0.8$ in Fig. 5.5(b) in double logarithmic scale. The magnitudes of $\chi_\infty(\max)$ are found to be independent of g at a given L for $g \leq 0.5$ whereas they increase with g at a given L for $g \geq 0.8$. The exponent γ/ν is determined by linear least square fit through the data points. For $g \leq 0.5$, it is found to be $\gamma/\nu = 1.79 \pm 0.01$ whereas for $g \geq 0.8$, it is found to be $\gamma/\nu = 2.0 \pm 0.01$. The solid straight lines with desire slopes in Fig. 5.5(a) and (b) are guide to eye. It is important to note that the value of γ/ν for $g \leq 0.5$ is that of the OP (43/24) which corresponds to continuous transitions whereas for $g \geq 0.8$ it is that of the space dimension as it appears in discontinuous transitions[42,121]. For $0.5 < g < 0.8$, the exponent γ/ν is found to change continuously from 1.79 to 2.0 that defines a region of crossover. The values of γ/ν for different values of g are also confirmed by estimating the average cluster size of all the finite clusters (excluding the spanning cluster) at their respective percolation thresholds. However, there are evidences in some other percolation models such as k-core percolation[163] that the scaling behavior of order parameter fluctuation and that of the average cluster size are not identical.

Phase diagram and Percolation threshold: A phase diagram separating the percolating and non-percolating regions is obtained by plotting the variation of $p_c(L)$ against g for a system of size $L = 1024$ in Fig. 5.6. The phase line starts at $p_c(L) \approx 0.6$ and $g = 0$, has a dip at $g = 0.65$ then increases almost linearly with g. It is obvious that the area fraction would be ≈ 0.6 at the criticality for $g = 0$ as this corresponds to OP. If g is finite but small, the growth of small clusters will stop mostly because of less growth probability besides rarely merging with another small cluster or a newly added nucleation center. A large number of smaller clusters will be

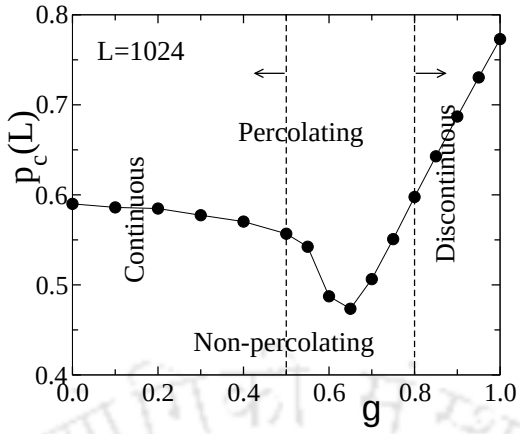

Figure 5.6: Plot of $p_c(L)$ against g for $L = 1024$. The line joining the data points separates the percolating region from the non-percolating region. The dotted lines with arrow towards left and towards right denote the regions of continuous and discontinuous transitions respectively.

there in the system before transition and merging of such small cluster will lead to a spanning cluster which will have many voids in it. As a result, the area fraction will be less. Such an effect will be more predominant when g is around the percolation threshold of OP as at this growth probability large fractal clusters will be grown. PT occurs due to the merging of such large fractal clusters which will contain maximum void space in it. Hence, the area fraction is expected to be the lowest around p_c(OP). It is interesting to note that the critical area fraction has a minimum, as low as ≈ 0.45, at a growth probability $g = 0.65$ little above the critical threshold of OP (≈ 0.5927). Beyond such growth probability, compact clusters start appearing which will occupy most of the space at the time of transition. Area fraction will increase almost linearly with g in this regime. Such variation of p_c is also observed in a percolation model with a repulsive or attractive rule in site occupation[164]. Moreover, the region left to the vertical dashed lines at $g = 0.5$ corresponds to $\gamma/\nu = 1.79$ as that of usual continuous PT whereas the region right to the vertical dashed line at $g = 0.8$ corresponds to $\gamma/\nu = 2.0$ as that of a discontinuous PT. In the intermediate region, though the transitions are continuous they do not belong to the same universality class of OP.

The critical area fraction $p_c(L)$ is expected to scale with the system size L as

$$p_c(L) - p_c(g) \approx L^{-1/\nu} \tag{5.8}$$

in case of continuous PT as in OP[11]. In the limit $L \to \infty$, the value of $p_c(L)$ should correspond to $p_c(g)$, the percolation threshold of the model for a given g.

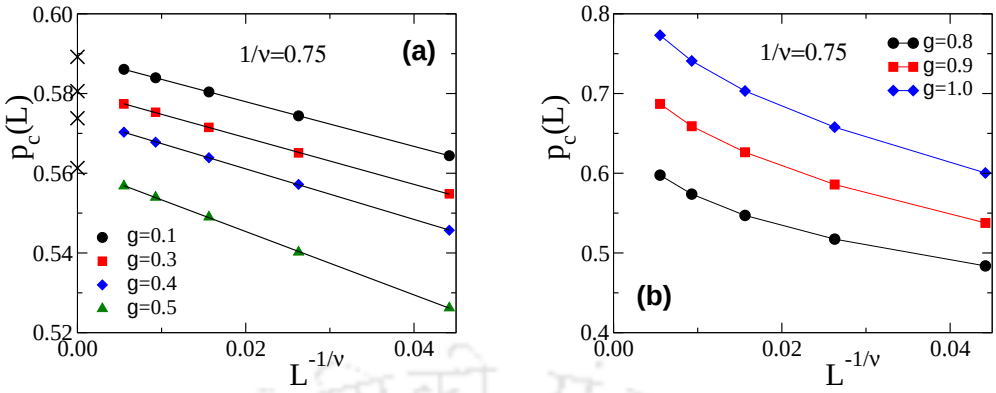

Figure 5.7: Plot of $p_c(L)$ against $L^{-1/\nu}$ taking $1/\nu = 0.75$, for $g = 0.1(\bullet)$, $0.3(\blacksquare)$, $0.4(\blacklozenge)$, $0.5(\blacktriangle)$ in (a) and for $g = 0.8(\bullet)$, $g = 0.9(\blacksquare)$, $1.0(\blacklozenge)$ in (b).

In Figs. 5.7, $p_c(L)$ is plotted against $L^{-1/\nu}$ taking $1/\nu = 0.75$, that of the OP, for $g \leq 0.5$ in (a) and for $g \geq 0.8$ in (b). The scaling form given in Eq.5.8 is found to be well satisfied for $g \leq 0.5$ with $1/\nu = 0.75$ and the plots intersect the $p_c(L)$-axis at different $p_c(g)$ values as seen in Fig. 5.7(a). Whereas for $g \geq 0.8$, since γ/ν is different from that of OP, the data do not obey Eq.5.8 with $1/\nu = 0.75$ as that of OP, shown in Fig. 5.7(b). As it is already mentioned in the previous chapter that in equilibrium thermal discontinuous phase transitions the difference of the size dependent critical point from the true critical point scales with the system size as $1/L^d$ where d is the space dimension[59,157], it is rarely observed in non-equilibrium discontinuous PTs[100,121,128]. It is verified that the plots neither found to be linear when plotted against L^{-2}. Tuning the exponent $1/\nu$ to certain smaller values that depend on g (for $g \geq 0.8$) the linearity in the plot might be obtained. However, such small values of $1/\nu$ will correspond to $p_c(g)$ far beyond the critical point at which a connected phase trivially occurs with almost a fully occupied lattice. As the FSS ansatz given in Eq.5.8 found to not valid for $g \geq 0.8$, the numerical value of $1/\nu$ will be then determined later by performing FSS analysis of $\chi_\infty(t)$ corresponding to the best possible collapse in this regime.

FSS of $\chi_\infty(t)$: The FSS form of $\chi_\infty(t)$ is verified plotting the scaled fluctuation $\chi_\infty(t)/L^{\gamma/\nu}$ against the scaled variable $[p(t) - p_c(g)]L^{1/\nu}$ for $g = 0.1$ in Fig. 5.8(a). For $g = 0.1$, a good collapse of data is obtained with $\gamma/\nu = 1.79$ and $1/\nu = 0.75$ as those of OP. Since no $p_c(g)$ can be identified for $g \geq 0.8$, FSS of $\chi_\infty(t)$ is performed against the scaled variable $[p(t) - p_c(L)]L^{1/\nu}$ replacing $p_c(g)$ by the size dependent threshold $p_c(L)$. For $g = 0.8$, $\chi_\infty(t)/L^{\gamma/\nu}$ is plotted against $[p(t) - p_c(L)]L^{1/\nu}$ in Fig. 5.8(b) taking $\gamma/\nu = 2.0$ for a discontinuous transition[42,165]. The best possible collapse is obtained by tuning the value of $1/\nu$ to 0.5 as in Bohman-Frieze-Wormald

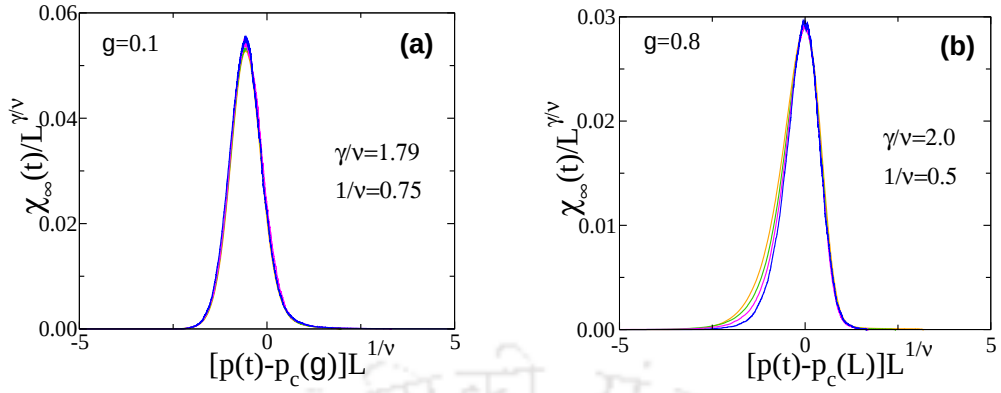

Figure 5.8: Plot of $\chi_\infty(t)/L^{\gamma/\nu}$ against the scaled variable $[p(t)-p_c(g)]L^{1/\nu}$ for $g = 0.1$ (a) and against $[p(t)-p_c(L)]L^{1/\nu}$ for $g = 0.8$ (b) respectively.

model of EP[100] which represents a first-order transition. Such collapse for all other values of $g > 0.8$ is also found to occur for $\gamma/\nu = 2.0$ and $1/\nu = 0.5$. However, the plots of $p_c(L)$ against $1/L^{0.5}$ are not found to be linear possibly due to higher order corrections to scaling[111]. The collapse of the peak values confirms the values of the scaling exponent γ/ν as 1.79 for $g \leq 0.5$ corresponding to continuous transition and 2.0 for $g \geq 0.8$ corresponding to discontinuous transition.

5.2.4 Dimension of spanning cluster

For the system size $L \ll \xi$, the size of the spanning cluster $S_{\max}$ at the criticality varies with the system size L as

$$S_{\max} \approx L^{d_f} \tag{5.9}$$

where d_f is the fractal dimension of the spanning cluster. Since the clusters are grown here applying PBC, the horizontal and vertical extensions of the largest cluster are stored. If either the horizontal or the vertical extension of the largest cluster is found to be greater than or equal to L, it is identified as a spanning cluster. The value of $S_{\max}$ are noted at the respective thresholds for several lattice sizes L for a given g. For a continuous PT, the spanning cluster is a random object with all possible sizes of holes in it and is expected to be fractal whereas in the case of a discontinuous transition it becomes a compact cluster whose size is expected to scale with the system size as L^d where d is the space dimension[39,119]. The values of $S_{\max}$ are plotted against L in double logarithmic scale for the different values of $g \leq 0.5$ in Fig. 5.9(a) and for $g \geq 0.8$ in Fig. 5.9(b). For $g \leq 0.5$, $S_{\max}$ scales with L as a power law with $d_f = 1.895 \pm 0.002$ almost that of OP (91/48). On the other

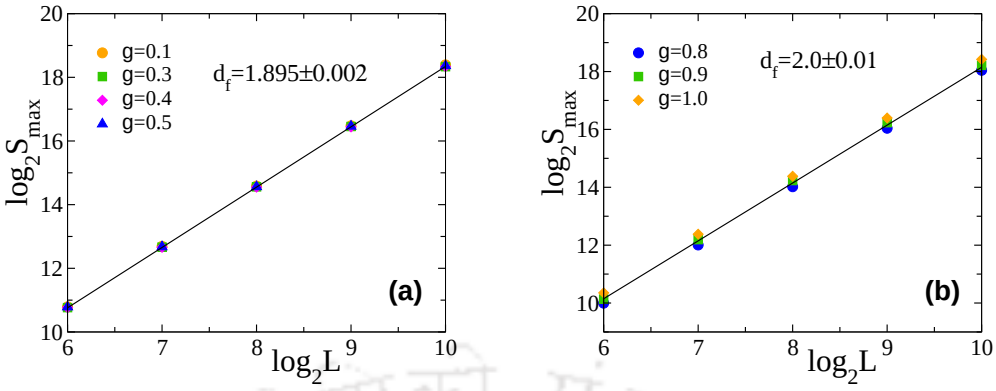

Figure 5.9: Plot of $S_{\max}$ against lattice size L at their respective thresholds for $g \leq 0.5$ (a) and for $g \geq 0.8$ (b). The solid straight line of slope 1.896 in (a) and that of slope 2.0 in (b) are guide to eye.

hand, for $g \geq 0.8$, $S_{\max}$ scales with L as a power law with $d_f = 2.0 \pm 0.01$ as that of the space dimension d. The solid lines with desire slopes 1.896 and 2.0 in Fig. 5.9(a) and (b) respectively are guide to eye. Thus for $g \leq 0.5$, the spanning cluster is found to be fractal as in OP whereas for $g \geq 0.8$ it is compact as expected in a discontinuous transition. As a result, there would be enclaves in spanning clusters for $g \leq 0.5$ whereas such enclaves would be absent in the spanning clusters for $g \geq 0.8$ as it is evident in the cluster morphology shown in Fig. 5.2. Such presence or absence of enclaves in the spanning cluster determines whether it would be fractal or compact which essentially determines the nature of the transition as continuous or discontinuous[49,158]. In the regime $0.5 < g < 0.8$ the dimension of spanning cluster d_f changes continuously from $d_f = 1.895$ to $d_f = d = 2.0$.

5.2.5 FSS study of $P_\infty(t)$

Following the scaling relations $\gamma/\nu = d - 2\beta/\nu$ and $d_f = d - \beta/\nu$, the exponent β/ν is found to be ≈ 0.105 as that of continuous PT in OP (5/48) for $g \leq 0.5$ and 0 as that of a discontinuous PT for $g \geq 0.8$. Like previous chapters, the FSS form of

$$P_\infty(t) = L^{-\beta/\nu} \widetilde{P}_\infty[\{p(t) - p_c(g)\}L^{1/\nu}]$$

will be now verified taking the respective values of β/ν and $1/\nu$ in these regimes of g instead of direct measurement of the exponent β/ν. Variation of $P_\infty(t)$ is plotted against $p(t)$ for different lattice sizes for $g = 0.1$ in Fig. 5.10(a) and for $g = 0.8$ in Fig. 5.10(b). As the system size L increases, $P_\infty(t)$ becomes sharper and sharper for both $g = 0.1$ and $g = 0.8$. However, the plots of P_∞ have longer tails for

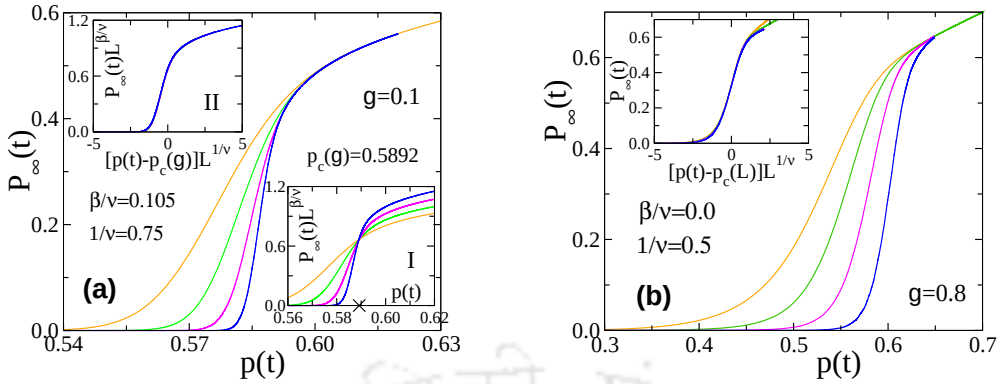

Figure 5.10: Plot of $P_\infty(t)$ against $p(t)$ for $g = 0.1$ (a) and $g = 0.8$ (b). In the inset-I of (a), $P_\infty(t)L^{\beta/\nu}$ is plotted against $p(t)$ taking $\beta/\nu = 0.105$ and in the inset-II of (a) it is plotted against the scaled variable $[p(t) - p_c(g)]L^{1/\nu}$ taking $1/\nu = 0.75$. In the inset of (b), $P_\infty(t)$ is plotted against $[p(t) - p_c(L)]L^{1/\nu}$ taking $1/\nu = 0.5$ as $\beta/\nu = 0$ for $g = 0.8$. Same set of color symbols of Fig. 5.4 for different system sizes are used.

$g \geq 0.8$ than the plots P_∞ for $g \leq 0.5$. This is expected because the value of $1/\nu$ is smaller for $g \geq 0.8$ than that of $g \leq 0.5$. To observe much sharper transition one needs to consider one order of magnitude higher lattice size than the considered one. Moreover, for $g = 0.1$, the plots of $P_\infty(t)L^{\beta/\nu}$ cross at a particular value of $p(t)$ corresponding to the critical threshold $p_c(g)$ taking $\beta/\nu = 0.105$ as shown in inset-I of Fig. 5.10(a). As $\beta/\nu = 0$ for $g = 0.8$, by no means they could make cross at a definite $p(t)$. For $g = 0.1$, a complete collapse of the plots is obtained by re-scaling both the axes taking $\beta/\nu = 0.105$ and $1/\nu = 0.75$ as shown in inset-II of Fig. 5.10(a). As $\beta/\nu = 0$ for $g \geq 0.8$, the collapse of $P_\infty(t)$ plots for $g = 0.8$ are obtained by re-scaling the $p(t)$ axis only by $[p(t) - p_c(L)]L^{1/\nu}$ taking $1/\nu = 0.5$ as shown in the inset of Fig. 5.10(b). Such collapse of data not only confirms the validity of the scaling forms assumed but also confirms the values of the scaling exponents obtained. The observations at $g = 0.1$ are found to be the same for all $g \leq 0.5$ and those are at $g = 0.8$ are same for $g \geq 0.8$. Though discontinuous jump in the order parameter is also observed in SFM, the PT is characterized as continuous[161]. On the other hand, in GCM, discontinuous transition is found to occur only in the vanishingly small fixed initial seed concentration[144] but for intermediate seed concentrations the transitions are found to continuous that belong to OP universality class[145,151]. For $0.5 < g < 0.8$, collapse of data is observed for continuously varied exponents β/ν that depend on g as also seen in other EP models[166,167].

The variations of the critical exponents γ/ν, β/ν and fractal dimension d_f with the growth probability g are presented in Fig. 5.11. The values of the critical exponents clearly distinguishes the discontinuous transitions for $g \geq 0.8$ from the

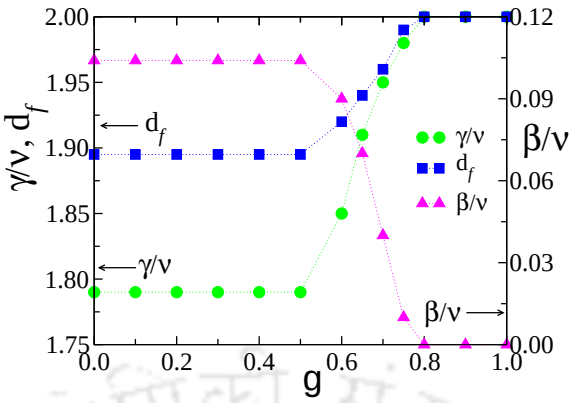

Figure 5.11: Plot of the values of γ/ν (green circle), β/ν (magenta triangle), and d_f (blue square) against the growth probability g.

continuous transitions for $g \leq 0.5$.

5.2.6 Binder cumulant

The evidences presented above shows a continuous transition for $g \leq 0.5$ and a discontinuous transition for $g \geq 0.8$. In order to confirm the order of transition in different regimes of the growth probability g, a dynamical Binder cumulant $B_L(t)$ [165,168], the fourth moment of $S_{\max}(t)$, is studied as function of area fraction $p(t)$. The dynamical Binder cumulant $B_L(t)$ is defined as

$$B_L(t) = \frac{3}{2}\left[1 - \frac{\langle S^4_{\max}(t)\rangle}{3\langle S^2_{\max}(t)\rangle^2}\right]. \tag{5.10}$$

The cumulants when plotted against the area fraction $p(t)$ for different system sizes L are expected to cross each other at a definite $p(t)$ corresponding to the critical threshold of the system for a continuous transition whereas no such crossing is expected to occur in the case of a discontinuous transition [39]. Though the cumulant has some unusual behavior [169,170], it is rarely used in the study of recent models of percolation. The values of $B_L(t)$ are plotted against $p(t)$ for different system sizes L in Fig. 5.12(a) for $g = 0.1$ and in Fig. 5.12(b) for $g = 0.8$. For $g = 0.1$, the plots of $B_L(t)$ cross at a particular $p(t)$ corresponding to $p_c(g)$, marked by a cross on the $p(t)$-axis whereas for $g = 0.8$ no such crossing of $B_L(t)$ is observed for different values of L. The value of the Binder cumulant at the critical threshold $B_L(p_c)$ is found to be 0.945 as shown by a dotted line in Fig. 5.12(a) for $g = 0.1$ and remains close to this for other values of $g \leq 0.5$. It is verified that the value of $B_L(p_c)$ is same as that of original site percolation though a little lesser value is reported for

the bond percolation[159].

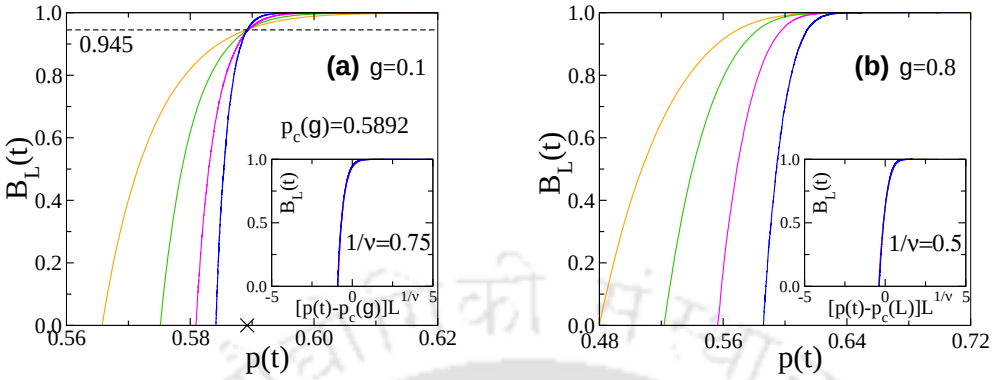

Figure 5.12: Plot of $B_L(t)$ against $p(t)$ for different L for $g = 0.1$ (a) and for $g = 0.8$ (b). The same color symbols of Fig. 5.4 for different L are used. Plot of $B_L(t)$ against $[p(t) - p_c(g)]L^{1/\nu}$ is given in the inset of (a) and against $[p(t) - p_c(L)]L^{1/\nu}$ is given in the inset of (b) taking appropriate values of $1/\nu$.

The FSS form of $B_L(t)$ is given by

$$B_L(t) = \widetilde{B}[(p(t) - p_c)L^{1/\nu}] \tag{5.11}$$

where $\widetilde{B}$ is a universal scaling function. The FSS form is verified by obtaining a collapse of the plots of $B_L(t)$ against the scaled variable $[p(t) - p_c(g)]L^{1/\nu}$ taking $1/\nu = 0.75$ for $g = 0.1$. For $g = 0.8$, however, such a collapse is obtained when the cumulants are plotted against $[p(t) - p_c(L)]L^{1/\nu}$ taking $1/\nu = 0.5$. The data collapse is shown in the insets of the respective plots. Such scaling behavior of $B_L(t)$ for $g = 0.1$ is found to occur for the whole range of $g \leq 0.5$ and that of $g = 0.8$ is found to occur for $g \geq 0.8$. Once again, Binder cumulant provides a strong evidence that the dynamical transition is continuous for $g \leq 0.5$ whereas it is discontinuous for $g \geq 0.8$. For $0.5 < g < 0.8$, a region of crossover, the cumulants do not cross at a particular value of $p(t)$ rather they cross each other over a range of $p(t)$ values but do collapse when plotted against the scaled variable $[p(t) - p_c(L)]L^{1/\nu}$ for the respective value of $1/\nu$ for a given value of g.

5.2.7 Cluster size distributions

Power law distribution of cluster sizes at the critical threshold is an essential criteria in a second-order continuous phase transition. Following OP, a dynamical cluster size distribution $n_s(t)$, the number of clusters of size s per lattice site at time t, is

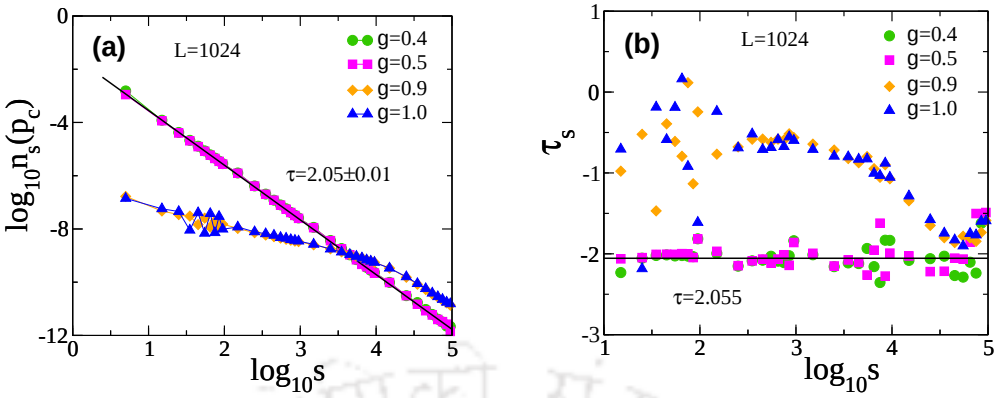

Figure 5.13: (a) Plot of $n_s(p_c)$ against s for different values of $g = 0.4$[●] (green), 0.5[■] (magenta), 0.9[♦] (orange) and 1.0[▲] (blue) for $L = 1024$. The solid black line with slope 187/91 is guide to eye. (b) Plot of the variation of the local slope τ_s against s for the same set of g values. The solid black line with slope 2.055 is guide to eye.

assumed to be

$$n_s(t) = s^{-\tau} \mathsf{f}[(p(t) - p_c)s^{\sigma}] \tag{5.12}$$

where τ and σ are two exponents and f is a universal scaling function. For OP, an equilibrium percolation model, the exponents are $\tau = 187/91$ and $\sigma = 36/91$[11]. The distribution at the percolation threshold $n_s(p_c)$ is expected to scale as $\approx s^{-\tau}$. The cluster size distributions $n_s(p_c)$ are determined taking $p_c(g)$ as threshold for $g \leq 0.5$ and taking $p_c(L)$ as threshold for $g \geq 0.8$ for a system of size $L = 1024$. The data obtained are binned of varying widths and finally normalized by the respective bin widths. In Fig. 5.13(a), the distributions $n_s(p_c)$ are plotted against s in double logarithmic scale for $g = 0.4$ (green circles), 0.5 (magenta squares), 0.9 (orange diamonds) and 1.0 (blue triangles)) for $L = 1024$. It is clearly evident that the distributions for $g \leq 0.5$ describes a power law behavior whereas for $g \geq 0.8$ the distributions develop curvature and deviate from power law scaling. The black solid line with slope $\tau = 187/91$ as that of OP drawn over the data points for $g \leq 0.5$ is a guide to eye. The exponent τ measured by linear least square fit to the data points of $g \leq 0.5$ is found to be 2.05 ± 0.01 as that of OP. Whereas no definite value of τ can be obtained for $g > 0.5$. In Fig. 5.13(b), the measured exponent $\tau_s = \partial \log_{10} n_s(p_c)/\partial \log_{10} s$ is plotted against $\log_{10} s$ for those g values. The value of τ_s remains constant to ≈ 2.055 as that of OP over a wide range of s for $g \leq 0.5$ whereas τ_s varies with s for $g \geq 0.8$ indicating no definite value of τ. Thus, a crossover from continuous transition of OP type with power law distribution of cluster sizes to a discontinuous percolation transition without power law distribution of cluster sizes in the different regimes of the growth probability g is found to occur

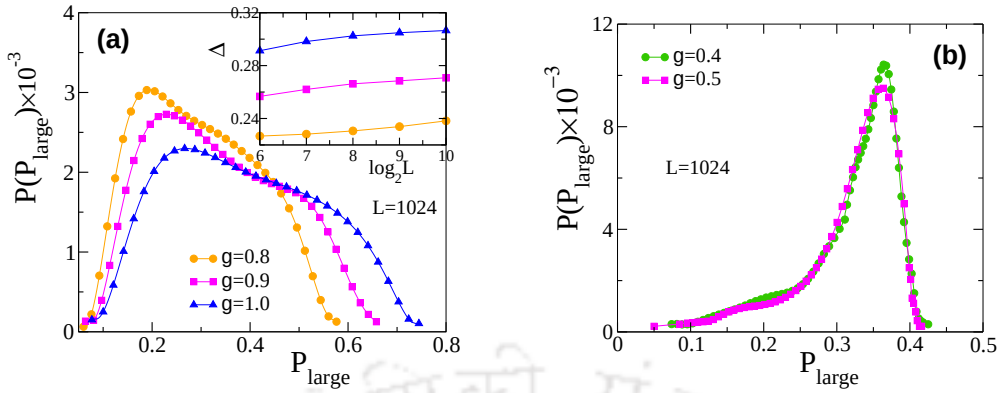

Figure 5.14: (a) Plot of $P(P_{\text{large}})$ against P_{large} for different values of $g = 0.8$[●] (orange), 0.9[■] (magenta) and 1.0[▲] (blue) for $L = 1024$. In the inset of Fig. (a), plot of Δ against L for $g = 0.8$[●] (orange), 0.9[■] (magenta) and 1.0[▲] (blue). (b) Plot of $P(P_{\text{large}})$ against P_{large} for $g = 0.4$[●] (green), 0.5[■] (magenta) and same L.

in this model. This is in contrary to the observations in SFM[161] or cluster merging model[50] where a power law distribution of clusters size is found to occur beside discontinuous transition.

5.2.8 Order parameter distributions

Beside the cluster size distribution, distribution of order parameter is also studied for different values of g as usually it is studied in thermal phase transitions[153]. A bimodal distribution of order parameter is expected in a discontinuous transition corresponding to coexisting phases whereas a single peaked distribution is expected in a continuous transition. An ensemble of largest clusters on different configurations are collected at the percolation threshold of a given g and the values of the order parameter $P_{\text{large}} = S_{\text{large}}/L^2$ are estimated. A probability distribution $P(P_{\text{large}})$ is then defined as

$$P(P_{\text{large}}) \sim L^{\beta/\nu} \widetilde{P}[P_{\text{large}} L^{\beta/\nu}] \tag{5.13}$$

where $\widetilde{P}$ is a scaling function. Bimodal nature of $\widetilde{P}$ is found to be a powerful tool to distinguish discontinuous transitions from continuous transitions in some of the recent percolation models[39,53,117,119]. The distributions of $P(P_{\text{large}})$s are plotted against P_{large} in Fig. 5.14(a) for $g = 0.8$ (circles), 0.9 (squares) and $g = 1.0$ (triangles) and in Fig. 5.14(b) for $g = 0.4$ (circles), 0.5 (squares). For $g \geq 0.8$, though not sharp but a broad distribution with two weak peaks for $\widetilde{P}$s are obtained. Such broad bimodal distributions of order parameter are also found in the study of mechanical yield in amorphous solids that represents a first-order transition[135]. No

FSS of the distributions is found as given Eq.5.13 but the width of the distribution $\Delta = 2[\langle P^2_{\text{large}}\rangle - \langle P_{\text{large}}\rangle^2]^{1/2}$ for a given g is found to increase with the system size L, shown in the inset of Fig. 5.14(a), as a signature of discontinuous transition. For a given L, the width of the distributions Δ is also found to increase with g. However, the distributions $P(P_{\text{large}})$ for $g \leq 0.5$ are found to be single-humped and follow the scaling form given in Eq.5.13 as shown in the other inset. The width of the distributions for a given $g \leq 0.5$ is found to decrease with L. The model, thus, exhibits characteristic properties of discontinuous transition for $g \geq 0.8$ and those of continuous transition for $g \leq 0.5$. Since no sharp double humped distribution is obtained for $g \geq 0.8$, discontinuous transitions occurring can be termed as a weak first-order transition.

5.3 Conclusion

A random cluster growth lattice filling percolation model with touch and stop rule is developed. As the growth probability, g is tuned from 0 to 1, a crossover from continuous to discontinuous PT is observed in this model. For $g \leq 0.5$, the order parameter continuously goes to zero and the geometrical quantities follow the usual FSS at the critical threshold with the critical exponents that of OP. The cluster size distribution is found to be scale-free and a single-humped distribution of order parameter is found to occur in this regime of g. On the other hand, for $g \geq 0.8$, the PT occurs with a discontinuous jump at the threshold, the order parameter fluctuation per lattice site becomes independent of system size, the spanning cluster becomes compact with fractal dimension $d_f = 2$ as that of discontinuous transitions. No scale-free distribution is found for the cluster sizes and the order parameter distribution is given by a broad double humped distribution of increasing width with the system size. The discontinuous transition observed here can be termed as a weak first-order transition. The occurrence of the true first-order transition should be verified in the thermodynamic limit. The order of transitions in different regimes of g is further confirmed by the estimates of Binder cumulant. The intermediate regime of growth probability $0.5 < g < 0.8$ remains a region of crossover without a definite tricritical point.

Chapter 6

Summary and Conclusion

In this thesis, a search of discontinuous first-order percolation transition has been performed with simple toy models. The search started with a new two-parameter equilibrium constant growth percolation model. Complexities such as suppression in the growth of the clusters or preferential growth of clusters are incorporated in a controlled manner in order to identify the criteria for discontinuous transition to occur in a geometrical model like percolation which is known to exhibit a robust second order continuous transition. In total, three equilibrium models and one non-equilibrium percolation model are developed. The models are studied via extensive numerical computation. Out of the three equilibrium models, only the two-parameter preferential growth model could exhibit a discontinuous transition in the low initial seed concentration limit. Though the constant growth model is found to belong to the same universality class of original percolation (OP), the suppressed cluster growth model however, deviates from that in the low initial seed concentration. The non-equilibrium growth model of percolation exhibits a novel critical behaviour and in the limit of high growth rate, a weak first-order transition is observed. Appropriate scaling theories are developed and verified. Below we provide a brief chapter wise summary.

In chapter 2, a new two-parameter percolation model (TPPM) with the simultaneous growth of multiple clusters is developed in order to expand the parameter space of original percolation model as well as to incorporate partial hindrance in growing a cluster due to the presence of other clusters. There are two tunable parameters, the initial seed concentration ρ and the cluster growth probability g. A phase line of second-order continuous phase transition points is found to separate the $\rho - g$ parameter space into a connected region and disconnected regions. A scaling theory of such percolation transition (PT) involving ρ and g is proposed and

verified numerically. Though the scaling variable is found to be modified by the presence of ρ, the values of the critical exponents describing the scaling functions at the criticality are found to be that of the original percolation for all values of ρ. Hence, all such transitions are continuous second order transitions and belong to the same universality class of the original percolation model. No discontinuous percolation transition is found may be because the partial hindrance due to the presence of other clusters remains a weak effect in an overall random growth process.

An improved version of TPPM incorporating suppression in cluster growth process is developed and studied in chapter 3. The suppressed growth percolation model is studied extensively developing a novel finite size scaling hypothesis and the results are compared with those of the previous constant growth model. Two regimes of the initial seed concentration are found to exist. For $\rho \geq 0.2$, the values of the critical exponents describing the scaling functions at the criticality are found to be that of ordinary percolation. Hence, all such transitions are continuous and belong to the same universality class of ordinary percolation. On the other hand, for $\rho < 0.2$, suppression of the growth of larger clusters seems to have a certain effect on the critical properties. The transitions though are found to be continuous, the values of the critical exponents are found to deviate from those of the OP model. Hence, the model is found to belong in new universality classes. However, such an effect is not found to be strong enough to change the order of transition apart from the fact that the cluster size distribution develops curvature and the order parameter distribution broadens in the limit $\rho \to 0$. Though no discontinuous percolation transition is found in this model, the broadening of the order parameter distribution in this model in the dilute limit of ρ indicates a possibility of obtaining a bimodal distribution of the order parameter corresponding to a first-order transition under stronger suppression of the growth of the larger clusters.

In chapter 4, the model TPPM is further improved incorporating stronger preferential growth of clusters following usual spanning cluster approach of original percolation. Depending on the initial seed concentration ρ, the model finally is found to exhibit distinctly first-order transitions for $\rho \leq 0.05$ and continuous percolation transitions for $\rho > 0.45$. The continuous transitions are found to belong to the same universality class of OP. The first-order transitions, however, are characterized by a discontinuous jump in the order parameter, the coexistence of spanning and non-spanning large clusters, and the appearance of compact spanning clusters. A compact spanning cluster in this region is an outcome of merging of the compact finite clusters that were grown with probability $g_0 \gg p_c$ of OP. The region of co-

existence is found to be confined within a double-humped bimodal distribution of the order parameter. In the intermediate range of $0.05 < \rho < 0.45$, the nature of percolation transition still remains inconclusive as the characteristic features of both continuous and discontinuous percolation transitions appear concurrently and can only be resolved in the true thermodynamic limit. After Bootstrap percolation, TPPM with preferential growth is another equilibrium percolation model where first-order transitions occur.

A random cluster growth lattice filling percolation model with touch and stop rule is developed in chapter 5. As the growth probability g is tuned from 0 to 1, a crossover from continuous to discontinuous PT is observed in this model. For $g \leq 0.5$, the order parameter continuously goes to zero and the geometrical quantities follow the usual FSS at the critical threshold with the critical exponents that of OP. The cluster size distribution is found to be scale free and a single humped distribution of order parameter is found to occur in this regime of g. On the other hand, for $g \geq 0.8$, the PT occurs with a discontinuous jump at the threshold, the order parameter fluctuation per lattice site becomes independent of system size, the spanning cluster becomes compact with fractal dimension $d_f = 2$ as that of discontinuous transitions. No scale free distribution is found for the cluster sizes. Though the order parameter distribution is not given by a sharp a double humped distribution but found to be a broad double humped distribution of increasing width with the system size. Hence the transitions are weak first-order transitions. The order of transitions in different regimes of g are further confirmed by the estimates of Binder cumulant. The intermediate regime of growth probability $0.5 < g < 0.8$ remains a region of crossover without a definite tricritical point.

The evidences of the different order of phase transitions in the thesis, the models are investigated via extensive numerical simulations. The scaling behaviour developed for these models are rigorously verified performing scaling analysis on the largest lattice as well as performing finite size scaling analysis. The first order transitions in all these models are justified by the presence of phase coexistence, bimodal distribution of the order parameter, compact spanning cluster, constant per lattice site fluctuation in order parameter, etc. whereas the second-order transitions are characterized by the power law distribution of cluster sizes and a definite set of critical exponents which satisfy usual scaling relations among them. The order of transition is further verified by estimating Binder cumulant in each case.

To conclude, the study in this thesis is able to identify criteria for the first-order transition in percolation such as correlated growth, the rapid growth of smaller clus-

ters than the larger clusters beside nucleation and overall growth. The models can be generalized in many different contexts where a discontinuous or abrupt transition occurs in physical sciences or nature.

Bibliography

[1] S. R. Broadbent and J. M. Hammersley, Proc. Cambridge Phill. Soc. **53**, 629 (1957).

[2] P. J. Flory, J. Am. Chem. Soc. **63**, 3083, 3091, 3906 (1941).

[3] C. Domb, Nature **184**, 509 (1959).

[4] P. R. King, S. V. Buldyrev, N. V. Dokholyan, S. Havlin, Y. Lee, G. Paul, and H. E. Stanley, Physica A **274**, 60 (1999).

[5] J. L. Cardy and P. Grassberger, J. Phys. A **18**, L267 (1985).

[6] R. Cohen, D. ben Avraham, and S. Havlin, Phys. Rev. E **66**, 036113 (2002).

[7] H. J. Herrmann and S. Roux, editors, *Statistical Models for the Fracture of Disordered Media*, North-Holland, 1990.

[8] Z. Ball, H. M. Phillips, D. L. Callahan, and R. Sauerbrey, Phys. Rev. Lett. **73**, 2099 (1994).

[9] H. E. Roman, A. Bunde, and W. Dieterich, **34**, 3439 (1986).

[10] M. Sahimi, *Applications of Percolation Theory*, Taylor and Francis, London, 1994.

[11] D. Stauffer and A. Aharony, *Introduction to Percolation Theory*, Taylor and Francis, London, 2nd edition, 1994.

[12] P. W. Kasteleyn and C. M. Fortuin, J. Phys. Soc. Jpn. **26**, 11 (1969).

[13] C. Fortuin and P. Kasteleyn, Physica **57**, 536 (1972).

[14] M. P. M. den Nijs, Journal of Physics A: Mathematical and General **12**, 1857 (1979).

[15] H. E. Stanley, *Introduction to Phase Transitions and Critical Phenomena*, Oxford University Press, New York, 1971.

[16] K. Binder, Reports on Progress in Physics **50**, 783 (1987).

[17] H. J. Herrmann, Journal of Physics: Conference Series **681**, 012003 (2016).

[18] N. Araújo, P. Grassberger, B. Kahng, K. Schrenk, and R. Ziff, The European Physical Journal Special Topics **223**, 2307 (2014).

[19] A. Saberi, Physics Reports **578**, 1 (2015).

[20] S. Boccaletti et al., Physics Reports **660**, 1 (2016).

[21] D. S. Callaway, J. E. Hopcroft, J. M. Kleinberg, M. E. J. Newman, and S. H.

Strogatz, Phys. Rev. E **64**, 041902 (2001).
[22] P. S. Dodds and D. J. Watts, Phys. Rev. Lett. **92**, 218701 (2004).
[23] H.-K. Janssen, M. Müller, and O. Stenull, Phys. Rev. E **70**, 026114 (2004).
[24] J. M. Schwarz, A. J. Liu, and L. Q. Chayes, EPL (Europhysics Letters) **73**, 560 (2006).
[25] X. Yuan, Y. Dai, H. E. Stanley, and S. Havlin, Phys. Rev. E **93**, 062302 (2016).
[26] P. Echenique, J. Gmez-Gardees, and Y. Moreno, EPL (Europhysics Letters) **71**, 325 (2005).
[27] D. Achlioptas, R. M. D'Souza, and J. Spencer, Science **323**, 1453 (2009).
[28] R. M. Ziff, Phys. Rev. Lett. **103**, 045701 (2009).
[29] Y. Cho, S. Hwang, H. Herrmann, and B. Kahng, Science **339**, 1185 (2013).
[30] S. V. Buldyrev, R. Parshani, G. Paul, H. E. Stanley, and S. Havlin, Nature **464**, 1025 (2010).
[31] D. Zhou, A. Bashan, R. Cohen, Y. Berezin, N. Shnerb, and S. Havlin, Phys. Rev. E **90**, 012803 (2014).
[32] F. Radicchi, Nature Physics **11**, 597 (2015).
[33] G. Bizhani, P. Grassberger, and M. Paczuski, Phys. Rev. E **84**, 066111 (2011).
[34] C. Christensen, G. Bizhani, S.-W. Son, M. Paczuski, and P. Grassberger, EPL **97** (2012).
[35] S. Boettcher, V. Singh, and R. Ziff, Nature Communications **3** (2012).
[36] K. J. Schrenk, M. R. Hilário, V. Sidoravicius, N. A. M. Araújo, H. J. Herrmann, M. Thielmann, and A. Teixeira, Phys. Rev. Lett. **116**, 055701 (2016).
[37] P. Grassberger, Phys. Rev. E **95**, 010103 (2017).
[38] B. Roy and S. Santra, Croatica Chemica Acta **86**, 495 (2013).
[39] B. Roy and S. B. Santra, Phys. Rev. E **95**, 010101 (2017).
[40] A. Bunde and S. Havlin, *Fractals and Disordered Systems*, Springer-Verlag, Berlin, 1991.
[41] Y. S. Cho, B. Kahng, and D. Kim, Phys. Rev. E **81**, 030103 (2010).
[42] N. A. M. Araújo and H. J. Herrmann, Phys. Rev. Lett. **105**, 035701 (2010).
[43] H.-K. Janssen and O. Stenull, EPL **113**, 26005 (2016).
[44] P. Shu, L. Gao, P. Zhao, W. Wang, and H. Stanley, Scientific Reports **7** (2017).
[45] N. A. M. Araújo, J. S. Andrade, R. M. Ziff, and H. J. Herrmann, Phys. Rev. Lett. **106**, 095703 (2011).
[46] L. Cao and J. M. Schwarz, Phys. Rev. E **86**, 061131 (2012).
[47] K. Chung, Y. Baek, M. Ha, and H. Jeong, Phys. Rev. E **93**, 052304 (2016).
[48] F. Radicchi and S. Fortunato, Phys. Rev. E **81**, 036110 (2010).
[49] M. Sheinman, A. Sharma, J. Alvarado, G. H. Koenderink, and F. C. MacK-

intosh, Phys. Rev. Lett. **114**, 098104 (2015).
[50] Y. S. Cho, J. S. Lee, H. J. Herrmann, and B. Kahng, Phys. Rev. Lett. **116**, 025701 (2016).
[51] R. A. da Costa, S. N. Dorogovtsev, A. V. Goltsev, and J. F. F. Mendes, Phys. Rev. Lett. **105**, 255701 (2010).
[52] O. Riordan and L. Warnke, Science **333**, 322 (2011).
[53] P. Grassberger, C. Christensen, G. Bizhani, S.-W. Son, and M. Paczuski, Phys. Rev. Lett. **106**, 225701 (2011).
[54] N. Bastas, P. Giazitzidis, M. Maragakis, and K. Kosmidis, Physica A: Statistical Mechanics and its Applications **407**, 54 (2014).
[55] J. M. Yeomans, *Statistical Mechanics of Phase Transitions*, Oxford University Press, New York, 1994.
[56] J. J. Binney, N. J. Dowrick, A. J. Fisher, and M. E. J. Newman, *The Theory of Critical Phenomena*, Oxford University Press, Oxford, 1992.
[57] M. Plischke and B. Bergersen, *Equilibrium Statistical Physics*, WORLD SCIENTIFIC, 3 edition.
[58] K. Binder, Reports on Progress in Physics **50**, 783 (1987).
[59] W. Janke, *First-Order Phase Transitions*, pages 111–135, Springer Netherlands, Dordrecht, 2003.
[60] R. Zallen, *The Physics of Amorphous Solids*, Wiley, New York, 1983.
[61] A. Bunde and S. Havlin, *Fractals and Disordered Systems*, Springer-Verlag, Berlin, 1991.
[62] A. G. Hunt, *Percolation Theory for Flow in Porous Media*, Springer-Verlag, New York, 2005.
[63] A. Bovier, *Statistical Mechanics of Disordered Systems: a mathematical perspective*, Cambridge University Press, 2006.
[64] D. Ben-Avraham and S. Havlin, *Diffusion and Reactions in Fractals and Disordered Systems*, Cambridge University Press, UK, 2000.
[65] P. R. King, S. V. Buldyrev, N. V. Dokholyan, S. Havlin, Y. Lee, G. Paul, and H. E. Stanley, **274**, 60 (1999).
[66] P. R. King, S. V. Buldyrev, N. V. Dokholyan, S. Havlin, E. Lopez, G. Paul, and H. E. Stanley, **314**, 103 (2002).
[67] J. L. Cardy and P. Grassberger, J. Phys. A: Math. Gen. **18**, L267 (1985).
[68] R. Cohen, D. Ben-Avraham, and S. Havlin, **66**, 036113 (2002).
[69] A. Acin, J. I. Cirac, and M. Lewenstein, Nature Physics **3**, 256 (2007).
[70] D. F. Fu, S. V. Buldyrev, M. A. Salinger, and H. E. Stanley, **74**, 036118 (2006).
[71] J. Brzychczyk, **73**, 024601 (2006).
[72] M. Dolz, F. Nieto, and A. J. Ramirez-Pastor, **72**, 066129 (2005).

[73] N. I. Lebovka, S. Tarafdar, and N. V. Vygornitskii, **73**, 031402 (2006).
[74] I. Brovchenko, A. Krukau, A. Oleinikova, and A. K. Mazur, Phys. Rev. Lett. **97**, 137801 (2006).
[75] I. Breskin, J. Soriano, E. Moses, and T. Tlusty, Phys. Rev. Lett. **97**, 188102 (2006).
[76] K. Kosmidis and A. Bunda, **376**, 699 (2007).
[77] T. Chelidze and T. Matcharashvili, Tectonophysics **431**, 49 (2007).
[78] T. Abete, A. de Canadia, E. D. Gado, A. Fierro, and A. Coniglio, Phys. Rev. Lett. **98**, 088301 (2007).
[79] A. Oleinikova and I. Brovchenko, Molecular Phys. **104**, 3841 (2006).
[80] K. H. Schatten, Astrophysical J. Suppl. Series **169**, 137 (2007).
[81] K. Christensen and N. R. Moloney, *Complexity and Criticality*, Imperial College Press, London, 2005.
[82] B. Bollobás and O. Riordan, *Percolation*, Cambridge University Press, 2006.
[83] G. R. Grimmett, *Percolation*, Springer-Verlag, New York, 1999.
[84] M. P. M. den Nijs, **12**, 1857 (1997).
[85] B. Nienhuis, **15**, 199 (1982).
[86] R. M. Ziff and B. Sapoval, **19**, L1169 (1987).
[87] D. Stauffer, Phys. Rep. **54**, 1 (1979).
[88] P. Erdos and A. Rényi, Publ. Math. Inst. Hung. Acad. Sci **5**, 17 (1960).
[89] R. D'Souza and J. Nagler, Nature Physics **11**, 531 (2015).
[90] Y. Cho, J. Kim, J. Park, B. Kahng, and D. Kim, Phys. Rev. Lett. **103**, 135702 (2009).
[91] F. Radicchi and S. Fortunato, Phys. Rev. Lett. **103**, 168701 (2009).
[92] Y. S. Cho and B. Kahng, Phys. Rev. Lett. **107**, 275703 (2011).
[93] R. M. D'Souza and M. Mitzenmacher, Phys. Rev. Lett. **104**, 195702 (2010).
[94] E. J. Friedman and A. S. Landsberg, Phys. Rev. Lett. **103**, 255701 (2009).
[95] H. Hooyberghs and B. Van Schaeybroeck, Phys. Rev. E **83**, 032101 (2011).
[96] W. Chen and R. M. D'Souza, Phys. Rev. Lett. **106**, 115701 (2011).
[97] Y. Zhang, W. Wei, B. Guo, R. Zhang, and Z. Zheng, Phys. Rev. E **86**, 051103 (2012).
[98] W. Chen, Z. Zheng, and R. D'Souza, EPL **100** (2012).
[99] H. Chen, G. He, F. Huang, C. Shen, and Z. Hou, Chaos **23** (2013).
[100] K. J. Schrenk, A. Felder, S. Deflorin, N. A. M. Araújo, R. M. D'Souza, and H. J. Herrmann, Phys. Rev. E **85**, 031103 (2012).
[101] T. Bohman, A. Frieze, and N. C. Wormald, Random Structures and Algorithms **25**, 432 (2004).
[102] R. M. Ziff, Phys. Rev. E **82**, 051105 (2010).
[103] N. Bastas, K. Kosmidis, and P. Argyrakis, Phys. Rev. E **84**, 066112 (2011).

[104] W. Choi, S.-H. Yook, and Y. Kim, Phys. Rev. E **84**, 020102 (2011).
[105] W. Choi, S.-H. Yook, and Y. Kim, Phys. Rev. E **86**, 051126 (2012).
[106] W. Choi, H. Chae, S.-H. Yook, and Y. Kim, Phys. Rev. E **90**, 022123 (2014).
[107] S. D. S. Reis, A. A. Moreira, and J. S. Andrade, Phys. Rev. E **85**, 041112 (2012).
[108] S. Squires, K. Sytwu, D. Alcala, T. Antonsen, E. Ott, and M. Girvan, Physical Review E - Statistical, Nonlinear, and Soft Matter Physics **87** (2013).
[109] A. Waagen, R. M. D'Souza, and T.-C. Lu, Phys. Rev. E **96**, 012317 (2017).
[110] Y. S. Cho, S.-W. Kim, J. D. Noh, B. Kahng, and D. Kim, Phys. Rev. E **82**, 042102 (2010).
[111] J. Li and M. Östling, Phys. Rev. E **86**, 040105 (2012).
[112] J. Nagler, A. Levina, and M. Timme, Nature Physics **7**, 265 (2011).
[113] J. S. Andrade, H. J. Herrmann, A. A. Moreira, and C. L. N. Oliveira, Phys. Rev. E **83**, 031133 (2011).
[114] P. Giazitzidis and P. Argyrakis, Phys. Rev. E **88**, 024801 (2013).
[115] J. Qian, D. Han, and Y. Ma, EPL **100** (2012).
[116] H. K. Lee, B. J. Kim, and H. Park, Phys. Rev. E **84**, 020101 (2011).
[117] L. Tian and D.-N. Shi, Physics Letters A **376**, 286 (2012).
[118] S. Manna and A. Chatterjee, Physica A: Statistical Mechanics and its Applications **390**, 177 (2011).
[119] S. Manna, Physica A: Statistical Mechanics and its Applications **391**, 2833 (2012).
[120] A. A. Moreira, E. A. Oliveira, S. D. S. Reis, H. J. Herrmann, and J. S. Andrade, Phys. Rev. E **81**, 040101 (2010).
[121] K. J. Schrenk, N. A. M. Araújo, and H. J. Herrmann, Phys. Rev. E **84**, 041136 (2011).
[122] R. Ziff, Science **339**, 1159 (2013).
[123] Y. S. Cho and B. Kahng, Phys. Rev. E **84**, 050102 (2011).
[124] Y. Cho, Y. Kim, and B. Kahng, Journal of Statistical Mechanics: Theory and Experiment **2012** (2012).
[125] J. Chalupa, P. L. Leath, and G. R. Reich, Journal of Physics C: Solid State Physics **12**, L31 (1979).
[126] S. N. Dorogovtsev, A. V. Goltsev, and J. F. F. Mendes, Phys. Rev. Lett. **96**, 040601 (2006).
[127] A. V. Goltsev, S. N. Dorogovtsev, and J. F. F. Mendes, Phys. Rev. E **73**, 056101 (2006).
[128] W. Chen, J. Nagler, X. Cheng, X. Jin, H. Shen, Z. Zheng, and R. M. D'Souza, Phys. Rev. E **87**, 052130 (2013).
[129] W. Choi, D. Lee, and B. Kahng, Phys. Rev. E **95**, 022304 (2017).

[130] Y. Kim, Y.-K. Yun, and S.-H. Yook, Physical Review E **82** (2010).
[131] R. K. Pan, M. Kivelä, J. Saramäki, K. Kaski, and J. Kertész, Phys. Rev. E **83**, 046112 (2011).
[132] G. Bizhani, M. Paczuski, and P. Grassberger, Phys. Rev. E **86**, 011128 (2012).
[133] H. D. Rozenfeld, L. K. Gallos, and H. A. Makse, The European Physical Journal B **75**, 305 (2010).
[134] C. L. N. Oliveira, N. A. M. Araújo, J. S. Andrade, and H. J. Herrmann, Phys. Rev. Lett. **113**, 155701 (2014).
[135] P. K. Jaiswal, I. Procaccia, C. Rainone, and M. Singh, Phys. Rev. Lett. **116**, 085501 (2016).
[136] Radicchi, Filippo and Arenas, Alex, Nat Phys **9**, 717 (2013).
[137] J. Gao, S. V. Buldyrev, H. E. Stanley, and S. Havlin, Nat Phys **8**, 40 (2012).
[138] L. Bttcher, M. Lukovi, J. Nagler, S. Havlin, and H. Herrmann, Scientific Reports **7** (2017).
[139] J. Gmez-Gardees, L. Lotero, S. Taraskin, and F. Prez-Reche, Scientific Reports **6** (2016).
[140] J. Adler, Physica A: Statistical Mechanics and its Applications **171**, 453 (1991).
[141] J. Hoshen and R. Kopelman, Phys. Rev. B **14**, 3438 (1976).
[142] P. L. Leath, Phys. Rev. B **14**, 5046 (1976).
[143] Y. A. Andrienko, N. V. Brilliantov, and P. L. Krapivsky, Journal of Statistical Physics **75**, 507 (1994).
[144] N. Tsakiris, M. Maragakis, K. Kosmidis, and P. Argyrakis, The European Physical Journal B **81**, 303 (2011).
[145] N. Tsakiris, M. Maragakis, K. Kosmidis, and P. Argyrakis, Phys. Rev. E **82**, 041108 (2010).
[146] W. H. Press, *Numerical Recipes in FORTRAN: The Art of Scientific Computing*, Cambridge University Press, 1992.
[147] B. Roy and S. B. Santra, arxiv:cond-mat , 1611.09497 (2016).
[148] V. Privman, *Finite Size Scaling and Numerical Simulation of Statistical Systems*, World Scientific Publication, Singapore, 1990.
[149] J. L. Cardy, *Finite Size Scaling*, North Holland, Amsterdam, 1988.
[150] A. D. Bruce, Journal of Physics C: Solid State Physics **14**, 3667 (1981).
[151] O. Melchert, Phys. Rev. E **87**, 022115 (2013).
[152] K. Binder, Reports on Progress in Physics **60**, 487 (1997).
[153] A. D. Bruce and N. B. Wilding, Phys. Rev. Lett. **68**, 193 (1992).
[154] M. Mueller, W. Janke, and D. A. Johnston, Phys. Rev. Lett. **112**, 200601 (2014).
[155] P. De Gregorio, A. Lawlor, P. Bradley, and K. A. Dawson, Phys. Rev. Lett.

93, 025501 (2004).
[156] F. Sausset, C. Toninelli, G. Biroli, and G. Tarjus, Journal of Statistical Physics **138**, 411 (2010).
[157] K. Binder, Reports on Progress in Physics **50**, 783 (1987).
[158] C. E. Fiore and M. J. de Oliveira, Phys. Rev. E **87**, 042101 (2013).
[159] E. Machado, G. M. Buendía, P. A. Rikvold, and R. M. Ziff, Phys. Rev. E **71**, 016120 (2005).
[160] B. Roy and S. B. Santra, arxiv:cond-mat , 1705.03780 (2017).
[161] A. Chakraborty and S. S. Manna, Phys. Rev. E **89**, 032103 (2014).
[162] T. Vicsek, *Fractal Growth Phenomena*, World Scientific, 1989.
[163] D. Lee, M. Jo, and B. Kahng, Phys. Rev. E **94**, 062307 (2016).
[164] Giazitzidis, Paraskevas, Avramov, Isak, and Argyrakis, Panos, Eur. Phys. J. B **88**, 331 (2015).
[165] K. Binder and D. P. Landau, Phys. Rev. B **30**, 1477 (1984).
[166] R. F. S. Andrade and H. J. Herrmann, Phys. Rev. E **88**, 042122 (2013).
[167] M. Liu, J. Fan, L. Li, and X. Chen, European Physical Journal B **85** (2012).
[168] M. S. S. Challa, D. P. Landau, and K. Binder, Phys. Rev. B **34**, 1841 (1986).
[169] S.-H. Tsai and S. R. Salinas, Brazilian Journal of Physics **28**, 58 (1998).
[170] A. Hasmy, R. Paredes, O. Sonneville-Aubrun, B. Cabane, and R. Botet, Phys. Rev. Lett. **82**, 3368 (1999).

List of publications

Journal:

1. *Continuous percolation transitions in random cluster growth model*
   Bappaditya Roy and S. B. Santra, Croat. Chem. Acta **86**, 495 (2013).

2. *First order transition in a percolation model with nucleation and preferential growth*
   Bappaditya Roy and S. B. Santra, Physical Review E **95**, 010101(R) (2017).

3. *Finite size scaling study of a two parameter percolation model: constant and correlated growth*
   Bappaditya Roy and S. B. Santra, Physica A: Statistical Mechanics and its Applications **492**, 969-979 (2018).

4. *Random growth lattice filling model of percolation: a crossover from continuous to discontinuous transition*
   Bappaditya Roy and S. B. Santra, to appear in JSTAT (2018).

Conferences:

1. *Anti-percolation in the etching of a random solid*, Bappaditya Roy, H. Bhaumik and S. B. Santra, CMDAYS 2011, Gauhati University, Guwahati, India.

2. *Random cluster growth and explosive percolation*, Bappaditya Roy and S. B. Santra, CMDAYS 2012, BIT, Mesra, Ranchi, India.

3. *Does explosive percolation occur away from the critical point?*, Bappaditya Roy and S. B. Santra, CCP 2012, Kobe University, Kobe, Japan.

4. *Random cluster growth site percolation with suppression*, Bappaditya Roy and S. B. Santra, CMDAYS 2013, NIT, Rourkela, India.

5. *Random cluster growth with suppression: No evidence of Explosive percolation*, Bappaditya Roy and S. B. Santra, 2nd Indian Statistical Physics Community Discussion Meeting 2015, IIScB, Bangalore, India.

6. *Explosive Percolation in Growing Cluster model from randomly added growth centers*, Bappaditya Roy and S. B. Santra, CCP 2015, IIT Guwahati, Guwahat.

7. *Continuous percolation transitions in suppressed random cluster growth model* B. Roy and S. B. Santra, AIP Conf. Proc. **1728**, 020132 (2016), ICC, Govt. Engineering College, Bikaner, India.

8. *Nature of transition in a touch and stop model with varying growth probability*, Bappaditya Roy and S. B. Santra, STATPHY-2016, Kolkata, India.

9. *Percolation and First-order Transition*, Bappaditya Roy and S. B. Santra, STATPHY-2016, Kolkata, India.